BIOAVAILABILITY OF ORGANIC CARBON FROM FE(II) REACTED FERRIHYDRITE NATURAL ORGANIC MATTER COPRECIPITATES

by

NADIA NOOR

(Under the Direction of Aaron Thompson)

ABSTRACT

Ferrihydrite (Fh) mineral associated soil organic matter (SOM) is considered to be protected. But the multiplicity of interactions between Fh and OM suggest OM protection can be disrupted. Under anoxic conditions, Fh that comes in contact with aqueous Fe(II) can be transformed into more stabilized iron minerals such as lepidocrocite, goethite, hematite, etc. While previous studies have shown that the presence of OM and the ratio of C/Fe can impact this transformation process, it is unknown how reaction with Fe(II) will impact the bioavailability of OM in the Fh-OM association. To investigate this, I first synthesized C isotope-labeled Fh-OM coprecipitates with a range of molar C/Fe ratios and reacted them with Fe(II) for the different time periods. Changes in the coprecipitate were then characterized using mössbauer spectroscopy (MBS) and ultrahigh-resolution scanning transmission electron microscopy (STEM). I found that reaction with Fe(II) drove a localized increase in Fh crystallinity, especially in the low C/Fe coprecipitates and also resulted in the partial release of OM from the coprecipitates. Higher C/Fe containing coprecipitates forestalled this transformation, but longer reaction times resulted in the

higher release of OM and in a localized increase in Fh crystallinity. Then I further incubated the Fh-OM coprecipitates with microbes under oxic conditions and measured the mineralization of CO_2-C, and changes in dissolved organic carbon (DOC) and solid phase C. I found that the Fe(II) reacted coprecipitates protected more of the coprecipitated C than the unreacted coprecipitates when the C/Fe ratio of the coprecipitates was low. While the significant OM was solubilized from the coprecipitates only a small amount of OC was mineralized to CO_2. Following the microbial incubation, the crystallinity of the Fe in the coprecipitates decreased. Lastly, I examined the OM bioavailability in naturally occurring Bacteriogenic Fe-OM coprecipitates using the same methods and found the native OM was more protected than the OM in the synthesized Fe-OM coprecipitates.

INDEX WORDS: Fe(II) catalyzed transformation, Ferrihydrite-Natural organic matter coprecipitate, Aerobic microbial respiration, Mössbauer spectroscopy, High resolution scanning transmission electron microscopy, bacteriogenic iron (oxyhydr)oxide

BIOAVAILABILITY OF ORGANIC CARBON FROM FE(II) REACTED FERRIHYDRITE NATURAL ORGANIC MATTER COPRECIPITATES

by

NADIA NOOR

BA, University of Dhaka, Bangladesh, 2011

MA, University of Dhaka, Bangladesh, 2013

A Dissertation Submitted to the Graduate Faculty of The University of Georgia in Partial Fulfillment of the Requirements for the Degree

DOCTOR OF PHILOSOPHY

ATHENS, GEORGIA

2021

BIOAVAILABILITY OF ORGANIC CARBON FROM FE(II) REACTED FERRIHYDRITE NATURAL ORGANIC MATTER COPRECIPITATES

by

NADIA NOOR

Major Professor:	Aaron Thompson
Committee:	Paul A. Schroder
	Mussie Habteselassie
	Patricia M. Medeiros
	Chunmei Chen

Electronic Version Approved:

Ron Walcott
Vice Provost for Graduate Education and Dean of the Graduate School
The University of Georgia
December 2021

DEDICATION

I dedicate this dissertation to my sister, Dr Nazia Noor. Thank you for motivating me throughout my life.

ACKNOWLEDGEMENTS

I would like to offer my utmost respect to my major professor Dr. Aaron Thompson for his continuous support, guidance and patience throughout my research time at The University of Georgia. I have always been highly inspired by his work ethic and dedication to research. Every meeting with him made me more knowledgeable and more enthusiastic to try something new in my research field. His guidance helped me in my research career as well as in my personal life. I am also appreciative of the guidance and support from my committee members, Dr. Paul A. Schroder, Dr. Mussie Habteselassie, Dr. Patricia M. Medeiros and Dr. Chunmei Chen.

I would like to thank the SusChEM project research group and National Science Foundation (NSF) for financial support. I would also like to thank Thomas R. Maddox and Eric Formo for helping with sample analysis.

I would like to thank the faculty members of the Crop and Soil Sciences, Department of The University of Georgia for sharing their knowledge and experience with me. I would extend my appreciation to the staff members of the Crop and Soil Sciences department for their support.
This research would not be possible without the technical assistance of Nehru Mantripragada, Kim Kauffman and all the lab members of the Soil Chemistry lab in the Department of Crop and Soil Sciences at the University of Georgia. I would like to thank Diego Barcellos, Jared Wilmoth, Taylor Cyle, Stephanie Fulton for sharing their research experience with me.

I would like to convey my gratitude to my Family members and my friends for believing in me and supporting me throughout my good and bad times. I would like to thank Kishan Mahmud for being there for me no matter what the situation was.

A big thanks to my son Nahwan Addoy Noor. Your beautiful smile inspired me every day and gave me the strength to continue working through thick and thins.

TABLE OF CONTENTS

Page

ACKNOWLEDGEMENTS v

LIST OF TABLES x

LIST OF FIGURES xii

CHAPTER

1. INTRODUCTION AND LITERATURE REVIEW 1

Explanation of Dissertation Format 1

Literature Review 3

Objectives 12

2 BIOAVAILABILITY OF C FROM SUWANNEE RIVER NATURAL ORGANIC MATTER -FERRIHYDRITE COPRECIPITATES AFTER REACTION WITH FE(II) 14

Abstract 15

Introduction 15

Materials and methods 18

Results and discussion 22

Conclusion 26

3 LOCALIZED ALTERATION OF FERRIHYDRITE NATUTAL ORGANIC MATTER COPRECIPITATES FOLLOWING REACTION WITH FE(II) 33
Abstract 34
Introduction 35
Materials and methods 37
Results 41
Discussion 44
Conclusion 48
4 BIOAVAILABILITY OF ORGANIC MATTER COPRECIPITATED WITH FERRIHYDRITE AND PRE-REACTED WITH FE(II) 56
Abstract 57
Introduction 58
Materials and methods 60
Results 66
Discussion 70
Conclusion 71
5 CONCLUSION 90
Summary 90
Environmental implication 92
REFERENCES 94

APPENDICES

A BIOAVAILABILITY OF ORGANIC MATTER IN BACTERIOGENIC IRON (OXYHYDR) OXIDES (BIOS) AND THE RELEASE OF HEAVY METALS 111

Abstract 112

Introduction 112

Materials and methods 115

Results 120

B SUPPLEMENTAL INFORMATION OF CHAPTER 3 133

C SUPPLEMENTAL INFORMATION OF CHAPTER 4 139

D BIODEGRADATION OF FERRIHYDRITE HUMIC ACID COPRECIPITATE ... 153

LIST OF TABLES

Page

Table 2.1: Change in C content in the SRNOM-Fh coprecipitates during incubation 31

Table 2.2: Percent (%) contribution of added lactate in the SRNOM-Fh during incubation 31

Table 2.3: Mass balance calculation for total C content (mg) in each reactor containing 20mg of coprecipitates in 15ml of media, initial and after incubation study.....32

Table 2.4: The temperature with max CO_2 peak was measured in SRNOM-Fh coprecipitates…32

Table 3.1: Elemental composition of the synthesized coprecipitates (Initial) and after reacting with Fe(II) (Final) in PIPES buffer.....49

Table 4.1: Change in the C/Fe molar ratio of the Fe(II) reacted and unreacted coprecipitates after 1d (Fresh) and 14d(Aged). The initial C/Fe indicates the synthesized C/Fe molar ratio of the coprecipitates 89

Table A.1: Elemental composition of the BIOS and synthesized coprecipitates, Ferrihydrite ..132

Table B.1: Magnetic susceptibility of the Fh mineral and Fh-NOM coprecipitates.....138

Table C.1: Total C and added ^{13}C-NOM content of the solids before and after incubation study (mg 30mg^{-1} unit) for fresh samples. The same treatment names indicating replications139

Table C.2: Total C and added ^{13}C-NOM content of the solids before and after incubation study (mg 30mg^{-1}) for aged samples. The same treatment names indicating replications.....140

Table C.3: Percent contribution of added ^{13}C-NOM released as DOC and CO_2-C (% of solid ^{13}C-NOM initially present in the solids) in fresh and aged reactors 141

Table C.4: Mass balance calculation for the added ^{13}C-NOM in each fresh reactor. The calculation has been done based on 30mg solid in 55 ml solution basis 142
Table C.5: Mass balance calculation for the added ^{13}C-NOM in each aged reactor. The calculation has been done based on 30mg solid in 55 ml solution basis 143
Table C.6: Mass balance calculation for total C in the fresh reactor. The calculation has been done based on 30mg solid in 55 ml solution basis.....144
Table C.7: Mass balance calculation for total C in the aged reactor. The calculation has been done based on 30mg solid in 55 ml solution basis.....145
Table C.8: Description of each reactor along with their designated names that have been used in this chapter 146
Table C.9: Change in pH during the incubation period in fresh reactor 147
Table C.10: Change in pH during the incubation period in aged reactor 148

LIST OF FIGURES

Page

Figure 1.1: Five principal carbon pools and fluxes between them 4

Figure 1.2: Common pathways of iron oxide formation and transformation 9

Figure 2.1: (a) Percent (%) loss of C from the SRNOM-Fh solids during incubation (b) Percent (%) contribution of added lactate C sorbed on the coprecipitate. 28

Figure 2.2: (a) CO_2-C (μg $g^{-1}h^{-1}$) respiration from added lactate (b) cumulative CO_2 respiration from added lactate and (c) per cent contribution of CO_2-C from added lactate to total CO_2 respiration 29

Figure 2.3: (a) CO_2-C respiration from SRNOM_FH coprecipitate (b) cumulative CO_2 respiration from SRNOM-Fh 30

Figure 2.4: DOC (mmol L^{-1}) concentration in the reactors after incubation 30

Figure 3.1: STEM image of fresh low unreacted (a,b)and reacted coprecipitate with Fe(II)(c-e) 50

Figure 3.2: STEM image of aged low unreacted (a) and reacted coprecipitate with Fe(II) (b,c) ..51

Figure 3.3: STEM image of fresh high unreacted(a,b)and reacted coprecipitate with Fe(II)(c-e) 52

Figure 3.4: STEM image of aged high unreacted(a,b)and reacted coprecipitate with Fe(II)(c-e) 53

Figure 3.5: Mössbauer spectra (at 35K, 13K, and 5K) of the fresh low (a.b) and aged low (c,d) C/Fe coprecipitates both unreacted and Fe(II) reacted, respectively 54

Figure 3.6: Mössbauer spectra (at 35K, 13K, and 5K) of the fresh high (a.b) and aged high (c,d) C/Fe coprecipitates both unreacted and Fe(II) reacted, respectively 55

Figure 4.1: Added ^{13}C-NOM (mg 30mg^{-1}) and total C (mg 30mg^{-1}) in the fresh (a, b) and aged (c, d) sample before and after biotic incubation 73

Figure 4.2: Added ^{13}C-NOM in DOC and total DOC in fresh (a,b)and aged (c,d)biotic reactors 74

Figure 4.3: Added ^{13}C-NOM mineralization as CO_2-C, cumulative ^{13}C-NOM and cumulative CO_2 respiration from the fresh (a,b,c) and aged (d, e, f) biotic reactors, respectively.....75

Figure 4.4: Mössbauer spectra (at 35K, 13K, and 5K) of before and after incubation solids of fresh low C/Fe unreacted (a, b) and Fe(II) reacted (c, d) coprecipitates 77

Figure 4.5: Mössbauer spectra (at 35K, 13K, and 5K) of before and after incubation solids of aged low C/Fe unreacted (a, b) and Fe(II) reacted (c, d) coprecipitates.....79

Figure 4.6: Mössbauer spectra (at 35K, 13K, and 5K) of before and after incubation solids of fresh high C/Fe unreacted (a, b) and Fe(II) reacted (c, d) coprecipitates 81

Figure 4.7: Mössbauer spectra (at 35K, 13K, and 5K) of before and after incubation solids of aged high C/Fe unreacted (a, b) and Fe(II) reacted (c, d) coprecipitates.....83

Figure 4.8: Mössbauer spectra (at 35K, 13K, and 5K) of before(a) and after (b) incubation solids of fresh Fh.....83

Figure 4.9: STEM image of fresh low C/Fe molar coprecipitates before (a,b) and after (c) incubation.....84

Figure 4.10: STEM image of fresh low C/Fe with Fe(II) reacted coprecipitates before (a-c) and after (d,e) incubation.....84

Figure 4.11: STEM image of aged low C/Fe with Fe(II) reacted coprecipitates before (a-c) and after (d-f) incubation.....85

Figure 4.12: STEM image of fresh high C/Fe coprecipitates before (a,b) and after (c,d) incubation.....86

Figure 4.13: STEM image of fresh high C/Fe with Fe(II) reacted coprecipitates before (a,b) and after (c-e) incubation 87
Figure 4.14: STEM image of aged high C/Fe before (a,b) and after (c-e) incubation 87
Figure 4.15: STEM image of aged high C/Fe with Fe(II) reacted coprecipitates before (a-c) and after (d-f) incubation 88
Figure 4.16: STEM image of aged Fh mineral before and after reacted with Fe(II) 88
Figure A.1: Percent (%) loss of carbon from the solid during incubation 123
Figure A.2: Percent (%) contribution of added lactate to the solid during incubation 124
Figure A.3: Dissolved organic carbon concentration (DOC) during microbial incubation 124
Figure A.4: (a) CO_2 mineralization over time and (b) cumulative CO_2 mineralization 125
Figure A.5: Aqueous concentration of (a) Zn, (b) Ni (c) Pb (d) Cr (e) As (f) Cu and (g) Al during microbial incubation 127
Figure A.6: Scanning transmission electron microscopy image of BIOS before incubation 127
Figure A.7: Scanning transmission electron microscopy image of BIOS after incubation 128
Figure A.8: Scanning transmission electron microscopy image of coprecipitate (a) before and (b) after incubation as we as (c) Fh treatment after incubation, illustrating the formation of new crystal structure 129
Figure A.9: X-ray diffraction pattern of collected BIOS 130
Figure A.10: (a) GPS map of the sampling site where the yellow pin pointing out the exact position. (b,c) the iron-containing flocks in the wetland from where the sampling occurs, (d,e) collected sample in the tube 131
Figure B.1: EDS mapping of results of fresh low unreacted (a-b) and reacted coprecipitate with Fe(II) (c,d) 133

Figure B.2: EDS mapping of results of aged low unreacted (a,b) and reacted coprecipitate with Fe(II) (c,d) 134
Figure B.3: EDS mapping of results of fresh high unreacted (a-c) and reacted coprecipitate with Fe(II) (d-f) 135
Figure B.4: EDS mapping of results of aged high unreacted (a,b) and reacted coprecipitate with Fe(II) (c,d) 136
Figure B.5: STEM image of aged unreacted (a-c) and Fe(II) reacted (d-f) Fh, (g) fresh Fe(II) reacted Fh 137
Figure B.6: Van Krevelen space diagram (VKD) of the ^{13}C-DOM used as C source for preparing the coprecipitate from FTICR analysis 138
Figure C.1: Added ^{13}C-NOM (mg 30mg^{-1}) in the (a) fresh and (b) aged solid sample before and after incubation without microbial inoculum 149
Figure C.2: Added ^{13}C-NOM in DOC and DOC in fresh (a,b) and aged (c,d) reactors without microbial inoculum 150
Figure C.3: Added 13C-NOM to CO_2 respiration, cumulative 13C-NOM and cumulative CO2 respiration from the fresh (a,b,c) reactor during the without microbial incubation and .151
Figure C.4: Van Krevelen space diagram (VKD) of the ^{13}C-DOM used as C source for preparing the coprecipitate from FTICR analysis 152
Figure C5: Image of the 1d reacted coprecipitates along with control 152
Figure D.1: HCL extracted Fe(II) over time under anoxic condition 156
Figure D.2: HCL extracted Fe(II) over time under oxic condition 157
Figure D.3: Dissolved organic carbon concentration over time under anoxic condition 159
Figure D.4: Dissolved organic carbon concentration over time under oxic condition 160

Figure D.5: CO_2 emission over time under anoxic condition 161

Figure D.6: CO_2 emission over time under oxic condition 162

Figure D.7: Growth curve of *Schwenella oneidensis* MR1 over time 163

CHAPTER 1

INTRODUCTION AND LITERATURE REVIEW

Explanation of dissertation format

This dissertation comprises Five chapters. Chapter one provides a review of the current literature and introduces the research problem. Chapters two to four and Appendix A comprise the core experimental work discussed in detail (present study). Chapter Five is a conclusion that reconnects the results of this dissertation and discusses its application in soil systems. Below I briefly outline each of the core experimental chapters.

Chapter 2 focuses on the bioavailability of organic matter contained in coprecipitates of ferrihydrite and Suwanee river natural organic matter that reacted with Fe(II). This study expands on collaborative work I was a part of that characterized the electron-transfer and atom exchange during Fe(II) catalyzed transformation of Organic matter-Ferrihydrite coprecipitates. This study was published in Environmental Science & Technology in 2018 (Zhou et al., 2018). In Chapter 2, I measured the bioavailability of organic matter from those coprecipitates using a microbial incubation technique common for assessing soil carbon availability, but I used ^{13}C-labeled substrates and microbial communities to distinguish between the microbes, media, and the co-precipitated organic matter. This work suggested that the Fe(II) reacted coprecipitates showed protection against the biodegradation of the coprecipitated C but the reason behind this was unclear from this study. To investigate the reason I focused on the change in the coprecipitates that occurred after Fe(II) reaction. In Chapter 3, I expanded my work to examine natural plant litter extracted organic matter as the base for the co-precipitates, here using ^{13}C-labeled plant material

and unlabeled microbes. In this chapter, I quantified changes in the crystallinity and morphological of the Ferrihydrite- natural organic matter coprecipitates after reacting with Fe(II). I have submitted this chapter for publication (*In review*) in the Soil Science Society of America Journal (Special issue). This study demonstrated that the Fe(II) reaction can develop localized increased crystallinity in the coprecipitates and this process may result in the release of some coprecipitated C. Chapter 4 is a parallel to Chapter 2, this time examining the bioavailability of the plant-litter derived coprecipitates I generated for Chapter 3. This study showed that the product of Fe(II) reacted coprecipitate protects the coprecipitated C compared to the unreacted coprecipitated and the bioavailability of C was related to the changes that occurred in the coprecipitates during the reaction with Fe(II). In the Chapters discussed so far, I examined synthesized coprecipitates, which are often less complex than naturally occurring coprecipitates, which can also have other elements (e.g., aluminum and heavy metals) associated with them. In Appendix A, I expand my work to examine the bioavailability of organic matter in naturally occurring coprecipitates collected from an iron floc emerging from a local wetland. In addition to assessing the bioavailability, I have also evaluated the release of some heavy metals during the aerobic microbial incubation. This work demonstrated that the iron floc showed higher protection against the biodegradation of the associated C than the synthesized coprecipitates.

LITERATURE REVIEW

Soil organic matter as a carbon reservoir

Soil is a large reservoir of carbon (C) and the soil C pool is 3.3 times the size of the atmospheric pool and 4.5 times the size of the biotic pool (Lal, 2004). Among the global soil carbon (SC) pool of 2500 Gigatons (Gt), about 1550 Gt is soil organic carbon (SOC) and 950 Gt is soil inorganic carbon (SIC) (Lal, 2004). Due to the high amount of SOC, a small amount of C release as carbon dioxide (CO_2) or methane can cause quantitatively relevant variation in the atmospheric concentration of greenhouse gases (Ciais et al., 2013). Soil organic matter (SOM) also retains nutrients as well as pollutants, and thus it supports plant growth and also prevents contamination of aquatic systems (Lal, 2004). The release of SOC plays a vital role in the biogeochemical processes in rivers, lakes and estuaries as well (Marín-Spiotta et al., 2014).

There are several mechanisms to protect SOM against decomposition. These processes can be separated into three major groups: (1) chemical stabilization, (2) physical protection and (3) biochemical stabilization (Christensen, 1996; Stevenson, 1994). Chemical stabilization results from the chemical and physiochemical binding between SOM and soil minerals (Feller & Beare, 1997; Hassink, 1997; Ladd et al., 1985). Physical protection is the influence of aggregation formation (Edwards & Bremner, 1967; Elliott, 1986; Jastrow, 1996; Tisdall & OADES, 1982), which protects SOM by forming a physical barrier between the microbes and enzymes and their substrates (Coleman & Elliot, 1988). Biochemical stabilization is the stabilization of SOM due to recalcitrant compounds and through chemical complexation processes in soil.

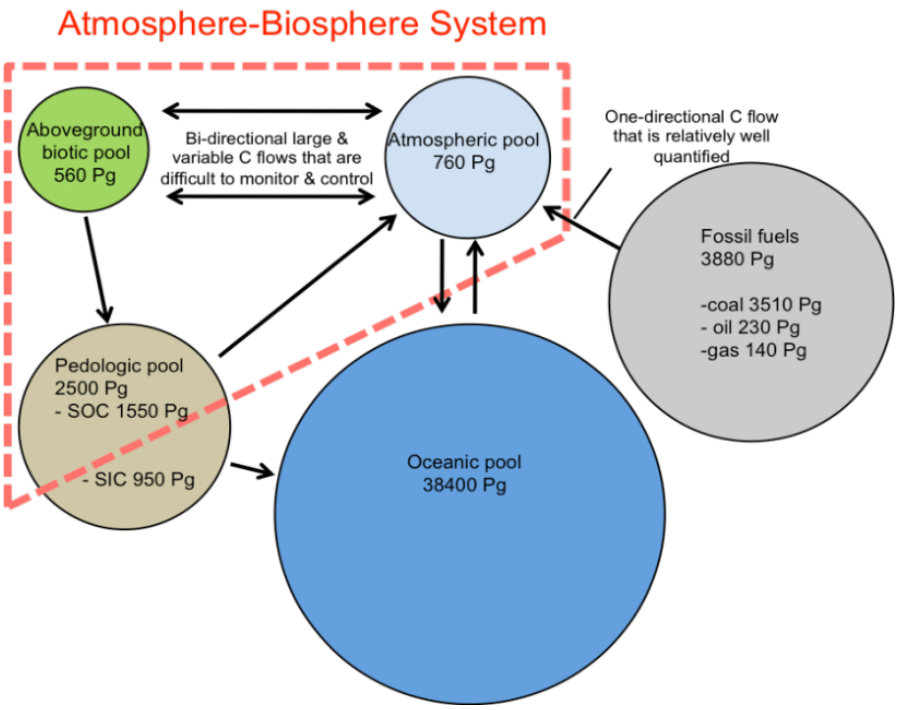

Figure 1.1: Five principal carbon pools and fluxes between them (SOC= soil organic carbon, SIC= soil inorganic carbon). Source: (Ascenso et al., 2018).

Interaction of Fe oxide mineral and organic matter

In soil, the organo-mineral associations can protect OM by imposing chemical, physical and biogeochemical stabilization (Kaiser & Guggenberger, 2003). Direct correlation between the specific surface area of minerals and concentration of OC have shown surface adsorption to be one of the major processes to preserve OM in soil and marine sediments (Keil et al., 1994; Mayer, 1994). But later studies have also shown that a broader set of interactions occur on the surface of minerals that can impact organic matter. For instance, mineral surfaces can act as a catalyst for organic reactions, they can serve as redox partners for the decomposition of OM through direct electron transfer or by generating reactive oxygen species that can oxidise OM, and they can compartmentalize soil and sediments by creating unique microsites that host diverse microbial communities with different modes of interacting with OM. (Kleber et al., 2021).

Among soil minerals, studies showed that the reactive iron oxide minerals alone store 20% of OM in soil and sediments (Lalonde et al., 2012; Wagai & Mayer, 2007). The higher sorption capacity of short-range-ordered (SRO) iron oxide minerals compared to layered silicate clays, for instance, is an important feature of these minerals in biogeochemical cycles and the stabilization of SOM (Kaiser & Guggenberger, 2003). Although iron oxide minerals are considered to retain significant OM in soil, iron minerals are also redox-sensitive and this can impact its interaction with SOM. The resulting interaction between the Fe(III) and Fe(II) dictates the speciation, mobility, and reactivity of iron in the environment (Melton et al., 2014), which can ultimately impact the interaction of the Fe oxide minerals and the OM associated with them.

Natural organic matter (NOM) can associate with Fe minerals through adsorption and coprecipitation. Where an adsorption complex forms simply by the sorption of OM on pre-existing Fe oxides surface, the coprecipitation complex forms due to the formation of Fe oxide mineral in presence of dissolve organic carbon that incorporates in the mineral during its formation process. Coprecipitation is a common feature of redox fluctuation soil where the molar C/Fe ratio of soil pore water is 0.2 – 6 (Chen et al., 2014; Cheng et al., 2010; Katoh et al., 2004) and upon aeration Fe(II) quickly oxidized to insoluble Fe(III), which sorbs surrounding NOM and precipitates as a Fe oxide mineral-NOM coprecipitate (Cheng et al., 2010; Riedel et al., 2013). Compared to adsorption, coprecipitation is a more dominant feature of sediments (Henneberry et al., 2012; Katoh et al., 2004; Mikutta et al., 2014; Pokrovsky & Schott, 2002), retains more OC, and may provide stronger C stability (Chen et al., 2014). However, studies have also observed no difference in the bioavailability of adsorbed and coprecipitated C following microbial incubation (Eusterhues et al., 2014b).

Whether OC coprecipitated with an iron oxide mineral is "stable" is a matter of current debate as the release of OC can be triggered by both biotic, abiotic factors and also can change if the iron oxide minerals transform (Kleber et al., 2021; Lalonde et al., 2012). Changes in redox conditions can alter the behavior of iron oxide minerals, which can impact the availability of associated OC. For example, anoxic conditions can promote the reductive dissolution of ferric iron oxide minerals and this can result in substantial release of associated OC (Adhikari et al., 2016; Grybos et al., 2007; Grybos et al., 2009). Although several studies are examining the reductive release of OC from iron minerals, only a handful of studies have been conducted on OC availability under oxic conditions(Adhikari et al., 2019; Porras et al., 2018).

Aerobic respiration of mineral associated OM

Aerobic microbial respiration is the most thermodynamically favourable pathway for mineralizing soil organic carbon (SOC) to CO_2 (Lal, 2004, 2008) and adds around 60 Pg C y^{-1} to the atmosphere (Lal, 2004). As a majority portion of SOC is associated with the soil minerals, understanding the bioavailability of mineral associated OC is critical for understanding the global C cycle. (Kögel-Knabner et al., 2008; Mikutta et al., 2007; Porras et al., 2018). Thus far, only a few studies have directly investigated the bioavailability of OC from the mineral-SOM associations (Adhikari et al., 2019; Eusterhues et al., 2014a; Mikutta et al., 2006; Porras et al., 2018; Torn et al., 1997).

Among different factors enhancing the respiration of SOC, the labile source of OM tends to increase respiration by enhancing microbial growth (Fontaine et al., 2007; Porras et al., 2018; Wild et al., 2014). Fontaine et al. 2003, suggested that the fresh labile SOC can enhance microbial growth and increase the rate of SOC respiration through co-metabolism. However, the type of OM and different iron oxide minerals can have a different effects. For example, Mikutta et al. 2007,

found a 50 – 90% decrease in the decomposition of OM from forest floor extract over 90 days when sorbed to goethite, where other studies have shown 27.9% Ferrihydrite (Fh) associated fulvic acid and 4.2% Fh associated glucose respiration occurred under aerobic conditions (Adhikari et al., 2019). Porras et al. 2018, found less than 3% of the Fh-associated glucose was respired after 80 days. It is important to note that most of the studies examining Fh associated OC mineralization were conducted with glucose, fulvic acid or a single C compound containing OM. There is a knowledge gap regarding the bioavailability of OC from Fh-NOM coprecipitates that needs to be addressed.

Iron oxide minerals in the soil

Different types of iron oxide minerals can be present in the soil depending on the pedogenic condition favouring the formation mechanism of Fe^{III} oxide minerals. Due to their higher thermodynamic stability, goethite (Gt) and hematite (Hm) are the most common Fe-oxides in soil, especially in older soils, e.g. oxisols, and ultisols. Ferrihydrite (Fh) which is an excellent well studied short-ranged order (SRO) mineral is thermodynamic most unstable or metastable and lepidocrocite (Lp) is of intermediate stability. Despite the lower stability, SRO minerals are predominant in the younger soils characterizing the non-equilibrium state in the pedo-environment, which favours the formation of these minerals kinetically but hinders the transformation into more stable minerals by an association with adsorbed ions or molecules, such as phosphate and organics (Chesworth, 2007; Schwertmann & Taylor, 1989).

Formation of Iron oxide mineral in the soil

The formation of different iron oxide minerals in soil depends on the soil physicochemical condition. Gt mineral forms through either slow oxidation of Fe^{II} ions, or solid Fe^{II} compounds such as pyrite or siderite, or from Fh. For the formation of Hm, Fh is the precursor(Chesworth,

2007). Whereas, Gt forms from dissolved, partly hydrolyzed Fe^{III} ions (e.g., $Fe(OH)_2^+$) in solution by nucleation and crystal growth, Hm nucleates and grows within nano-sized Fh aggregates. The success of the formation of one mineral over another in this competing process of Gt and Hm formation is highly dependent on several factors especially temperature, water activity, pH and Al concentration. (Chesworth, 2007). Ferrihydrite minerals form due to quick aeration of Fe^{2+}containing soil water or the aeration occurs in presence of compounds with high affinity for Fe oxide surfaces such as organic matter, phosphate, silicate etc. These adsorbates inhibit the formation of more crystalline FeOOH forms or proper structural order and also retard the transformation into a more stable mineral. Ferrihydrites usually occur in cool climate temperate soil, especially in concretions, oxidation of horizons of glayed soils, Podzol B horizons, drains and ditches of lowland soil. As these soils are prone to waterlogged conditions, it can result in the redissolution of Ferrihydrite by reduction. Lp forms in soils through the oxidation of dissolved Fe^{2+} directly or via a green rust intermediate. It frequently occurs in non-calcareous redoximorphic soils, where Fe^{2+} is formed by biotic reduction. *Schwertmannite* forms only in the presence of high concentrations of sulfate and at very low pH. Magnetite in the soil is usually inherited from rocks, but a recent study reported pedogenic magnetite likely from the bacterial origin (Geiss et al., 2008). It results from the intracellular reaction of ferrihydrite with dissolved Fe^{2+} at ambient temperature and neutral pH. (Chesworth, 2007).

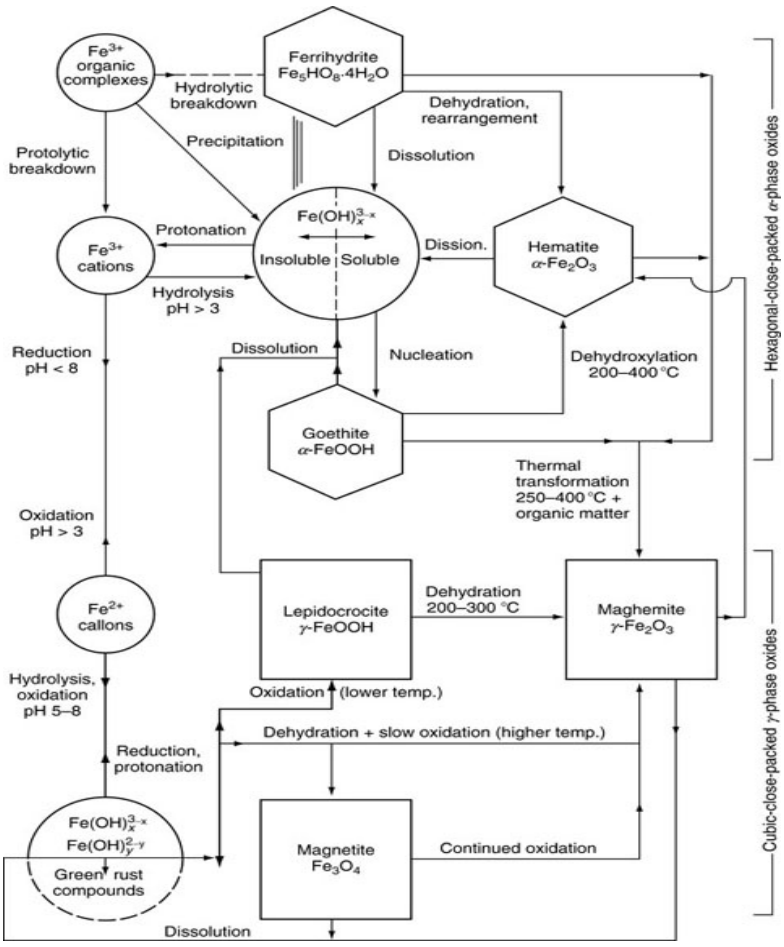

Figure 1.2: Common Pathways of iron oxide formation and transformation. (Source: (Chesworth, 2007))

Fe(II) catalyzed mineral transformation

The association of aqueous Fe^{2+} with iron oxides often leads to the transformation of less stable iron oxide minerals, such as Fh, into more stable phases, such as Hm and Gt (Hansel et al., 2003; Jang et al., 2003; Jeon et al., 2003), or to mixed-valence compounds such as green rust or Magnetite. Fh mineral transformation is thought to occur via classical Oswald ripening, where larger particles grow at the expense of smaller particles (Hiemstra, 2018; Hiemstra et al., 2019) and oriented aggregation, where nanoparticles rearrange themselves through Brownian motion to achieve a more stabilized structure (Li et al., 2012). The reducing capacity of Fe(II) induces

interfacial electron transfer to structural Fe(III) (Tronc et al., 1992; Williams & Scherer, 2004) and stimulates atom for atom dissolution and re-precipitation as a more thermodynamically stable phase (Cornell & Schneider, 1989), hence accelerating the transformation process often called Fe(II) catalyzed recrystallization (Jiang et al., 2014; Tronc et al., 1992). The reaction between the aqueous Fe(II) and Fe(III) oxides is extremely complex. Previously the reaction between the Fe(III) and Fe(II) was conceptualized as simply the adsorption of Fe(II) onto the surface of Fe(III) minerals (Coughlin & Stone, 1995; Sørensen & Thorling, 1991). But later application of Mössbauer spectroscopy helped to demonstrate electron transfer between the Fe(II) and Fe(III) minerals (Géhin et al., 2007; Williams & Scherer, 2004). ^{57}Mössbauer spectroscopy can only detect the ^{57}Fe isotope, making the other Fe isotopes, such as ^{56}Fe, transparent. The use of Fe isotopes (to differentiate between the structural Fe and Fe in the solution) and Mössbauer spectroscopy has proven the atom exchange process involved more than just the sorption and increased reduction potential of adsorbed Fe(II) (Zhou, 2018). Studies following these processes have shown that along with electron transfer and mineral transformation, atom exchange between the aqueous and solid phases can occur without visible mineral transformation. The outcome of Fe(II) catalyzed atom exchange on Fh minerals depends on multiple factors such as the Fe(II) concentration, pH, the presence of anion or other impurities, etc. (Boland et al., 2014; Chen et al., 2015; Hansel et al., 2005; Liu et al., 2008). In general, the Fe(II)/ Fe(III) ratio has a large influence, where the higher Fe(II) concentrations can lead to the formation of Gt and Mt, and lower concentration can result in Lp mineral formation (Boland et al., 2014; Hansel et al., 2005). Moreover, the presence of impurities such as chloride tends to favour Lp formation (Hansel et al., 2005; Liu et al., 2008). Atom exchange during the Fe(II) catalyzed Fe oxide recrystallization can also drive the re-arrangement or loss of co-precipitated elements and potentially organic matter

(Zhou et al., 2021). Studies have shown that the presence of organic carbon, both sorbed and coprecipitated with Fh does not influence the Fe atom exchange kinetics during the Fe (II) catalyzed recrystallization (Pasakarnis, 2013). In some instances, the presence of organic carbon was also found not to influence the rapid transformation of Fh to Lp, but it did end up stabilizing Lp and preventing its further transformation to Mt to Gt (Pasakarnis et al.). Another study showed that the amount of Fh transformation is indirectly related to the C/Fe ratios (Chen et al., 2015). Although it is clear that the presence of OM creates some sort of resistance towards the Fh mineral transformation, the mechanism behind this inhibition is unclear. In addition, most of the studies examining the Fe(II) catalyzed OC associated Fh mineral transformation were conducted using single organic ligands or relatively homogenous OM isolates (Daugherty et al., 2017; Royer, Burgos, Fisher, Jeon, et al., 2002). That raises the question that how the Fe(II) catalyzed the mineral transformation of Fh minerals will occur when it is associated with Natural Organic Matter (NOM).

Bacteriogenic Iron (oxyhydr) oxide (BIOS):

Bacteriogenic iron oxides (BIOS) are common in environments with strong redox gradients such as natural water, sediments, wetlands, groundwater etc. (Duckworth et al., 2009; Emerson & Weiss, 2004; Ferris, 2005; Weiss et al., 2004). In the redox gradient suboxic zone where high ferrous iron containing fluids meet oxygenated conditions such as groundwater seeps (Fleming et al., 2014; James & Ferris, 2004), wetland soils (Emerson & Weiss, 2004; Weiss et al., 2004) and in the rhizosphere Fe(II) oxidizes via both abiotic and biotic process (Druschel et al., 2008; Neubauer et al., 2007; Weiss et al., 2003; Weiss et al., 2007). Iron oxidizing bacteria can accelerate the Fe(II) oxidation process and stimulate the formation of ferric oxide co-precipitates with cell exudates and other forms of organic matter (Druschel et al., 2008). There is growing recognition

that the Fe(III) (oxyhydr) oxide minerals, especially Fh, prevails in BIOS that forms at redox gradients (Duckworth et al., 2009; Emerson, 2019; Emerson et al., 2010; Ferris, 2005). Most of our knowledge regarding the OC stability in Fh coprecipitates is based on abiotically synthesized Fh, but there are substantial structural differences between synthesized Fh-OM coprecipitates and BIOS. Compared to synthesized Fh-OM coprecipitates, BIOS has a lower crystallinity, a smaller crystal domain size, and a lower surface area. BIOS has an affinity for metal cations and oxyanions of arsenic and chromium (Cismasu et al., 2011; Kikuchi et al., 2019; Posth et al., 2010; Whitaker & Duckworth, 2018). Moreover, cell-derived OM is incorporated (2 – 5% OC) in BIOS (Muehe et al., 2013; Schmid et al., 2014; Sowers et al., 2017). Although it has been acknowledged that OM can be associated with BIOS, what is not known is the bioavailability of this OM.

OBJECTIVES

The iron oxide mineral associated with organic matter is considered to be less accessible for microbial degradation than other forms of OC. However, recent studies have illustrated that a broad set of interactions control organic matter stability associated with minerals. Such as, the mineral surface catalyzes organic reactions, electron transfer process occurs or reactive oxygen species generates from the mineral that can oxidize OM, compartmentalization of soil and sediments by mineral can create unique microsites that host diverse microbial communities, which interact with OM etc. (Kleber et al., 2021). These multiplicities of interactions indicate that "mineral associate OM is protected" is a highly simplistic general assumption of this complex system. Moreover, the redox-sensitive change of the iron oxide mineral-OM coprecipitates and its impact on the bioavailability of iron oxide mineral associated OM is yet to unveil.

Accordingly, the objectives of this study are:

(i) To measure the bioavailability of OC from Ferrihydrite-Suwanee river natural organic matter reacted with Fe(II) (Chapter 2).

(ii) To investigate the change in Ferrihydrite natural organic matter coprecipitate morphology and crystallinity following reaction with Fe(II) and ageing (Chapter 3).

(iii) To investigate the bioavailability of OC from Ferrihydrite natural organic matter coprecipitates after reacting with Fe(II) (Chapter 4).

(iv) Compare the bioavailability of OC from Bacteriogenic iron (oxyhydr) oxide (BIOS) with synthesized Fh-NOM coprecipitates, along with the release of heavy metal from the BIOS (Appendix A).

CHAPTER 2

Bioavailability of carbon from Suwannee river natural organic matter-ferrihydrite coprecipitates after reaction with Fe(II)

Noor, N., and A. Thompson. To be submitted to the Soil Science Society of America Journal.

ABSTRACT

The iron oxide mineral and organic matter (OM) association consider being a stabilization mechanism of OM in soil. In redox fluctuating conditions, the interaction of Fe(II) with Fe(III) in the iron oxide mineral result in mineral transformation, electron exchange or atom exchange which can impact the stability of the associated OM. To measure the bioavailability of the OM, Suwannee River natural organic matter-Ferrihydrite coprecipitates (SRNOM-Fh) was reacted with Fe(II) for 1,7, and 14 days and incubated under the oxic condition with soil microbial community. Additional ^{13}C labeled Na-lactate was also used to ensure the activity of the microbial community. We found that the 1 day Fe(II) reacted SRNOM-Fh protected 9±3% more of the coprecipitated C than the unreacted coprecipitate. For 7 and 14 days reacted coprecipitates no significant impact on the OM protection was observed. All the coprecipitates sorbed 1-2% of the added lactate regardless of the treatments. The mineralization of CO_2-C from the coprecipitates was low and a higher concentration of coprecipitated C was released in the solution. During the first few days of the incubation, around 10% of the lactate was mineralized by the microbial community and later they continued using the coprecipitated C as an energy source. This study suggests that under the oxic condition, the product of freshly Fe(II) reacted Fh-OM coprecipitate can introduce protection to the associated OM against biodegradation.

INTRODUCTION

Mineral association with organic matter (OM) is one of the major mechanisms stabilizing OM in the soil (Lehmann & Kleber, 2015; Schmidt et al., 2011) and comprises OM associations via chemical bonds to minerals and also OM that is physically protected by minerals in micro-aggregates or coprecipitates (Kleber et al., 2015; Kögel-Knabner et al., 2008). Short-range ordered

(SRO) minerals (e.g., allophane, ferrihydrite, nano-goethite, etc.) are often found in close association with OM owing to their high surface areas. The SRO iron (Fe) mineral ferrihydrite (Fh) is commonly studied as an index of various SRO-Fe phases found associated with OM. However, the soil Fe plays multiple roles in the ecosystem biogeochemistry (Chen et al., 2020) and among them, electron transfer or exchange can impact the fate of OM associated with Fh mineral.

Fe minerals can protect OM from extracellular enzymes and heterotrophic microbes by sorption and create structural protection during coprecipitation reactions (Kaiser & Guggenberger, 2003; Kleber et al., 2015; Oades, 1988; Totsche et al., 2018). But, when anoxic conditions occur, microbial use of Fe (III) as an electron acceptor results in the reductive dissolution of Fe(III) to Fe^{2+}(aq) (Lipson et al., 2010; Roden & Wetzel, 1996), which may release the associated OM in the Fe-OM coprecipitates or OM that was protected in the Fe(III) cemented micro-aggregates (Chen et al., 2020; De-Campos et al., 2012; Pan et al., 2016). Under oxic conditions, the oxidation of Fe(II) by O_2 can generate hydroxyl free radicals that can either mineralize OM to CO_2 or increase OM bioavailability (Hammel et al., 2002; Wood, 1994). Despite the complexity of Fe playing both a role in protecting OM (Gentsch et al., 2015; Mikutta et al., 2007; Porras et al., 2018) as well as promoting OM release and mineralization (Dubinsky et al., 2010; Huang & Hall, 2017), few studies have looked directly at the bioavailability of OM in Fe-OM associations via classic aerobic microbial respiration incubations (Adhikari et al., 2019; Porras et al., 2018).

When Fe oxide minerals, especially the metastable ones such as Fh and lepidocrocite (Lp), react with aqueous Fe(II) they undergo secondary mineralization and transform to more stable forms (Hansel et al., 2005; Pedersen et al., 2005). The more stable Fe minerals, such as goethite(Gt) and hematite (Hm), do not go through such transformation but forms Fe(III) coating on the mineral

surface due to electron transfer with Fe(II) or a stable sorbed Fe(II) phase (Catalano et al., 2010; Gorski & Scherer, 2011; Larese-Casanova & Scherer, 2007). The Fe(II) interaction with the Fe(III) in the mineral itself is a complex process and the presence of coprecipitated or adsorbed OM complicates the Fe mineral transformation process even complex as discussed in chapter- 3 and 4. The objective of this study is to determine the fate of OM associated with Fe oxide minerals that have gone through electron transfer and atom exchange in the presence of Fe(II), which has not yet been reported. To test this, we synthesized a Suwannee River natural organic matter-Ferrihydrite (SRNOM-Fh) coprecipitate with a C/Fe molar ratio of 1.2 and reacted it with Fe(II) under anoxic conditions for 1d, 7d and 14d in presence of PIPES buffer. Then the resulted products were incubated in presence of a soil microbial inoculum under oxic conditions in the presence of lactate and we measured the change in C content and also an evolution of CO_2. In a previous study Eusterhuse, et al., 2014a measured the mineralization of OM from Fh-OM coprecipitate with no labile C source where a very low amount of C utilization was observed from the coprecipitate especially when sulfonated lignin was used as OM source in the coprecipitate. This could result from a less active microbial community due to the lack of labile C source during the 68 days of incubation time. In soil, the microbial community can utilize different labile C sources that can keep them alive and active to work on the mineral associate C. Chen, et al., 2020 also showed that the use of added C during the incubation study increased the decomposition of native soil OC. To ensure the activity of the microbial community and also to imitate the natural soil condition we used lactate as a labile C source for the microbes. Moreover, ^{13}C labeled lactate was used to differentiate the coprecipitated C from the added lactate. We hypothesize that the interaction of Fe(II) with Fh-OM coprecipitates will increase the bioavailability of the OC.

MATERIALS AND METHODS

Organic matter- Ferrihydrite coprecipitate synthesis and characterization

Suwannee River natural organic matter (SRNOM) was purchased from the International Humic Substances Society (IHSS) and used without further treatment as an OM source to prepare the coprecipitates. Its C content was 50.7% and its functional group composition includes carboxyl, phenolic, aromatic and aliphatic functional groups at 11.2, 2.5, 23 and 27% respectively, as reported by IHSS (Compositions). To prepare SRNOM-Fh coprecipitate, required masses of SRNOM was dissolved in 1L of ultrapure 18.2 MΩ water at pH 9.0 under vigorous stirring. The solution pH was adjusted back to pH 7.0 and 1g ferric nitrate ($Fe(NO_3)_3.9H_2O$) was added to generate an initial molar C/Fe ratio of 1.2. The pH of the solution was readjusted at 7.5 with 1M KOH under stirring to produce SRNOM-Fh coprecipitate. Synthesized coprecipitates were centrifuged and washed with ultrapure 18.2 MΩ water twice and the final C content was measured using a Thermo Flash 2000 Elemental Analyzer. The solids were transferred into an anoxic glove box chamber filled with mixed gas (7% H_2, and 93% N_2) and dispersed in ultrapure water by sonication. The coprecipitates were used in slurry form within a few days after preparation. A detailed characterization of the coprecipitates including X-ray diffraction (XRD, Rigaku Mini Flex II), ^{57}Fe Mössbauer spectrometer (Web Research Inc., Edina, MN) equipped with a closed-cycle cryostat (CCS-850 System, Janis Research Co., Wilmington, MA), surface area measurement etc. were done and described in details in our previously published manuscript (Zhou et al., 2018). In the analysis, Fh was the only Fe mineral detected by XRD and Mössbauer spectroscopy. The specific surface area of freeze-dried SRNOM-Fh (C/Fe=1.2) coprecipitate was determined by N_2 adsorption BET analysis (Quantachrome Nova 1200) to be 15.5 $m^2\ g^{-1}$, which was smaller than pure ferrihydrite (269 $m^2\ g^{-1}$) but consistent with Fh in aggregated form based on prior published

studies (Chen & Sparks, 2018; Eusterhues et al., 2008). The presence of OM in association with Fh can result in a decreased surface area.

Secondary mineral transformation experiment

Natural isotopic abundance Fe(II) stock solution was made by dissolving Fe(0) in concentrated hydrochloric acid (Notini et al., 2018). The deionized water was degassed with N_2 over 2h and equilibrated in the glove box at least overnight before use. The SRNOM-Fh coprecipitate in 15mL of piperazine-N, N′-bis (ethanesulfonic acid) (PIPES) buffer (10 mM, pH 7.0) was reacted for 1d, 7d and 14d with 2mM Fe(II) in three different batches on an end-over-end shaker (Zhou et al., 2018) in an anaerobic glovebox chamber. The Coprecipitate solid loading rate was ~10 mM Fe(III) in the reactors. The resulting Fe(II) reacted coprecipitates were then centrifuged and washed with anoxic ultrapure water twice before analysis.

Carbon bioavailability measurement

To study the bioavailability of carbon from SRNOM-Fh coprecipitates after reacting with Fe(II), incubation studies were performed under oxic conditions for 26 d using SRNOM-Fh samples reacted with Fe (II) for either 1 d, 7 d, or 14 d at molar C/Fe ratio of 1.2 (along with associated Fe(II)-free controls). The microbial inoculum was extracted from freshly collected soil (0 to 15cm depth) from J. Phil Campbell Sr. Research and Education Center of the University of Georgia, Athens. Briefly, the inoculum was isolated by incubating the soil at 24 ºC for 7 d at 60% water holding capacity and then shaking it in a 4mM $CaCl_2$ solution for 24 h before passing the slurry through a 5 µm filter (Eusterhues et al., 2014b). A small amount (0.1 ml) of this inoculum was then transferred to a selective growth media containing (per liter): 0.5 g KH_2PO_4, 1.0 g $NaSO_4$, 2.0 g NH_4Cl, 0.5 mM $CaCl_2$, 0.1 mM $MgSO_4$, and ^{13}C labeled 1mM Na-lactate. The solution was placed inside the incubator on a rotatory shaker at 29º C overnight to target an exponential growth

phase of the microbial community (the target was an optical density reading minimum of 0.36 – 0.37 at 600 nm). The incubation studies were carried out in 30 ml opaque serum bottles containing 20 mg of coprecipitate, 15 ml of selective media, and microorganisms added at 2×10^8 cells ml^{-1}. 1mM ^{13}C labeled Na-lactate (98% enriched) in the selective growth media was used to ensure enough carbon for the survival of the microorganisms during the incubation period.

To investigate the difference in the bioavailability of OC from the SRNOM-Fh samples with and without Fe(II), four treatments with duplicates were conducted as follows: (1) SRNOM-Fh + Media + Microorganisms; (2) SRNOM-Fh reacted with Fe(II) + Media + Microorganisms; (3) Media + Microorganisms; (4) Only media. Here, treatment #3, 'Media + Microorganisms' and treatment #4, 'Only media' served as controls. With three different levels of SRNOM-Fh aging (1 d, 7d, 14 d aged) with or without reaction with Fe (II), a total of 16 parallel reactor bottles were set up in this experiment. The pH was maintained at 7 for all reactors. During the whole incubation period, the bottles were rotated on a rotatory shaker under a laminar flow hood under laboratory atmospheric conditions. To measure the emission of $CO_{2(g)}$ from each reactor, gas sampling was done at 1, 2, 3, 5, 7, 10, 13, 16, and 26 d from crimp sealed butyl rubber stoppers on the reactors. After finishing each sampling, the reactors were uncapped and kept open for at least six hours, to circulate the air from the atmosphere to the reactor bottles to reach an equilibrium. Then the reactors were crimp sealed with butyl rubber stoppers again and kept sealed until the next sampling date. Initial (time zero) sampling was also done from all the reactors. Gas samples were collected with gastight syringes and stored in pre-evacuated gas collection vials. The $CO_{2(g)}$ concentration was measured using LI -840A CO_2/H_2O gas analyzer and $^{13}CO_2$ concentration were measured using Picarro G2201-i isotope analyzer. The pH and the dissolved organic carbon (DOC) content after incubation were measured using a pH meter and Shimadzu TOC-500 analyzer. The total C

and ^{13}C isotope content of the solids before and after incubation were measured using a Thermo Flash 2000 Elemental Analyzer coupled to a Thermo Delta V Isotope Ratio Mass Spectrometer via the Thermo Conflo IV open split Interface.

Thermogravimetric analysis

To thermal stability of the SRNOM-Fh coprecipitate was assessed by thermal analysis using ramped combustion in the University of Pennsylvania lab. 6mg sample were heated to 105°C at 10°C min^{-1}, held at 105 °C for 15 minutes to dry and equilibrate the sample, then heated at 10°C min-1 to 800°C. Experiments were performed in an oxidizing atmosphere of 40 mL min-1 of CO_2-free synthetic air (20% O_2 and N_2 balance) using a Netzsch STA 449PC Jupiter simultaneous thermal analyzer equipped with an automatic sample carrier (ASC) and a type-S platinum/ rhodium (Pt/PtRh) sample carrier (Netzsch– Gerätebau GmbH, Selb, Germany). The gas outlet of the thermal analyzer was coupled to a LICOR LI-820 infrared gas analyzer (Licor Biosciences, Lincoln, NE) for evolved gas analysis of CO_2 during the ramped combustion. The thermal stability of the SRNOM-Fh coprecipitates was determined using the temperature at which the peak in CO_2 evolution occurred.

Data analysis

The amount of CO_2-C mineralized from the coprecipitates, as well as the per cent (%) contribution of added lactate to CO_2-C respiration, was calculated using a two-source mixing model.

The per cent contribution of added ^{13}C-lactate to CO_2 respiration (P $^{13}C_{\_lactate}$),

$$P^{13}C_{\text{lactate}} = \frac{x13[CO2]_{\_Fh-SRNOM} - x13[CO2]_{no\ lactate}}{x[13C]_{lactate} - x[13C]_{Fh-SRNOM}} * 100$$

Where, $x13[CO2]_{Fh-SRNOM}$ and $x13[CO2]_{no\ lactate}$ are atom fraction of ^{13}C of CO_2 respired from Fh-SRNOM coprecipitates reactor with added lactate and Fh-SRNOM coprecipitates reactor

without added lactate, respectively; x[13C]lactate and x[13C]Fh_SRNOM are the initial atom fraction of ^{13}C content of the lactate and Fh-NOM coprecipitate, respectively.

Statistical analysis

Statistical analysis was conducted between the Fe(II) reacted and unreacted coprecipitates using T-test in JPM software and excel.

RESULTS AND DISCUSSION

Change in solid-phase C content

SRNOM-Fh coprecipitates were reacted with Fe(II) for 1d, 7d and 14d under anoxic conditions along with the unreacted controls and later the products were incubated under oxic conditions with a microbial inoculum to measure the bioavailability of C. The before and after incubation solid sample C content (Figure 2.1, Table 2.1 and 2.2) suggest that the reaction of Fe(II) with the coprecipitate (in all treatments) reduced C degradation relative to the unreacted treatments, although these reductions were minor. For example, the SRNOM-Fh reacted with Fe(II) for 14 d lost 31±1 % of the coprecipitated C, whereas the unreacted control lost 35± 6 % (p value 0.49). For 7 day treatments these values were 32±1 % and 34±1 %, respectively and they were significantantly different (p value 0.05). In the 1d Fe(II) reacted SRNOM-Fh coprecipitate 31±2.0 % of the coprecipitated C was lost compared to 40±3.6 of the C lost in the unreacted control (p value 0.14), suggesting aging may offer additional protection against C degradation (Figure 2.1a and Table 2.1). Although the statistical analysis showed no significant differences in the Fe(II) reacted and unreacted controls of the 1d and 14 days treatments but the small amount of sample size and difference in the values suggest protection of the coprecipitated C in the Fe(II) reacted treatments, especially in case of 1d reacted treatment.

We used ^{13}C labeled lactate to distinguish between external C and the co-precipitate C during the incubation. The data suggest that the coprecipitates sorbed minor amounts of C from the solution regardless of the treatment i.e. this occurred in both the reacted and unreacted controls (Figure 2.1b, Table 2.2). There was no effect of reaction with Fe(II) on the amount of solid phase lactate accumulation (Table 2.2), with Fe(II) reacted and unreacted coprecipitates in all the treatments sorbing between 1.7 – 2% of ^{13}C-lactate. However, the buffer PIPES may have contributed to the sorbed C during the reaction with Fe(II) and this was not isotopically labeled and thus would not be distinguished from the co-precipitate C.

Coprecipitate characterization

To characterize the stability of C in SRNOM-Fh coprecipitates after reaction with Fe(II), we characterized SRNOM-Fh coprecipitates before and after Fe(II) reaction using thermal analysis during ramped combustion. We used the temperature where we saw the max CO_2 peaks as a guide for C thermal stability and found no C thermal stability change in SRNOM-Fh before and after Fe(II) reaction (Table 2.1). We further compared the C thermal stability in SRNOM-Fh with a C/Fe molar ratio of 0.8 where Fe(II) usually start the mineral transformation. The temperature where we observed max CO_2 peak increased after mineral transformation occurred, indicating the C thermal stability in SRNOM-Fh coprecipitates increased by Fh transformation.

CO_2-C Mineralization

Our result suggests that only a small amount of coprecipitated C (around 2%) was respired as CO_2 and the flux was higher during the first five days of incubation (Figure 2.2 and 2.3). The total CO_2-C respiration from the unreacted controls was a little higher than the Fe(II) reacted treatments (14d and 7d) except for the 1d reacted coprecipitates (Figure 2.3). For 14d Fe(II) reacted coprecipitate, the total CO_2-C respired was 800±19 μg g^{-1}, whereas it was 891μg g^{-1} for

unreacted controls. For the 7d treatments, the values were 733 µg g^{-1} and 756 µg g^{-1} for the reacted and unreacted, respectively. In the 1d Fe(II) reacted SRNOM-Fh reactor the total CO_2-C respired was 667±134

µg g^{-1} and in the unreacted controls it was 442±67 µg g^{-1}. The control reactor vial with the media and microbial inoculum had higher CO_2-C respiration than all our treatments indicating that the microbial inoculums were alive and well active.

The per cent contribution of added lactate to CO_2-C respiration indicates around 7 to 10% of the added lactate was respired as CO_2-C in different treatments (Figure 2.2). The microbial inoculums were grown in the ^{13}C-lactate containing media before adding to the incubation experiment. In our experiment, we have observed only 7.4 % of the total CO_2 respired from the "Media with inoculum" control. This indicates inspite of our best effort the microbes were not fully labeled and also during the incubation study under the oxic condition the ambient microbes might have interacted with the media in the reactors.

The $^{13}CO_2$-C respiration occurred only during the first 3 to 5 days of the incubation and later no such respiration occurred. This suggests that the microbial community used the added lactate during the first 5 days of the incubation. Moreover, for both the 14d and 1d reacted coprecipitate, the total CO_2-C respired from added lactate in the Fe(II) reacted treatments was higher i.e. 10 µg g^{-1} (for both) than the unreacted coprecipitates i.e. 7 µg g^{-1} and 4 µg g^{-1} respectively. This could indicate that the reaction of Fe(II) with the coprecipitate offered some protection for the coprecipitated C, which biased the microbial community to further prefer the lactate as their energy or C source initially. Unfortunately, the CO_2-C respiration data from the 7d reacted treatments got contaminated and we cannot come to any conclusion regarding that treatment.

From solid C measurements, a decrease in the C content after incubation in all treatments was seen, but not much of this released C was emitted as CO_2. The total DOC measurement data and the mass balance calculation indicated that 30-65% of the coprecipitated C that was released from the coprecipitates during incubation remained in the solution rather than emission as CO_2 (Table 2.3, Figure 2.4).

In our previous study (Zhou et al., 2018) we have conducted a detailed examination regarding the changes that occurred in the SRNOM-Fh C/Fe 1.2 coprecipitate after reacting with Fe(II). The SRNOM-Fh coprecipitate after reacting with Fe(II) for 14d showed no transformation into secondary mineral where Fh coprecipitated with humic acid transformed into Gt. Although the complete mineral transformation was not observed in the SRNOM-Fh coprecipitates after reaction with Fe(II), the Mössbauer spectroscopic temperature profile revealed that the blocking temperature for Fe(II) reacted SRNOM-Fh was higher than the SRNOM-Fh coprecipitate aged in the buffer solution without the Fe(II). This is consistent with an increased crystallinity, particle size or particle aggregation through particle-particle magnetic interactions (Berquó et al., 2007; Berquó et al., 2009). Moreover, Fe atom exchange and electron transfer between the structural Fe(III) and the Fe(II) in the solution was also observed.

To get a better understanding of the change in the coprecipitate after reacting with Fe(II) the thermal stability of the SRNOM-Fh coprecipitate (Table 2.4) following Thermogravimetric analysis (TGA) (Plante et al., 2009) was also measured. The result showed no difference in the maximum CO_2 peak temperature suggesting that there is no difference in the stability of C in the Fe(II) reacted SRNOM-Fh C/Fe 1.2 coprecipitate and the unreacted SRNOM-Fh coprecipitate. To compare this data with a lower C/Fe molar ratio 0.8 coprecipitate both Fe(II) reacted and unreacted were also analyzed following the TGA method, which showed increased thermal stability with

coprecipitate reacted with Fe(II) compared to the unreacted coprecipitate. This suggested that the increasing C content may have prevented the transformation after reacting with Fe(II) resulted in no increased thermal stability of the coprecipitate.

A few studies have been conducted before focusing on the bioavailability of C from Fe-OM coprecipitates under oxic conditions (Adhikari et al., 2019; Eusterhues et al., 2014b; Porras et al., 2018). Eusterhues et al. 2014 (Eusterhues et al., 2014b) found that the microbial community could not immediately mineralized organo-mineral associated C but needed adaptation before starting slow degradation. Another study showed that the Fh bound organic compounds had lower bioavailability than the free organic compounds and the glucose bioavailability was lesser than the bioavailability of Fulvic acid (Adhikari et al., 2019). In our study, we have observed that the microbial inoculum used the lactate only first three to five days of the incubation along with the coprecipitate C and later used the coprecipitated C as their C source

Overall, this study suggests that SRNOM-Fh coprecipitates with a C/Fe molar ratio of 1.2 after reacting with Fe(II) has the potential to increase the stability of coprecipitated C. But it is also important to notify that the difference between the Fe (II) reacted and unreacted coprecipitate was very negligible. This could be due to a lack of wholesale secondary mineral transformation, although the Mössbauer data reveals the SRNOM-Fh coprecipitate increases crystallinity after reaction with Fe(II) and that could be the cause of seeing some differences in C stability in the reacted coprecipitate compared to the unreacted coprecipitate.

CONCLUSION

This study demonstrated that the product of Fe(II) reacted SRNOM-Fh coprecipitates with a C/Fe ratio of 1.2 can increase the stability of coprecipitated C by reducing biodegradation. This

effect is more prominent in the freshly Fe(II) reacted coprecipitates. The previous study has suggested that the Fh mineral can protect its associated C from biodegradation (Adhikari et al., 2019) and our study emphasizes that this effect can be more prominent after the coprecipitates went through Fe(II) reaction. Moreover, we also suggest the use of some labile form of C as the initial food source for the microbial community during the incubation study as we have seen around 10% of the added lactate being used in the first few days of the incubation and later the inoculum continued using the coprecipitated C as their food source. This initial use of the available labile C source ensured the activity of the microbial inoculum during the incubation that has previously been not observed (Eusterhues et al., 2014a). In the natural environment, the Fh-OM coprecipitate under reducing conditions can react with the Fe(II) which can result in the mineral transformation, electron exchange, atom exchange between Fe(III) and Fe(II) (Zhou et al., 2018). Our study demonstrated that even without complete mineral transformation the freshly Fe(II) reacted coprecipitate can retain more associated C in the soil following an oxic condition. Although this is a highly complex process and the reaction time, C/Fe ratio, pH, types of organic matter etc. can change this scenario.

TABLES AND FIGURES

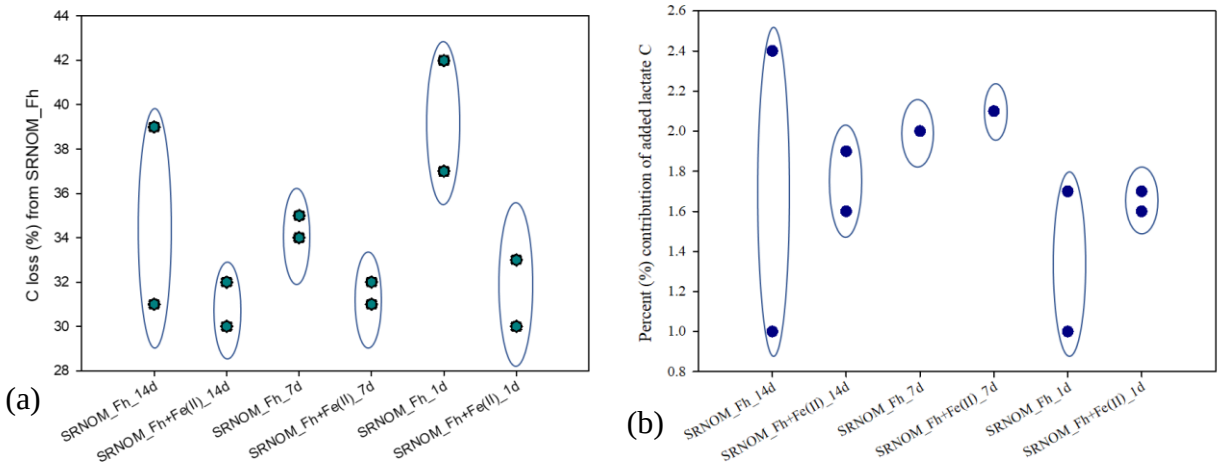

Figure 2.1: (a)Percent (%) loss of C from the SRNOM-Fh solids during incubation(b) Percent (%) contribution of added lactate C sorbed on the coprecipitate. This calculation was done following a two-source mixing model. The two points for the same treatment represent replications in both graphs.

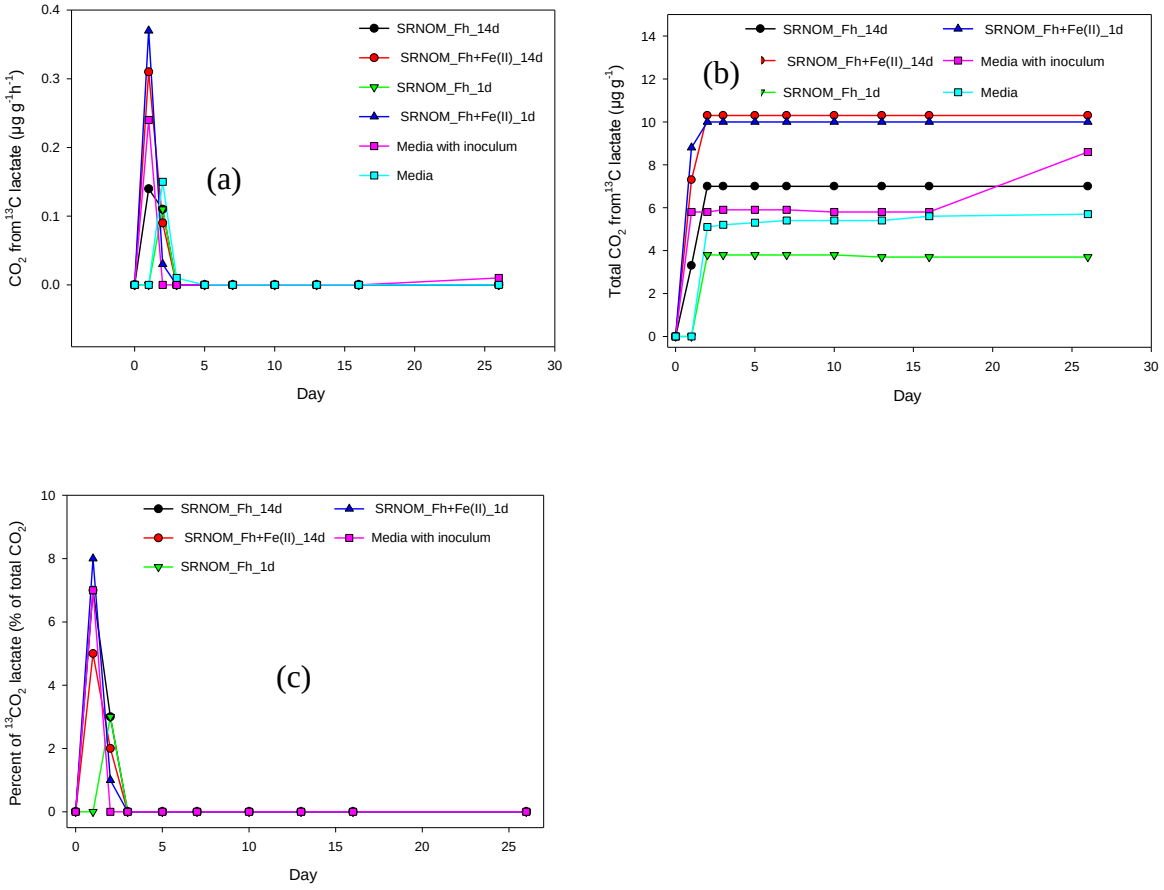

Figure 2.2: (a) CO_2-C (µg g^{-1} h^{-1}) respiration from added lactate; (b) cumulative CO_2 respiration from added lactate and (c) Percent contribution of CO_2-C from added lactate to total CO_2 respiration.

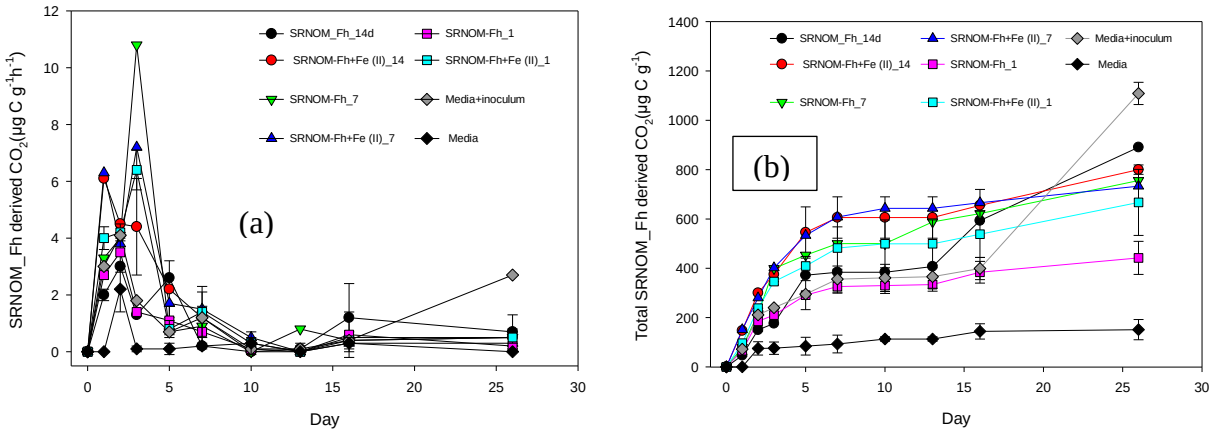

Figure 2.3: (a) CO_2-C respiration from SRNOM-Fh coprecipitate (b) Cumulative CO_2-C respiration from SRNOM-Fh. The CO_2-C respiration from the Media and Media+ inoculum treatments are also added to this graph for comparison purposes. The error bars indicate standard deviation between replicates.

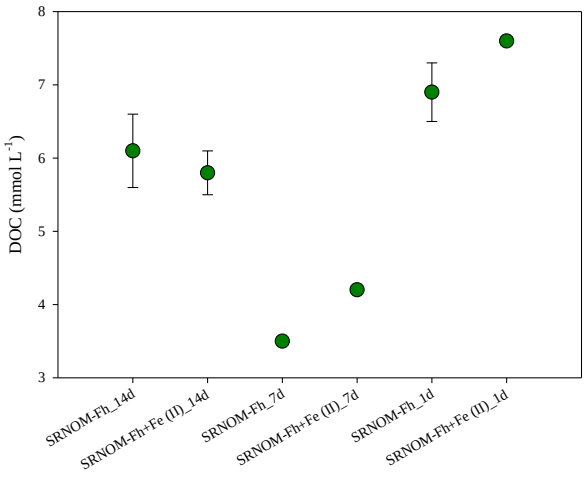

Figure 2.4: DOC (mmol L^{-1}) concentration in the reactors after incubation. This indicates that higher DOC was remained in the 1d treatment reactors after incubation compared to the 14 and 7days treatments reactors. The error bars indicate the standard deviation between replicates.

Table 2.1: Change in C content in the SRNOM-Fh coprecipitates during incubation.

Treatment	Replication	Before (mmol C /g soil)	After (mmol C/g solid)	% loss of C from SRNOM-Fh	Average % loss of C from SRNOM-Fh
SRNOM_Fh_14d	Rep 1	8.3	5.0	39	35±5.6
	Rep 2	8.3	5.7	31	
SRNOM_Fh+Fe(II)_14d	Rep 1	7.8	5.3	32	31±1.2
	Rep 2	7.8	5.4	30	
SRNOM_Fh_7d	Rep 1	8.4	5.6	34	34±0.8 [a]
	Rep 2	8.6	5.6	35	
SRNOM_Fh+Fe(II)_7d	Rep 1	7.7	5.3	32	32±0.5[a]
	Rep 2	7.7	5.3	31	
SRNOM_Fh_1d	Rep 1	8.5	4.9	42	40±3.6
	Rep 2	8.5	5.3	37	
SRNOM_Fh + Fe(II)_1d	Rep 1	8.1	5.7	30	31±2.0
	Rep 2	8.2	5.5	33	

[a] = indicates a significant difference.

Table 2.2: Percent (%) contribution of added lactate in the SRNOM-Fh during incubation

Treatment	Replication	% contribution of added lactate C in the solid	Average
SRNOM_Fh_14d	Rep 1	1.0	1.7±1.0
	Rep 2	2.4	
SRNOM_Fh+Fe(II)_14d	Rep 1	1.6	1.8 ±0.2
	Rep 2	1.9	
SRNOM_Fh_7d	Rep 1	2.0	2.0±0.0
	Rep 2	2.0	
SRNOM_Fh+Fe(II)_7d	Rep 1	2.1	2.1±0.0
	Rep 2	2.1	
SRNOM_Fh_1d	Rep 1	1.0	1.3±0.5
	Rep 2	1.7	
SRNOM_Fh+Fe(II)_1d	Rep 1	1.6	1.7±0.0
	Rep 2	1.7	

Table 2.3: Mass balance calculation for total C content (mg) in each reactor containing 20mg of coprecipitates in 15ml of media, Initial and after incubation study.

Treatment	Initial			After			
	C content	Media+ Inoculum	Total	C content	CO_2-C release	DOC	Total
SRNOM_Fh_14d	1.98	0.23	2.2	1.22	0.015	1.1	2.4
SRNOM_Fh_14d	1.99	0.23	2.2	1.41	0.013	1.0	2.5
SRNOM_Fh+Fe(II)_14d	1.87	0.23	2.1	1.30	0.016	1.1	2.4
SRNOM_Fh+Fe(II)_14d	1.86	0.23	2.1	1.33	0.016	1.0	2.4
SRNOM_Fh_7d	2.03	0.23	2.3	1.37	0.015	0.6	2.0
SRNOM_Fh_7d	2.06	0.23	2.3	-			-
SRNOM_Fh+Fe(II)_7d	1.86	0.23	2.1	1.29	0.015	0.8	2.1
SRNOM_Fh+Fe(II)_7d	1.84	0.23	2.1	-			-
SRNOM_Fh_1d	2.04	0.23	2.3	1.19	0.008	1.3	2.5
SRNOM_Fh_1d	2.04	0.23	2.3	1.30	0.010	1.2	2.5
SRNOM_Fh+Fe(II)_1d	1.94	0.23	2.2	1.39	0.012	1.4	2.8
SRNOM_Fh+Fe(II)_1d	1.96	0.23	2.2	1.34	0.015	1.4	2.7

Table 2.4. The temperature at which max CO_2 peak was measured in SRNOM-Fh coprecipitates

Sample Information	Max CO_2 peak (°C)
SRNOM-Fh (C/Fe = 1.2)	289
SRNOM-Fh (C/Fe = 1.2) with Fe^{2+}	287
SRNOM-Fh (C/Fe = 0.8)	289
SRNOM-Fh (C/Fe = 0.8) with $Fe^{(II)}$	295

CHAPTER 3

Localized Alteration of Ferrihydrite Natural Organic Matter Coprecipitates Following Reaction with Fe(II)

Noor, N., and A. Thompson. Submitted to Soil Science Society of America Journal (special issue), June 30, 2021.

ABSTRACT

Coprecipitation of natural organic matter (NOM) with Ferrihydrite (Fh) can alter the trajectory of Fe(II) catalyzed transformation. High C/Fe molar ratio Fh-NOM coprecipitates are expected to resist transformation completely and preserve OM. However, most studies have examined this using only single organic compounds. To explore how heterogeneous NOM would influence this process, we reacted Low (0.8) and High (1.8) C/Fe molar ratio Fh-NOM coprecipitates (synthesized with a ^{13}C-labeled plant litter extract) with 2 mM Fe(II) for 1 and 14 days under anoxic conditions and examined changes in the solid phase with Mössbauer spectroscopy (MB) and ultrahigh-resolution scanning transmission electron microscopy (STEM). We found Fe(II) reaction drove localized increases in Fh crystallinity accompanied by partial expulsion of NOM from the coprecipitates. Higher initial solid phase C/Fe ratios forestalled this transformation but did not prevent it completely. STEM images of the Low C/Fe coprecipitate revealed localized lepidocrocite-like phases after only 1 day of reaction with Fe(II), whereas no changes were observed for the High C/Fe until 14 days when these phases had lost significant NOM (C/Fe ratio decreased to 0.7). MB spectra corroborate the STEM findings revealing increases in coprecipitate crystallinity. Fe(II) reaction stimulated the partial exchange of coprecipitate ^{13}C-NOM for the organic PIPES buffer, suggesting coprecipitate OM composition may evolve over time, especially when exposed to Fe(II). Our findings suggest that Fe(II) mediated Fh-NOM transformation is highly dynamic and has the potential to influence the stability of NOM in Fh even at higher C/Fe ratios.

INTRODUCTION

Ferrihydrite (Fh) is a common short-range-ordered (SRO) Fe(III) phase in soils and sediments (Cornell & Schwertmann, 2003; Jambor & Dutrizac, 1998). Fh is thermodynamically unstable and will transform into more stable iron (oxyhydr)oxide minerals such as goethite, hematite, magnetite, and lepidocrocite over time (Kukkadapu et al., 2003; Schwertmann & Murad, 1983). The sorption of $Fe(II)_{(aq)}$ to Fh accelerates this transformation through a process of electron transfer and atom exchange (Boland et al., 2014; Hansel et al., 2005; Pedersen et al., 2005; Williams & Scherer, 2004). Although many studies have examined Fe(II) catalyzed the transformation of Fh, there is no consensus regarding the transformation/crystallization pathway to product minerals (Boland et al., 2014; Hansel et al., 2005) as minor changes in the geochemical conditions such as pH, $Fe(II)_{(aq)}$ concentration, the presence of cations and counterions, and organic ligands can alter the composition of the secondary minerals (Boland et al., 2014; Chen et al., 2015; Hansel et al., 2005; Jones et al., 2009; Liu et al., 2016; ThomasArrigo et al., 2018; ThomasArrigo et al., 2019; Zhou et al., 2018).

During Fe(II) catalyzed recrystallization, the concentration of solid associated (sorbate) Fe(II) are major factors for the formation of secondary minerals (Chen et al., 2015). For example, lower sorbate Fe(II) concentrations can lead to lepidocrocite (Lp) formation whereas higher sorbate Fe(II) can lead to goethite (Gt) (Boland et al., 2014). Ferrihydrite, due to its higher available surface area, can adsorb more Fe(II) than Gt which facilitates the complete transform into secondary minerals within less than 3 d, whereas it often takes more than 7 d for Gt transformation to occur (Pedersen et al., 2005). However, in the natural environment especially in biologically active soils and sediments that have dissolved organic matter (OM) Fh is typically coprecipitated with natural organic matter (NOM) (Chen et al., 2014; Lalonde et al., 2012). Association of OC

can decrease Fh's available surface area and also block the adsorption of Fe(II) (Chen et al., 2014; Eusterhues et al., 2008; Jones et al., 2009). A coprecipitate C/Fe molar ratio greater than 2.8 is likely to result in complete blockage of the adsorption sites and prevent Fe(II) adsorption in mineral surface (Chen et al., 2014) and the threshold value to prevent transformation is 1.6 (Chen et al., 2015). Despite a consensus that OM can interfere with Fe(II) mediated Fh transformation, significant uncertainty remains regarding the specific interactions (Chen et al., 2015; ThomasArrigo et al., 2018; ThomasArrigo et al., 2019; Zhou et al., 2018). For example, some studies report coprecipitated OM retards Fh transformation progressively with increasing C/Fe molar ratios and secondary mineral formation dependent on Fe(II) concentrations (Chen et al., 2015), whereas other studies suggest longer reaction times and higher Fe(II) concentrations can cause Fh-OM transformation even when the initial C/Fe molar ratios are above 1.6 (ThomasArrigo et al., 2018). While, it is well accepted that various organic functional groups can drive transformations in consistent trajectories (Sheng et al., 2020; ThomasArrigo et al., 2019), our understanding of how Fh-OM coprecipitates behave when exposed to Fe(II) is largely based on experiments with single organic ligands or relatively homogenous OM isolates (Daugherty et al., 2017; Royer, Burgos, Fisher, Unz, et al., 2002). It remains unclear how Fh-NOM coprecipitates with more complex OM profiles will behave. In our previous study, we found that the reaction of Fe(II) with Fh coprecipitated with Suwannee River natural organic matter (SRNOM) resulted in electron exchange between the $Fe(II)_{(aq)}$ and Fe(III) and some minor increases in the Fe phase crystallinity, increased particle size, and aggregation (Zhou et al., 2018). Another recent study showed that Fh-SRNOM coprecipitates went through an electron exchange process after reacting with Fe(II) without secondary mineral transformation, but decreased their ability to retain nickel (Ni) (Zhou et al., 2021). These findings make it clear that changes are occurring in the Fh-NOM

coprecipitates during reaction with Fe(II) that affect Fh behavior. There is, however, considerable uncertainty on how those changes will manifest for more complex OMs. The majority of this uncertainty arises from experiments using various types of NOM as a C source for the coprecipitates. Resolving the Fe(II) mediated mineral transformation of Fh-NOM is critical for predicting the long-term impact of OM on the mineral binding of various constituents of interest. To address this, we examined the effects of NOM concentration and Fe(II) exposure (aging) time on NOM and Fe composition of Fh-NOM co-precipitates. We hypothesized that the C/Fe ratio and Fe(II) exposure time will govern the transformation product composition. To test this, we synthesized Fh-NOM coprecipitates at Low and High C/Fe ratios that based on prior literature should promote and hinder Fh transformation, respectively. Furthermore, we used ^{13}C-NOM (extracted from ^{13}C-Bermudagrass) as the source of C in the co-precipitates to distinguish co-precipitated NOM from the organic PIPES buffer in the media. Along with the elemental analysis of the co-precipitates before and after reacting with Fe(II), we examined the solids using Mössbauer spectroscopy and Ultra-high-resolution scanning transmission electron microscopy (STEM).

MATERIALS AND METHODS

Preparation of ^{13}C labeled DOM

Labeled dissolved organic matter (DOM) was prepared by extracting ^{13}C labeled Bermudagrass litter with water. Briefly, a pulse labeling method was used to label Tifton-85 bermudagrass (*Cynodon dactylon x Cynodon nlemfuencis*) with $^{13}CO_2$ (99.999 atom%, Cambridge Isotope Laboratories Inc.). Bermudagrass was grown in flats of C-free sand with some residual potting medium under greenhouse conditions for four weeks. All flats were fertilized with 0.7

mmol $(^{15}NH_4)_2SO_4$ once a week. For ^{13}C pulse labelling, bermudagrass was transported to a Conviron growth chamber with a temperature of 35°C and CO_2 concentration of 500 ppm maintained using a Qubit G400-2 gas mixing system coupled with a S157 infrared CO_2 analyzer (Kingston, Ontario, CA). Pulse labelling was carried out once a week for 6 weeks. Bermudagrass was exposed to $^{13}CO_2$ for 8 h with a flow rate of $^{13}CO_2$ approximately 0.5 L min^{-1}. Labeled above ground biomass was harvested and immediately frozen. The frozen material was freeze-dried and ground using Wiley mill to <1 mm. Ground materials were mixed with ultrapure 18.2 MΩ water with a solid to water ratio of 1/20 (w/v). The mixture was shaken at 140 rpm in a horizontal shaker for 48 h and filtered through a 0.45 μm polyvinylidene fluoride membrane filter. The total organic carbon concentration and ^{13}C isotope content was measured and later diluted with ultrapure water to achieve the required concentration to prepare the coprecipitates. Molecular composition characterization of dissolved NOM was done using Fourier transform ion cyclotron resonance spectroscopy (FTICR). The NOM was comprised predominantly of lignin-derived molecules and aliphatic compounds (according to the Van Krevelen diagram) with mean population O/C and H/C values of 0.2±0.08 and 1.5±0.3, respectively (SI Figure 6). Detailed information regarding the DOC extracted from similar material is available elsewhere (Chen et al., 2020). Here an O/C ratio around 0.2 was considered to identify as Lingin derived material but literature also considered an O/C ratio around 0.4 to identify Lingin derived formulae (Kim et al., 2003). Although we used the Van Krevelen space diagram but lately this diagram being avoided to show FTICRMS data with chemical classes (Koch & Dittmar, 2006; Šantl-Temkiv et al., 2013)as it does not ensures the structure and there can be discrepancies regarding the data interpretation.

Ferrihydrite (Fh) and Ferrihydrite-Natural organic matter (Fh-NOM) coprecipitates synthesis

All the chemicals used in this study were laboratory grade. Ferrihydrite was synthesized by dissolving $Fe(NO_3)_3.9H_2O$ in ultrapure water and pH was adjusted to 7 using 1M KOH (Schwertmann & Cornell, 2008). Fh-NOM coprecipitates with an initial solution C/Fe molar ratio of 0.8 or 1.8 were prepared by following the methods described by Chen et al. (Chen et al., 2014). Briefly, the required amount of $Fe(NO_3)_3.9H_2O$ was mixed with labeled ^{13}DOC solution under vigorous stirring. The pH of the suspension was raised from ~2.0 to 7 by slowly adding 0.1 M KOH. Synthesized Fh and Fh-NOM coprecipitate were centrifuged at 10,000 rpm for 10 min and washed twice using degassed ultrapure water and stored in the glove box (97% N_2 and 3% H_2) for at least 48 h to remove O_2 gas before reacting with Fe(II) in our experiments as described below.

Reacting Fh-NOM coprecipitates with Fe(II)

Freshly-synthesized, moist Fh and Fh-NOM coprecipitate were resuspended in anoxic PIPES (1,4-piperazinediethanesulfonic acid) buffer (10 mM, pH 7) and stirred for 1 d inside the glovebox (filled with 97% N_2 and 3% H_2) to remove residual O_2. A portion of the Fh and Fh-NOM coprecipitates were reacted with Fe(II) in 100 ml opaque serum bottles containing 33.6 mg of total Fe (as an Fh-NOM slurry) and 60 mL of anoxic PIPES buffer (10 mM, pH 7). $FeSO_4.7\ H_2O$ was added to the bottle (except the controls) to obtain a final Fe(II) concentration of 2 mM (Chen et al., 2015). The reaction was carried out in the anoxic glove box on a rotatory shaker in two batches: one reacted with Fe(II) for 24 h (henceforth "Fresh"); one reacted for 14 days (henceforth "Aged"). After the reactions, the Fe(II)-reacted Fh and Fh-NOM samples were rinsed with degassed 18.2 MΩ ultrapure water twice by centrifuging them at 10,000 rpm for 10 min. After washing the

samples, a small amount of degassed water was added to maintain a moist slurry and the samples were stored at -20 °C before analysis.

Analysis for ^{13}C, total C and Fe in the solid

The total C and ^{13}C isotope content of the solid phase were measured by lyophilizing a portion of the solid sample, crimped in a tin capsule, and analyzing it in a Thermo Flash 2000 Elemental Analyzer coupled to a Thermo Delta V Isotope Ratio Mass Spectrometer via the Thermo Conflo IV open split Interface. The total Fe content was measured using inductively coupled plasma mass spectrometry (ICP-MS, Perkin Elmer, Elan 9000) after the dissolution of 2 mg coprecipitates in 5 ml 30% HCl for 1hr and volume up to 30 ml with 1% HCl (Chen et al., 2014). We calculated the amount of ^{13}C-natural organic matter in the solid samples (P ^{13}C-NOM in solid) using a two-source mixing model.

$$P13\mathrm{C_{NOM}}\text{in solid} = \frac{\mathrm{x[13C]Fh\_NOM} - \mathrm{x[13C]}Fh}{\mathrm{x[13C]NOM} - \mathrm{x[13C]Fh}} * 100$$

where $\mathrm{x[13C]Fh_{\_NOM}}$ and $\mathrm{x[13C]Fh}$ are atom fraction of ^{13}C isotope in the coprecipitates and ^{13}C content of the Fh, respectively; $\mathrm{x[13C]NOM}$ is the initial atom fraction of ^{13}C content of the bermudagrass extract.

Mössbauer analysis

Mössbauer analysis (MB) was done using a 50-mCi ^{57}Co/Rh source under 5 K, 13 K, and 35 K (RT) to characterize Fe in the coprecipitates after reacting with Fe(II) along with the unreacted controls. Collected solid samples were washed twice with ultrapure water by placing the samples in a falcon centrifuge tube with a sufficient amount of water following gentle shaking and centrifuged at 3000g for 10 min. The supernatant was then poured off, the samples were placed in an O-ring and sealed between two pieces of Kapton tape, and immediately frozen in a −20 °C freezer. MB was analyzed using Recoil software and spectra fitting was done using Voigt-based

fitting (VBF). In addition, mass-specific magnetic susceptibility (MS) measurement was collected on coprecipitates at 295K in a Bartington magnetic susceptibility meter (MS2B). Measurements were calibrated against a well-characterized standard set used previously (Thompson et al., 2011).

Scanning transmission electron microscopic images (STEM)

STEM images were obtained using an ultra-high resolution scanning transmission electron microscopy (STEM-Hitachi SU 9000EA) with a resolution of 0.4 nm and operated at 30 kV. The solid sample slurry was placed on a silica chip and dried overnight, which was later analyzed under the microscope. A secondary electron detector was used for collecting the images and EDS spectra were recorded with Oxford Ultim Extreme software.

RESULTS

Total Fe and C content of the coprecipitates

Total Fe, C and ^{13}C isotope i.e. coprecipitated C contents were measured in the solids before and after reaction with Fe(II) (Table 3.1). In the Fresh samples, all treatments and unreacted controls retained nearly their initial measured C/Fe ratios of either 0.8 and 1.8, for the Low and High treatments, respectively. However, in the Aged samples, the C/Fe molar ratios decreased. For the Aged Low coprecipitates, the C/Fe molar ratio decreased from 0.8 to 0.5 and for the Aged High coprecipitates it decreased from 1.8 to 0.7. Interestingly, Fe(II) reaction drove up the total C content of the Fresh and Aged Low coprecipitates relative to the unreacted controls, although the Fe(II) reacted coprecipitates lost more ^{13}C NOM at the expense of unlabeled OC from the media than their paired unreacted controls. For instance, the OC in the Fe(II)-reacted Fresh-Low coprecipitate was comprised of 64% NOM, whereas the unreacted pared control was comprised of 88% NOM. For the Aged co-precipitates, which also experienced a decrease in C/Fe ratio, the loss

of NOM fraction was even greater, with the Aged Low coprecipitates comprising 34% NOM after reaction with Fe(II) compared to 56% NOM in its unreacted control. The High C/Fe treatments had similar trends, although the relative fractions of NOM after reaction were greater (Table 3.1). Finally, our pure Fh controls gained some OC after 1d and 14d of aging and the values were higher than the Fe(II) reacted Fh. The PIPES buffer could be the source of C although we did not see any change in the pH content of the reactors. This increased C content did not appear to influence the transformation of Fh, which was complete after 1 d (Figure B.5). This measured OC may also have been an experimental or analytical contaminant.

Changes in Fh-NOM Crystallinity and Morphology

Mössbauer spectroscopy

Mössbauer spectra (MB) collected at 35K, 13K and 5K were used to characterize changes in the crystallinity of the Fe(II)-reacted coprecipitates relative to the unreacted controls. At the lowest collection temperature (5K), the Fe(III) populations of all the samples were magnetically ordered into a sextet (Figure 3.5 and 3.6). Portions of the sample forming a sextet at higher temperatures (13K and 35K) are more crystalline than the remaining portions that require lower temperatures to magnetically order and this can be used to compare the relative crystallinity of the Fh-NOM coprecipitates (Thompson et al., 2006; Thompson et al., 2011).

Reaction with Fe(II) increased the crystallinity of the coprecipitates in all the treatments relative to the paired unreacted controls (Figure 3.5 and 3.6). For example, the emerging sextet for the Fe(II) reacted Fresh Low coprecipitate (Figure 3.5 a, b) is sharper at 13K than sextet for the unreacted control, indicating a greater crystallinity. For the Aged Low coprecipitates, (Figure 3.5 c, d) sextet development starts at a higher temperature (i.e. 35K) and already becomes fully developed at 13K, indicating the Low coprecipitates crystallinity increases with Fe(II) aging time.

The High C/Fe coprecipitates follow a similar trend (Figure 3.6), although the degree of crystallinity increase is much less than the Low C/Fe coprecipitates or the C-free Fh control (Figure 3.5 a, c and Figure 3.6 a, c). Thus, the C/Fe ratio appears to govern the degree of crystallinity increase upon reaction with Fe(II), likely by hindering crystal ripening as shown previously (Eusterhues et al., 2008; Mikutta, 2011; Schwertmann et al., 2005).

Scanning Transmission Electron Microscopy (STEM)

Scanning transmission electron microscopy (STEM) images of the unreacted and Fe (II) reacted coprecipitates along with EDS mappings (Figure 3.1- 3.4, Figure B.1- B.5) illustrate the variation in the crystallinity, morphology, and distribution of Fe in the coprecipitates. After reaction with Fe(II), all of the coprecipitates exhibited some morphological changes relative to their unreacted controls, although most of the changes were localized and did not extend over the full coprecipitate structure.

Fe(II) reacted Fresh (1d reacted) Low C/Fe coprecipitates (Figure 3.1) developed localized regions with ordered, crystalline-like phases that were absent in the paired unreacted controls. The coprecipitates had a bulk aggregated structure (1 – 8 μm) but also had localized nano-sized crystals growing within the aggregate with morphology suggestive of Lepidocrocite (Lp) (Figure 3.1, c-e) (Schwertmann & Thalmann, 1976). In places, the bulk aggregates were laminated in lath Lp-like crystals (Figure 3.1, e), while in other places they were covered in nm sized (<10nm) Lp-like phases (Figure 3.1, c), and elsewhere there appeared 10 – 65 nm sized Lp-like crystals (Figure 3.1, d) along with nanoclusters of the original Fh, similar to structures reported by ThomasArrigo et al. 2019.

As these Low Fe(II) reacted coprecipitates aged for 14 d exposed to Fe(II) they developed nano-sized phases resembling Fh minerals on the bulk Fh structure's surface (Figure 3.2) along with 80

– 100 nm sized mineral clusters in some parts of the samples. Fh nano-particles are usually ≤10 nm in size (Hochella et al., 2008; Michel et al., 2007) or for freshly precipitated, as small as 1 – 3 nm (Cismasu et al., 2011; Hochella et al., 2008) and above 8 nm Fh is thermodynamically unstable at room temperature and transforms into nano-goethite or hematite (Hiemstra, 2015; Navrotsky et al., 2008). To assess the possibility that magnetite may have formed, we ran magnetic susceptibility (MS) on these coprecipitates. The MS values of the coprecipitate ranged from 1.7×10^{-7}- 20.4×10^{-7} m^3 kg^{-1} except for the Fresh Fe(II) reacted Fh which was had a higher MS value (5.6×10^{-5} m^3 kg^{-1}) (Table B.1). Typically, Fh, Gt and Hm have MS values ~ 5.0×10^{-7} m^3 Kg^{-1}. The usual MS values for magnetite and maghemite are ~4.5×10^{-4} m^3 kg^{-1} (Michel et al., 2010; Thompson et al., 2011) suggesting magnetite or maghemite have not formed in the coprecipitates, but may have formed transitionally in the pure Fh control. EDS mapping of the Aged coprecipitates shows the *de novo* Fh deposits contained C and clusters of C appeared at the edge of the bulk Fh structure (Figure B.2). For the Fe(II) reacted High coprecipitates localized iron spherules (1.5 µm sized) (Franke et al., 2009) (Figure 3.3) appeared after 1d and developed into <10nm sized Lp-like crystals after 14 d (Figure 3.4).

DISCUSSION

C dynamics during Fe(II) reaction with coprecipitates

Our experiment involved the incubation of Fh-NOM coprecipitates generated using ^{13}C-labeled NOM in a solution containing an organic PIPES (1,4-Piperazinediethanesulfonic acid) buffer with natural C isotopic composition. Prior work has suggested PIPES buffer does not react significantly with Fe phases (Henneberry et al., 2012). However, our Fh-NOM coprecipitates progressed through a sequence whereby they first accumulated PIPES from the solution (after 1 d

of reaction) with concomitant loss of NOM and then lost a large fraction of both C sources as the reactions proceeded to 14 d. Reaction with Fe(II) uniformly drove the greater loss of the NOM but in some cases higher accumulation of PIPES. The point of zero charges (PZC) of Fh is between 7 and 9 (Cornell & Schwertmann, 2003; Parks, 1965). In our reactor vials, the pH was set between 7 and 6.8, which might have resulted in a slight positive surface charge on the Fh. The NOM was dominated by lignin-derived molecules, which likely contain an excess of negatively charged carboxyl groups (pKa 3 – 4) and thus the PZC of the coprecipitates was likely between 4 and 7 (ThomasArrigo et al., 2019) and the surface likely negatively charged. The pKa value for the PIPES buffer is 6.7 at 25°C which gives it a buffering range of 6.1 to 7.5. Therefore, the charged surface could result in some complex formation with the buffer. Chen et al. (Chen et al., 2015) observed no change in the total C content of Fh-NOM coprecipitates after reacting them with Fe(II) in a PIPES buffer but later found the resulting transformation products desorbed significant C when exposed to an anoxic 0.1 M NaH_2PO_4 desorption solution. Exchange between coprecipitate OM and PIPES could have occurred in the Chen et al (2015) study and not been detected as they did not use isotopes to distinguish C sources.

The coprecipitates (both Low and High) retained their approximate initial C/Fe ratio after reacting with Fe(II) for 1d, but after 14d the C/Fe molar ratio decreased substantially (Table 3.1). For the High coprecipitate, the C/Fe molar ratio decreased from 1.8 to 0.7. A slight decrease in the C/Fe ratio in the High coprecipitate after Fe(II) reaction might be expected, but this change was substantial. It could result from structural flaws in Fh-NOM coprecipitate that resulted in high dissolution rates, or simply the net consequence of 14 days of reaction in a solution containing PIPES buffer. ThomasArrigo et al. 2017 also found coprecipitate C/Fe ratio to decrease (from 1.2 to 0.9) after extended (70 d) reaction with 1mM Fe(II), and similar to our study they observed the

development of Lp in the coprecipitates. Conversely, other studies have shown no or only a slight change in the C/Fe molar ratio after reaction with Fe(II) (Chen et al., 2015; ThomasArrigo et al., 2019), however, these studies used lower C/Fe ratios or different OM sources.

Localized mineral transformation

The morphology of the Low coprecipitate changed after 1 d of reaction with Fe(II) (Figure 3.1) with the development of lepidocrocite (Lp)-like nano-sized crystal growths and this development was not uniform rather it was localized along with the bulk Fh structure. Interestingly, a similar change in the High C/Fe coprecipitates occurred after reaction with Fe(II) for 14 days (Figure 3.4). Higher OM loading on Fh typically hinders Fe(II) sorption to the Fh surface by blocking the mineral surface sites or micropore entrances and forestalls the Fh transformation process (Chen et al., 2014; Chen et al., 2015; Hiemstra et al., 2019). We suspect the emerging transformation of the High Fh-NOM coprecipitates that we observe results from the loss of OC (Table 3.1) and subsequent atom exchange between the Fe(II) and Fe(III) (Zhou et al., 2018). This loss of OC (decrease of C/Fe ratio of 1.8 to 0.7) likely then allowed further Fe(II) to adsorb on the Fh surface and promote localized mineral transformation. The EDS mapping data illustrated that the *de novo* Lp like phases were relatively C-poor (Figure B.4). Thus the Aged High C/Fe coprecipitates and the Fresh Low C/Fe coprecipitates behaved similarly suggesting that at some point during the 14d reaction time, the High C/Fe coprecipitates lost sufficient C to allow Fe(II) catalyzed transformations to begin in localized regions. A recent study has also suggested that higher Fe(II) concentrations and longer experimental durations can result in the mineral transformation of coprecipitates with Fe/C ratios >1.6 (ThomasArrigo et al., 2018).

The wide size distribution of Lp particles formed likely occurred due to the presence of a mixture of NOM compounds. The NOM used in our study is a heterogeneous mixture of soluble

compounds likely containing a range of sizes and functional groups (Kellerman et al., 2018; Newcomb et al., 2017). NOM with a variety of functional groups and diversity of size, charge, hydrophobicity, charge density, etc. likely results in multiple bonding mechanisms with Fh (Kappler et al., 2021; Kleber et al., 2021), which can impact the transformation of minerals over time. ThomasArrigo et al. 2019 showed that Fh coprecipitated with polygalacturonic acid results in thicker Lp, whereas Fh coprecipitated with citric acid results in thin hedge-hog like laminar Lp growth surrounding the aggregate structure. Moreover, the fast oxidation of Fe(II) usually results in a thin Lp structure development (Cornell & Schwertmann, 2003; Kassim et al., 1982; Schwertmann & Thalmann, 1976) and the presence of any excess carboxyl groups can facilitate this fast transformation process (ThomasArrigo et al., 2019). The NOM used in our study was dominated by lignin-derived molecules (Figure B.6) that likely contain significant carboxyl groups as it was soluble and this likely impacted the Fe(II) oxidation rate and resulted in localized Lp phases.

Pure Fh transformed into Gt within 1day reaction with Fe(II) (Figure B.5). The formation of Lp and Gt usually occurs through Oswald ripening of Fh where the presence of Fe(II) increases the dissolution rate and subsequent reprecipitation to a more thermodynamically stable phase via adsorption and electron transfer of Fe(II) with the structural Fe(III), with Lp the typical precursor of Gt formation (Cornell & Schwertmann, 2003). Therefore, the dissolution and reprecipitation of Fh as Lp may have resulted in OM association with Lp that prevented the further transformation into Gt. Moreover, after 14day Fe(II) reaction the Low coprecipitate crystallinity increased and EDS mapping showing OM accumulating on the edge of the mineral phases.

CONCLUSION

Our results suggest the C/Fe molar ratio of Fh-NOM coprecipitates has a governing effect on the morphological and crystallinity changes that occur during reaction with Fe(II). We found localized morphological changes in coprecipitates with Low C/Fe ratios (0.8) after only 1d of reaction with Fe(II) while High C/Fe ratio (1.8) coprecipitates remained unchanged. After 14 d of reaction with Fe(II), the C/Fe ratios decreased for all coprecipitates and localized transformations could then be observed also for the High C/Fe coprecipitates. Previous studies have generally set upper limits of C/Fe ratios for Fe-NOM coprecipitates, whereby no mineral transformation would take place upon exposure to Fe(II). Our work here suggests this assumption is not valid at least when coprecipitates are generated from diverse NOM sources and future studies should examine coprecipitates at the nano-scale to assess the potential for localized transformations. Our study also illustrates that OC exchange can occur between the coprecipitated C and the other C source in solution. Such OC exchange is likely a very common phenomenon in the natural environment and likely impacts the composition of OM associated with short-range-ordered (SRO) minerals, such as ferrihydrite. The interplay between minerals and organic matter is likely much more dynamic than typically appreciated and the potential for changes in soil solution conditions (i.e. redox shifts, changes in DOM composition or concentrations) are likely to have implications for the stability of mineral associated organic matter, especially for redox-active SRO Fe phases.

TABLES AND FIGURES

Table 3.1: Elemental composition of the synthesized coprecipitates (Initial) and after reacting with Fe(II) (Final) in PIPES buffer.

Sample		Initial			Final			
		Fe	Total C	C: Fe molar ratio	Fe	Total C	Fraction of ^{13}C - NOM	C: Fe molar ratio
		(mg g^{-1})		(mol/mol)	(mg g^{-1})		(%)	(mol/mol)
Fresh	Fh	819	-	-	534	43	n.d.	0.4
	Fh with Fe (II)	819	-	-	593	11	n.d.	0.08
	Low C/Fe	469	80	0.8	466	85	88	0.9
	Low C/Fe with Fe (II)	469	80	0.8	505	105	64	1.0
	High C/Fe	407	157	1.8	352	136	81	1.8
	High C/Fe with Fe (II)	407	157	1.8	381	136	76	1.7
Aged	Fh	972	-	-	563	70	n.d.	0.5
	Fh with Fe (II)	972	-		1426	28	n.d.	0.09
	Low C/Fe	949	163	0.8	511	59	56	0.5
	Low C/Fe with Fe(II)	949	163	0.8	671	71	34	0.5
	High C/Fe	850	328	1.8	460	70	72	0.7
	High C/Fe with Fe(II)	850	328	1.8	512	76	60	0.7

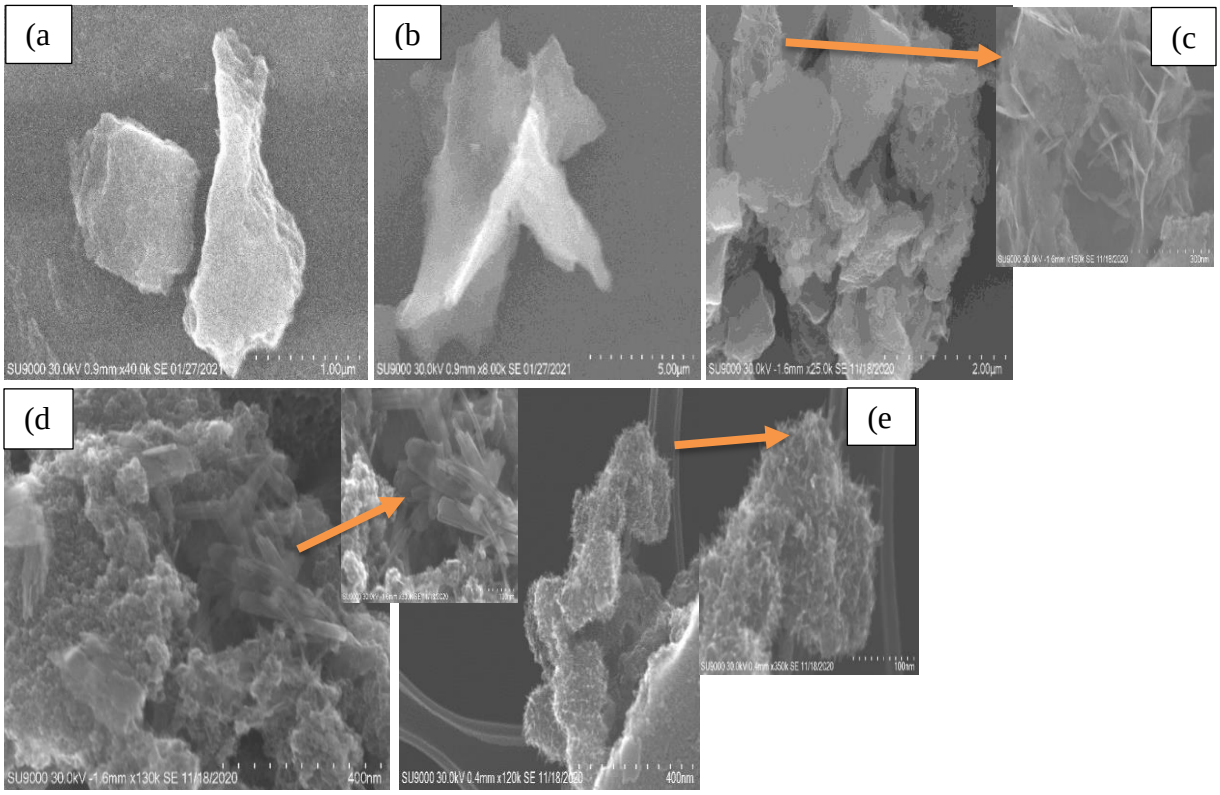

Figure 3.1: STEM image of Fresh Low unreacted (a,b) and reacted coprecipitate with Fe(II) (c-e).

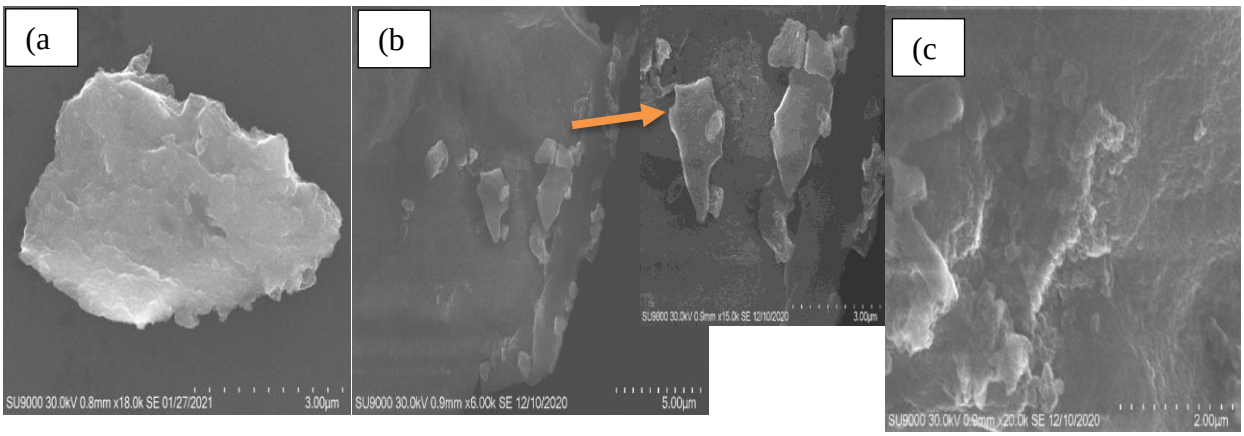

Figure 3.2: STEM image of Aged Low unreacted (a) and reacted coprecipitate with Fe(II) (b,c).

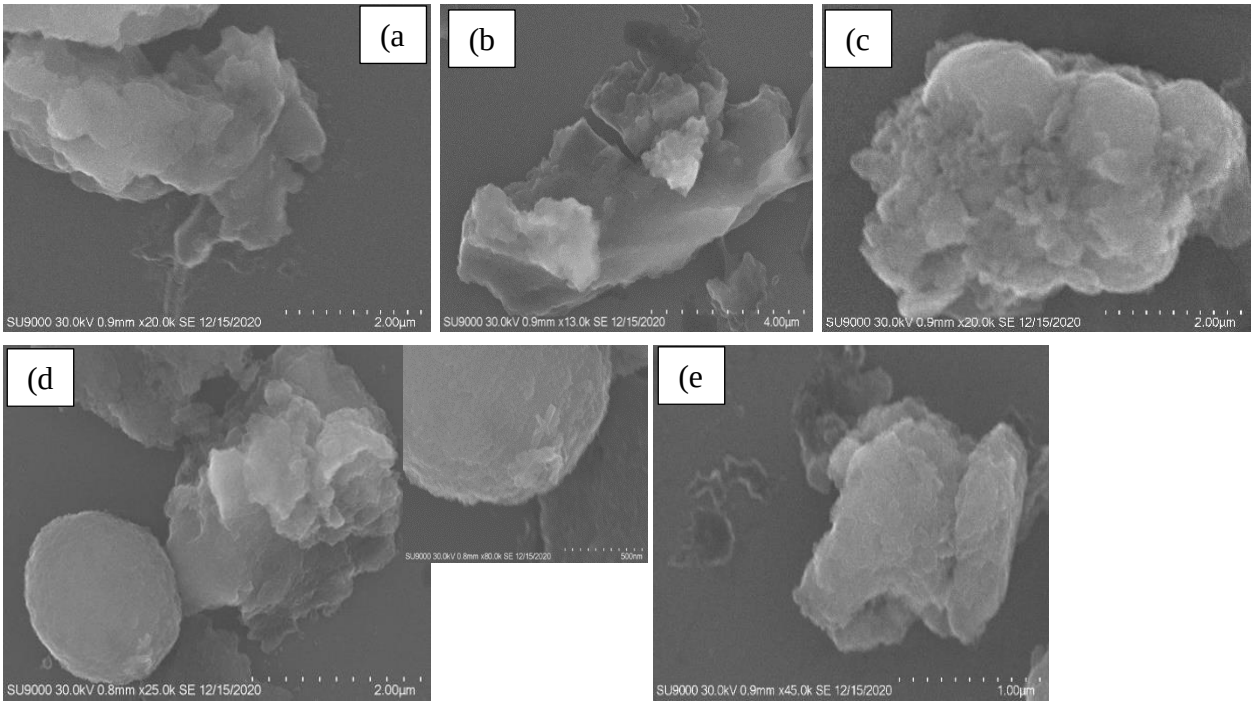

Figure 3.3: STEM image of Fresh High unreacted (a,b) and reacted coprecipitate with Fe(II) (c-e).

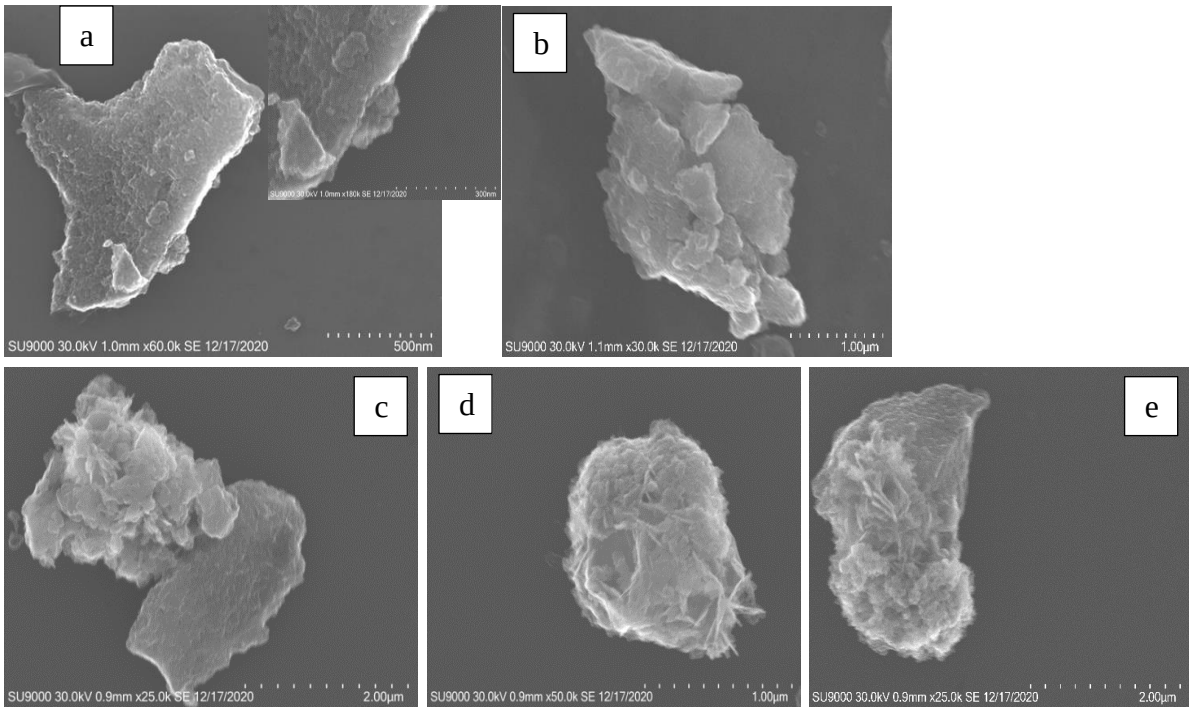

Figure 3.4: STEM image of Aged High unreacted (a,b) and reacted coprecipitate with Fe(II) (c-e).

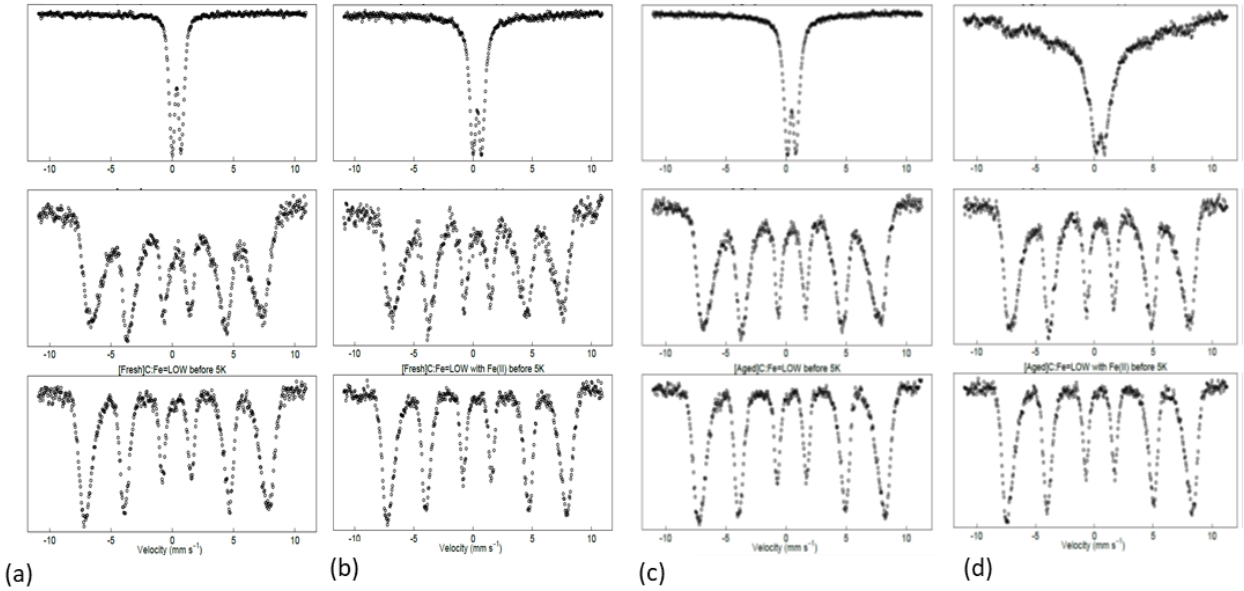

Figure 3.5: Mössbauer spectra (at 35K, 13K, and 5K) of the Fresh Low (a,b) and Aged Low (c,d) C/Fe coprecipitates both unreacted and Fe(II) reacted respectively.

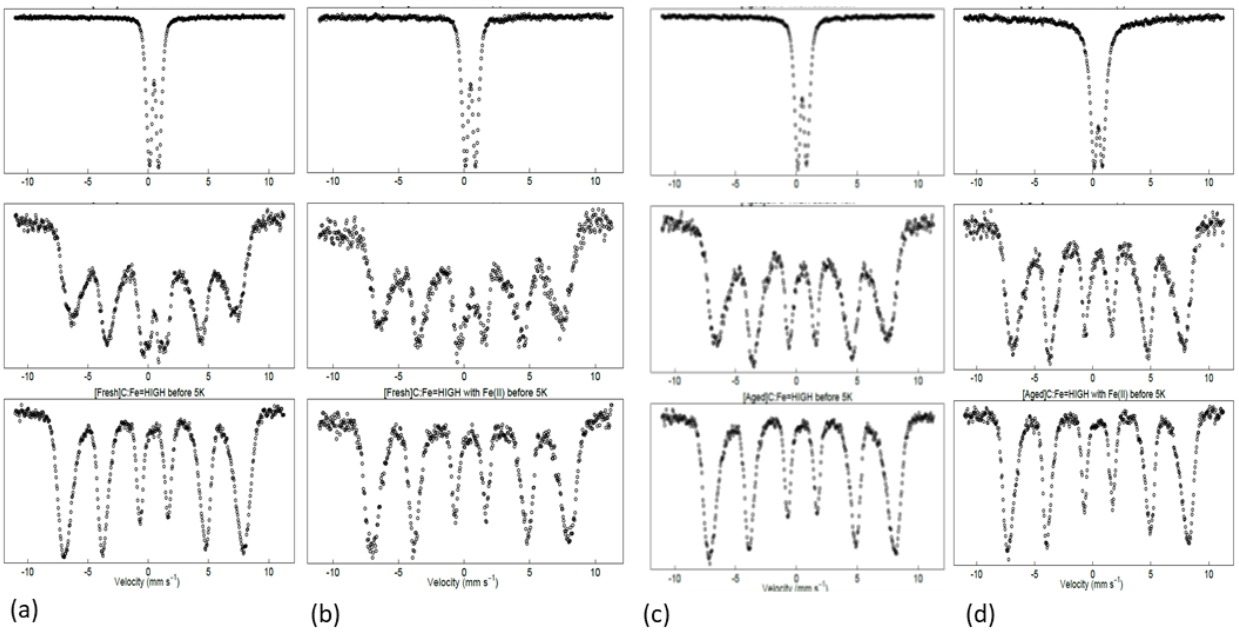

Figure 3.6: Mössbauer spectra (at 35K, 13K, and 5K) of the Fresh High (a,b) and Aged High (c,d) C/Fe coprecipitates both unreacted and Fe(II) reacted respectively.

CHAPTER 4

Bioavailability of natural organic matter coprecipitated with ferrihydrite and pre-reacted with Fe(II)

Noor, N., and A. Thompson. To be submitted to the Environmental Science & Technology Journal.

ABSTRACT

Ferrihydrite-Natural organic matter (Fh-NOM) coprecipitates stabilize organic matter (OM) against biodegradation. However, under anoxic conditions, the adsorption of $Fe(II)_{aq}$ to Fe(III) minerals can drive their transformation to more crystalline phases, which may impact the bioavailability of OM. To test if Fe(II)-catalyzed atom exchange and re-crystallization would alter OM availability, we assessed OM availability using a 45-day oxic microbial incubation of Fe-NOM coprecipitates before and after a 1-day and 14-day exposure to Fe(II). We found the Fe(II) reacted coprecipitates lost less OM than the unreacted controls, with 1-day Fe(II) reacted coprecipitates offering the most protection (28%). Mineralization of coprecipitated NOM-C was very low across all treatments (~1-5%), with most loss of solid-phase C retained as dissolved NOM-C (around 30 – 50% of the coprecipitated C). Moreover, the changes in the coprecipitate crystallinity and morphological appearance following the incubation experiment was also measured using Mössbauer spectroscopy and Scanning transmission electron microscopy. The crystallinity of the coprecipitates decreased and the initial C/Fe ratio before incubation impacted the extent of the changes. Our study suggests that the product of Fe(II) reacted Fh-NOM can protect the coprecipitated C but this depends on the C/Fe molar ratio and the changes that occur to the coprecipitates during Fe(II) reaction. Moreover, we have observed decreasing crystallinity during incubation which has the potential to impact other biogeochemical cyclings such as nutrients and heavy metals.

INTRODUCTION

Association with minerals is a major mechanism responsible for the accumulation and persistence of organic matter (OM) in soil (Eusterhues et al., 2003; Kaiser & Guggenberger, 2000; Mikutta et al., 2006; Mikutta et al., 2007; Schmidt et al., 2011), often terms Mineral Associated Organic Matter (MAOM). Strong chemical bonds between the mineral surfaces and organic molecules and the trapping of OM within mineral pores (which are inaccessible for microbes and enzymes) can protect OM from microbial mineralization (Jones & Edwards, 1998; Kaiser & Guggenberger, 2003, 2007). However, even in association with minerals, microorganisms can use the OM as an energy source and/or facilitate desorption of the OM (Kalbitz et al., 2005; McGhee et al., 1999; Singh et al., 2003).

Short-Range-Ordered (SRO) minerals are ubiquitous in soils (Cornell & Schwertmann, 2003; Jambor & Dutrizac, 1998) and are often investigated using a common SRO mineral, ferrihydrite (Fh). The abundance of OM in soil is strongly correlated with SRO minerals (Rasmussen et al., 2018). Fh mineral associated OM is often considered to be protected, however recent studies suggest that while SRO Fe minerals can facilitate short term protection of SOM, they may not promote long term C stabilization (Chen et al., 2020; Hall et al., 2018). Fh and OM can form associations through either adsorption or coprecipitation, with coprecipitation considered to protect OM better (Adhikari et al., 2019; Chen et al., 2014; Eusterhues et al., 2014b; Eusterhues et al., 2008; Mikutta et al., 2008; Riedel et al., 2013). However, exposure to anoxic conditions can result in a dissolution of Fh resulting in higher mineralization of the coprecipitated OM (Chen et al., 2020). Hall et al. (2018) found that in soils experiencing frequent redox fluctuations, older carbon is better correlated with crystalline Fe minerals than with SRO-Fe minerals. This recent

understanding suggests Fh-OM associations will likely require further protection in redox fluctuating conditions in order to for OM to persist (Chen et al., 2020).

The Fe(III) in Fh can continuously exchange electrons with Fe(II) sorbed to the surface under anoxic conditions (Zhou et al., 2018) and this can cause it to transform into more stabilized minerals such as lepidocrocite, goethite, hematite etc. through a process known as Fe(II) mediated transformation (Kukkadapu et al., 2003; Schwertmann & Murad, 1983). Whether this process provides some protective effect on the mineral associated OM is currently unknown. Previous studies have shown that Fe(II) mediated transformation of Fe oxide minerals can result in substantial release of co-precipitated Ni and Zn (Catalano et al., 2010), suggesting that the same may occur with OM. However, the degree of Fe mineral transformation and electron transfer is sensitive to the C/Fe ratio, Fe(II) concentration, and length of reaction, so the trajectory is not clear.

To investigate these questions, we reacted Fh-NOM with Fe(II) and then incubated the coprecipitates with microbes under oxic conditions to evaluate the OM bioavailability. Noting that the C/Fe molar ratio and Fe(II) reaction time are likely important, we examined coprecipitates at low and high C/Fe ratios exposed to Fe(II) for 1 or 14 days. We used a mixed microbial community extracted from the soil as a microbial inoculum and discriminated between the microbial C and media by producing co-precipitates with ^{13}C labeled NOM. In addition to assessing the bioavailability of the OM, we also evaluated changes in the crystallinity and morphological appearance of the coprecipitates.

MATERIALS AND METHODS

Preparation of ^{13}C isotope labeled NOM

Labeled natural organic matter (NOM) solution was prepared from a water extract of ^{13}C labeled Burmudagrass litter. Briefly, a pulse labeling method was used to label Tifton-85 bermudagrass (*Cynodon dactylon x Cynodon nlemfuencis*) with $^{13}CO_2$ (99.999 atom%, Cambridge Isotope Laboratories Inc.). Bermudagrass was grown in flats of C-free sand with some residual potting medium under greenhouse conditions for four weeks. All flats were fertilized with 0.7 mmol $(^{15}NH_4)_2SO_4$ once a week. For ^{13}C pulse labeling, bermudagrass was transported to a Conviron growth chamber with a temperature of 35°C and CO_2 concentration of 500 ppm maintained using a Qubit G400-2 gas mixing system coupled with a S157 infrared CO_2 analyzer (Kingston, Ontario, CA). Pulse labeling was carried out once a week for 6 weeks. Bermudagrass was exposed to $^{13}CO_2$ for 8 h with a flow rate of $^{13}CO_2$ approximately 0.5 L min^{-1}. Labeled above-ground biomass was harvested and immediately frozen before being transported to the laboratory. The frozen material was freeze-dried and ground using Wiley mill to <1 mm. Ground materials were mixed with 18.2 MΩ deionized water (DI) with a solid to water ratio of 1/20 (w/v). The mixture was then shaken at 140 rpm in a horizontal shaker for 48 h and filtered through a 0.45 μm polyvinylidene fluoride membrane filter. The total organic carbon concentration of the stock solution was measured by Shimadzu-500 TOC analyzer and later diluted with ultrapure DI water to achieve the required concentration to prepare the coprecipitates. Molecular composition characterization of dissolved NOM was done using Fourier- transform ion cyclotron resonance spectroscopy (FTICR), which revealed a composition dominated by lignin-derived molecules and aliphatic compounds (according to the Van Krevelen diagram) with mean population O/C and H/C values of 0.2±0.08 and 1.5±0.3, respectively (Figure C.4). Here an O/C ratio around 0.2 was

considered to identify as Lingin derived material but literature also considered an O/C ratio around 0.4 to identify Lingin derived formulae (Kim et al., 2003). Although we used the Van Krevelen space diagram but lately this diagram being avoided to show FTICRMS data with chemical classes (Koch & Dittmar, 2006; Šantl-Temkiv et al., 2013)as it does not ensures the structure and there can be discrepancies regarding the data interpretation.

Ferrihydrite (Fh) and Ferrihydrite-natural organic matter (Fh-NOM) coprecipitates synthesis

All the chemicals used in this study were laboratory grade. Ferrihydrite was synthesized following Schwertmann and Cornell, 2008, where, $Fe(NO_3)_3.9H_2O$ was dissolved in 18.2 MΩ water and pH was adjusted at 7 using 1M KOH. Fh-NOM Coprecipitates with a C/Fe molar ratio of 0.8 and 1.8 were prepared by following the well-accepted method described by Chen et al. 2014. Briefly, $Fe(NO_3)_3.9H_2O$ was mixed with dissolved labeled ^{13}C-NOM containing the required amount of C to achieve the required C/Fe ratio under vigorous stirring. The pH of the suspension was raised from ~2.0 to 7 by slowly adding 0.1 M KOH. Synthesized Fh and Fh-NOM coprecipitate was centrifuged at 3000rpm for 10 minutes and washed twice using degassed 18.2 MΩ ultrapure water and stored in the glove box to remove O_2 before preparing them for reaction with Fe(II).

Reacting Fh-NOM coprecipitates with Fe(II)

Freshly-synthesized, moist Fh, and Fh-NOM coprecipitate were resuspended in anoxic PIPES (1,4-piperazinediethanesulfonic acid) buffer (10 mM, pH 7) and stirred for 1 d inside the glovebox (filled with 97% N_2 and 3% H_2) to remove residual oxygen. A portion of the Fh and Fh-NOM coprecipitates were reacted with Fe(II) in 125 ml opaque serum bottles containing 33.6 mg of total Fe (as an Fh-NOM slurry) and 60 mL of anoxic PIPES buffer (10 mM, pH 7). $FeSO_4.7H_2O$

was added to the bottles (except the controls, listed as “unreacted control”) to obtain a final Fe(II) concentration of 2mM (Chen et al., 2015). The reaction was carried out in the anoxic glove box on a rotatory shaker in two batches: one reacted with Fe(II) for 24 h (henceforth “Fresh”); one reacted for 14 days (henceforth “Aged”). After the reactions, the Fe(II)-reacted Fh and Fh-NOM samples along with the unreacted controls were rinsed with degassed 18.2 MΩ ultrapure anoxic water twice by centrifuging them at 10,000 rpm for 10 min. A small amount of degassed water was added to maintain a moist slurry and two-thirds of each sample was stored at 4 °C and used within 24 h for this incubation study. The moisture content of the samples was measured on separate aliquots. The remainder of the samples were stored at -20 °C for characterization. Total Fe, total C, and the C isotopic composition were measured. The C/Fe ratio of the coprecipitates in the Fresh reactor remained unchanged but the C/Fe ratio decreased in the Aged reactors (Table 4.1). This change was higher for the 1.8 C/Fe ratios containing coprecipitates and it decreased from 1.8 to 0.7. To keep it simple in the literature we still addressed this coprecipitate as “High” but it's important to keep in mind that the ratio of it is almost similar to the Low coprecipitates. The crystallinity and morphological changes were also analyzed using Mössbauer spectroscopy (MB) and ultrahigh-resolution scanning transmission electron microscopy (STEM).

Collection of soil microbial inoculum

Soil microbial inoculum was obtained by enrichment from freshly collected soil (0 – 10 cm depth) from a field at the J. Phil Campbell Sr. Research and Education Center, University of Georgia, Athens-GA. The soil was shaken in a 4 mM $CaCl_2$ solution for 24 h and passed through 5 μm filters (Eusterhues et al., 2014b). A small portion of that filtrate was added to Luria broth (LB) media and incubated for 12 h at 25°C to stimulate active microbial growth. The resulting incubated solution was centrifuged at 3000 rpm for 10 min, and the supernatant was discarded.

The microbial enrichments were then washed with 18.2 MΩ ultrapure water twice to remove the remaining LB media and resuspended in a small amount of selective media containing 0.5 g KH_2PO_4, 1.0 g $NaSO_4$, 2.0 g NH_4Cl, 0.5 mM $CaCl_2$, 0.1 mM $MgSO_4$, and 3 mM glucose (per Liter basis).

Experimental setup and sample collection

An incubation study was conducted in 125ml opaque serum bottles containing 30 mg of the solid sample and 55ml of selective media containing 0.5 g KH_2PO_4, 1.0 g $NaSO_4$, 2.0 g NH_4Cl, 0.5 mM $CaCl_2$, 0.1 mM $MgSO_4$, and 1mM glucose (per Liter basis) (Ginn et al., 2014). The soil microbial inoculum was added at a rate of $2x10^8$ cells ml^{-1} (except in the non-inoculated controls, to which no inoculum was added). This concentration was based on a cell growth curve (cell numbers counted via agar plate count method) and targeted the late log phase of growth. A detailed description of the incubation setup is available in the supporting information section (Table C.8).

The vials were seal capped with butyl rubber stoppers and continuously shaken on a rotatory shaker at 20 °C for 45 d. To measure the dissolution and mineralization of the NOM, we sampled initially every day (for 3 d), then every three days (for the next 9 d), and then every five days (for the next 20 d), and then took a final sample at 45 d. For the Fresh and Aged reactors, the sampling dates varied slightly for two of the time points due to logistic issues, but variations were accounted in the calculations. During each sampling day, 4 ml of the solution was collected and filtered through a 0.22 µm polyvinylidene fluoride filter for dissolved organic carbon (DOC) analysis and 28.5 ml of reactor gas was collected and stored in pre-evacuated sealed sterile vials for further analysis. After each sampling, the vials were uncapped for at least 6 h and left under a laminar hood on the rotatory shaker to expose them to O_2 and prevent the development of anoxic conditions. At the end of the incubation experiment, the solid samples were washed twice with

18.2 MΩ ultrapure water and stored at -20 °C for further analysis. The incubation study was conducted with two biotic reactor replicates, but only one un-inoculated control. During the incubation, the pH varied only slightly within the range of 6.1 – 7.0 (Table C.9 and C.10).

Solid sample analysis for ^{13}C, total C and Fe content

The ^{13}C isotope (i.e. coprecipitated C) and total C content of the solid phase were measured by lyophilizing a portion of the solid sample, crimping it in a tin capsule, and analyzing it in a CHN Carlo Erba Elemental Analyzer. The total Fe content was measured using inductively coupled plasma mass spectrometry (ICP-MS, Perkin Elmer, Elan 9000).

The per cent contribution of added ^{13}C-NOM from bermudagrass extract remaining in the solid samples after incubation study (P ^{13}C-NOM in solid) was calculated using a two-way source mixing model.

$$P^{13}\mathrm{C_{NOM}}\text{in solid} = \frac{\mathrm{x[13C]}_{Fh-NOM}\ \text{after} - \mathrm{x[13C]}_{Fh}}{\mathrm{x[13C]}_{NOM} - \mathrm{x[13C]}_{Fh}} * 100$$

where, $\mathrm{x[13C]}_{\mathrm{Fh_NOM}}$after and $\mathrm{x[13C]}_{Fh}$ are atom fraction of ^{13}C isotope in the coprecipitates after incubation and ^{13}C content of the Fh, respectively; $\mathrm{x[13C]}_{\mathrm{NOM}}$ is the initial atom fraction of ^{13}C content of the bermudagrass extract.

Added ^{13}C-NOM in DOC and total DOC

The added ^{13}C-NOM in the dissolved organic carbon (DOC) content was measured by freeze-drying the sampled solution and analyzing the collected pallet in the CHN Carlo Erba Elemental Analyzer. The proportion of added ^{13}C-NOM in the DOC was calculated following a two-source mixing model.

$$P^{13}\mathrm{C_{NOM}}\text{in DOC} = \frac{\mathrm{x[13DOC]}_{Fh-NOM} - \mathrm{x[13DOC]}_{Fh}}{\mathrm{x[13DOC]}_{NOM} - \mathrm{x[13C]}_{Fh\_NOM}} * 100$$

where, $\mathrm{x[13DOC]}_{\mathrm{Fh\_NOM}}$ and $\mathrm{x[13DOC]}_{Fh}$ are atom fraction of ^{13}DOC isotope in the reactor at each data collection point and ^{13}DOC content of the Fh control reactor, respectively; $\mathrm{x[13DOC]}_{\mathrm{NOM}}$ is

the initial atom fraction of ^{13}DOC content of the bermudagrass extract and $x[13C]_{Fh\_NOM}$ is the initial added ^{13}C-NOM content of the solid coprecipitate.

Total DOC concentration of the solution was measured using a Shimadzu-500 TOC analyzer.

Gas sampling and measurement

To measure the CO_2 losses during the experiment and their ^{13}C isotopic content, gas samples were collected from the headspace of each experiment vial. Using gas-tight syringes, 3.5ml of gas was collected and over-pressurized in a pre-evacuated 3ml glass vial (Exetainer, Labco Inc., UK) for measurement of CO_2 concentration using Licor 640A. A separate 25-ml gas sample was collected from each experimental vial and over-pressurized into pre-evacuated 20-ml glass serum bottles capped with Teflon septa and sealed with aluminum crimps for the measurement of ^{13}C-CO_2 gas. The δ^{13}C values of CO_2 were measured by injecting 20-ml of headspace gas using a gas-tight glass syringe into a Piccaro G 220-i. A separate 2.5 ml aliquot of the gas sample was injected in a Licor LI-840A CO_2/H_2O gas analyzer using a gas-tight syringe and the CO_2 concentration was measured against standards ranging from 0% to 2.5% CO_2.

The per cent contribution of added ^{13}C-NOM to CO_2 respiration (P $^{13}C_{NOM}$) was calculated using a two-source mixing model.

$$P^{13}C_{NOM} = \frac{x13[CO2]_{Fh\_NOM} - x13[CO2]_{Fh}}{x[13C]_{Fh\_NOM} - x[13C]_{Fh}} * 100$$

Where, $x13[CO2]_{Fh\_NOM}$ and $x13[CO2]_{Fh}$ are atom fraction of ^{13}C of CO_2 respired from Fh-NOM coprecipitates and Fh during the incubation period, respectively; $x[13C]Fh\_NOM$ and $x[13C]Fh$ is the initial atom fraction of ^{13}C content of the solid phase Fh-NOM coprecipitate and Fh, respectively.

Fluxes of CO_2 derived from the added ^{13}C-NOM were calculated by multiplying total CO_2 fluxes by their fractional contributions.

Mössbauer analysis

Mössbauer spectroscopy was collected using 50-mCi ^{57}Co/Rh source at 5 K, 13 K, and 35 K to characterize Fe mineral phases and to compare phase crystallinity before and after incubation. Solid samples were washed twice with ultrapure water by suspending the samples in ~ 5 ml of water, gently shaking the samples, and then centrifuging them at 10,000 rpm for 10 min. The supernatants were then poured off, the pelleted samples were mounted in a nylon o-ring, sealed between two pieces of Kapton tape, and immediately frozen at −20 °C. Mössbauer spectra were analyzed using Recoil software and spectra fitting was done using Voigt-based fitting (VBF) as described elsewhere (Thompson et al., 2011).

Scanning transmission electron microscopy (STEM)

Electron microscopy images were obtained using an ultra-high resolution scanning transmission electron microscopy (STEM-Hitachi SU 9000EA) with a resolution of 0.4 nm operating at 30 kV. The solid sample slurry was placed on a silica chip and dried overnight before analysis. A secondary electron (SE) detector was used for collecting the images and EDS spectra were recorded with Oxford Ultim Extreme software.

RESULTS

Changes in crystallinity and morphological appearance of the coprecipitates

The Mössbauer spectra (MB) of the coprecipitate before and after incubation and scanning transmission electron microscopy (STEM) images and EDS mapping are presented in Figure 4.4 - 4.16. After incubation, the Fh controls (no NOM) (Figure 4.8) crystallinity increased but decreases in Fe phase crystallinity observed in the coprecipitates (Figure 4.4 - 4.7) except the Fresh High C/Fe coprecipitates (relative to the un-incubated samples). The Fe(II) reacted samples

generally had higher crystallinity than the un-reacted controls, and the Aged samples had higher crystallinity than the Fresh samples (Noor and Thompson, *In Review*); these relationships were maintained through the microbial incubation, again except the Fresh High C/Fe coprecipitate.

The ultrahigh resolution scanning transmission electron microscopy (STEM) images support the Mössbauer spectroscopy results (Figure 4.9-4.16) illustrating changes following microbial incubation consistent with decreasing iron phase crystallinity except for Fresh High C/Fe control. The Fresh Fe(II) reacted Low coprecipitate initially had localized Lp like phases that largely disappeared after microbial incubation revealing images similar to our unreacted Fh controls (Figure 4.10). Similarly, the Fe(II) reacted Aged High C/Fe coprecipitate also had Lp like phases before incubation which decreased in appearance frequency after microbial incubation (Figure 4.15) but did not completely disappear.

The behavior of the Fresh High C/Fe control coprecipitate was anomalous relative to the other samples. Following microbial incubation, its net Fe crystallinity increased (MBS Figure) and the STEM revealed the formation of some highly crystalline phases, with EDS mapping suggesting a high enrichment of Ca (Figure 13). This Ca enrichment may promote both the Fe crystallinity increase and different C behavior by blocking the adsorption of media C (Sowers et al., 2018). This source of Ca could be the media used that contained 0.5mM litre^{-1} $CaCl_2$.

Change in C content

To evaluate changes in the carbon content of the coprecipitates during the microbial incubation, we characterized changes in both the ^{13}C labeled (from co-precipitated NOM) and unlabeled C (from the media and microbes). Our previous work illustrated that during the reaction with Fe(II), some of the initial coprecipitated NOM-C was lost and the coprecipitates accumulated minor amounts of unlabeled C from the reaction solutions (likely from the PIPES buffer).

After incubation, less coprecipitated C was lost from the Fe(II) reacted samples than the unreacted controls, which suggests reaction with Fe(II) increased the stability of the coprecipitated C (Table C.1). The Fe(II) reacted Fresh Low coprecipitates retained 28% more coprecipitated C than its control (p-value 0.01), the highest among all the treatments. However, the Fe(II) reacted High coprecipitates exhibited wide variation between the Fresh and Aged treatments, with the Fresh coprecipitate retaining only 5% more than its paired control (p-value 0.09), while the Aged sample retained 19% more coprecipitated C than its paired control (p-value 0.01). This again likely reflects the alteration of the Aged High coprecipitates that resulted from their decrease in C/Fe ratio from 1.8 to 0.7 during reaction with Fe(II).

Mineralization of coprecipitated NOM-C and total CO_2-C

The fraction of total CO_2 represented by coprecipitated NOM-C was very low for all treatments (Figure 4.3 and Table C.3). For the Low, C/Fe coprecipitates, the Fe(II) reacted coprecipitates mineralized more NOM-C than the unreacted paired controls, with 3.2 ± 0.4% and 4.7±0.6% vs. 1.5 ± 0.1% and 2.9±0.1%, for the Fresh and Aged samples, respectively. However, in the High C/Fe coprecipitates, in Fresh controls mineralized more coprecipitated C (2.3± 0.6%) than the Fe(II) reacted coprecipitates (4.1± 0.7%), and for the Aged High samples, no differences in carbon mineralization were minor (Figure 4.3 and Table 4.3).

In our study, mineralization of coprecipitated C as CO_2 was very low and only around 1 to 5% of the coprecipitated C was respired in all the treatments. The reduced bioavailability of NOM-C from the coprecipitates is expected but this was extremely low. Mikutta et al., 2007 Found 50 – 90% decrease in the decomposition of organic matter from forest floor extract over 90 days when sorbed to Gt. Another study showed 27.9% Fh associate fulvic acid but 4.2% Fh associate glucose respiration occurred under aerobic conditions (Adhikari et al., 2019). Porras et al, 2018 conducted

a microbial incubation study with synthesized Fh-^{13}C labeled glucose association to measure bioavailability of C under aerobic condition and also found only less than 3% of the associated glucose was respired after 80 days. In our experiment, the higher CO_2 emission from the coprecipitates than the Fh control and the CO_2 emission rate from the "microbial inoculum and media containing" control ensure that the low respiration value of NOM-C was not experimental artifact and the microbial inoculums were healthy and active.

Dissolved OC

Total DOC at all the sampling points was tracked, but ^{13}DOC was measured only for three sampling points (day 1, day 3 and at the end of the incubation period). To do a mass balance calculation for each sampling day, an estimated ^{13}DOC concentration for all sampling points were calculated by linear interpolation (Figure 4.2).

The ^{13}DOC concentration increased over time in all the coprecipitates whereas total DOC concentration decreased over time. The coprecipitates released 30% to 50 % of the coprecipitated C (Figure 4.2 and Table C.3), but also resorbed other sources of C from the solution (i.e., glucose or microbial exudates). The linear interpolation of the values might have resulted in the overestimation of the ^{13}DOC values. Mass balance calculation also indicates that in some of the treatments the recovered coprecipitated C was a little higher than what was added (Table 4.4 and 4.5). Fe(II) reacted Fresh Low C/Fe coprecipitates released slightly more ^{13}C-NOM than unreacted controls, which was respectively 43% and 35% of their initial coprecipitated C in the solids (Figure 4.2 a, Table C.3). The opposite pattern observed in the Fe(II) reacted High C/Fe coprecipitate, where the Fe(II) reacted coprecipitates released 29% and the unreacted control released 40% of the coprecipitated C. A similar pattern was observed in the non-inoculated control as well (SI Figure 2 a, b). Fe(II) pre-reacted Aged, Low and High C/Fe molar ratio containing coprecipitates

released more coprecipitated C in the solution than the unreacted controls (Figure 4.2 c; Table C.3). For Fe(II) reacted Low C/Fe coprecipitates it was 51% and for unreacted control the 35% of the coprecipitated C. Similar trends were observed in the non-inoculated reactors (Figure C.2 c, d and Table C.2).

DISCUSSION

The Fe(II) reacted coprecipitates promoted protection against biodegradation for the coprecipitated C and this effect was prominent when the C/Fe ratio of the coprecipitates were below 0.8. This statement was true regardless of the reaction time (1 day or 14 day). During the reaction of the coprecipitates with Fe(II), the coprecipitates lost C and the crystallinity of the coprecipitates also increased. These changes in the coprecipitates likely resulted in a more organized arrangement in the coprecipitates where the remaining coprecipitated C (after reaction with Fe(II)) was strongly associated with the mineral structure and this could have thus resulted in higher retention of the OM. In the first day of reaction, the High C/Fe coprecipitates it did undergo detectable changes in crystallinity (by either TEM or Mössbauer) and offer no additional protection of the OM during microbial incubation than the unreacted controls. However, after 14 days of reaction, the High C/Fe coprecipitates lost significant coprecipitated C (the C/Fe ratio decreased from 1.8 to 0.7) and its crystallinity increased. These changes resulted in higher level of protection for the remaining coprecipitated C against biodegradation than controls. These findings suggest the reaction of Fe(II) with coprecipitates and resulting transformation of the coprecipitates is a key factor determining the bioavailability of the coprecipitated C. In previous laboratory incubation studies, mineral association has been shown to decrease C bioavailability (Jones & Edwards, 1998; Kleber et al., 2015; Mikutta et al., 2007). Adhikari et al. (2019) showed that Fh bound glucose and

fulvic acid has lower bioavailability compared to free organic compounds. In our study, we have also observed that the coprecipitated C was protected, even in the unreacted controls. More uniquely, our study suggests that reaction with Fe (II) can increase the level of of this protection.

In our experiment, the crystallinity of the coprecipitates decreased after the microbial incubation, during which non-labeled C from the glucose and microbial exudate-containing media sorbed to the coprecipitates. The sorption of non-labeled C could likely be responsible for the decreasing crystallinity as studies have shown that increased OC loading decreases crystallinity of Fh-OM coprecipitates (Chen et al., 2014; Eusterhues et al., 2008). After Fe(II) reaction, the 1d reacted Low C/Fe coprecipitates and 14 day reacted High C/Fe coprecipitates both developed Lp-like localized phases and the crystallinity increased, but after incubation, those Lp phases appeared to disappear from the 1d reacted Low coprecipitates while it decreased, but did not disappear in the 14 day reacted High coprecipitates. This suggests that the longer interaction between Fe(II) and the coprecipitates mediated the increase in crystallinity and increased the resistance of the co-precipitated OM to desorption during the microbial incubation.

CONCLUSION

Overall, Fe(II) pre-reacted coprecipitates can retain more coprecipitated C when the C/Fe molar ratio of the coprecipitates is 0.8 or less. The mineralization of coprecipitated C from the Fe(II) pre-reacted and unreacted coprecipitate is less than 5% where the dissolved C concentration can be up to 50% of the coprecipitated C. Moreover, the crystallinity of the coprecipitates decreased during the microbial incubation study. The C/Fe ratio, Fe(II) reaction and aging process can bring changes in the crystallinity and morphology of the coprecipitates, which can direct the later changes following microbial incubation. In the natural environment, under reducing

conditions the dissolution of Fh mineral can result in higher mineralization of the associated OM in presence of Fe(II) (Chen et al., 2020). Our results suggest that those Fe(II) interacted Fh-NOM coprecipitates when subject to an oxic condition can protect the coprecipitated C more than the Fe(II) unreacted Fh-NOM coprecipitates. Although this effect is sensitive to the C/Fe ratio of the coprecipitates and the interaction time of Fe(II) with the coprecipitates. Moreover, our finding regarding the decreasing crystallinity of the Fh-NOM coprecipitates during microbial incubation can also impact concurrent nutrient and heavy metal cycling in the soil.

FIGURES AND TABLES

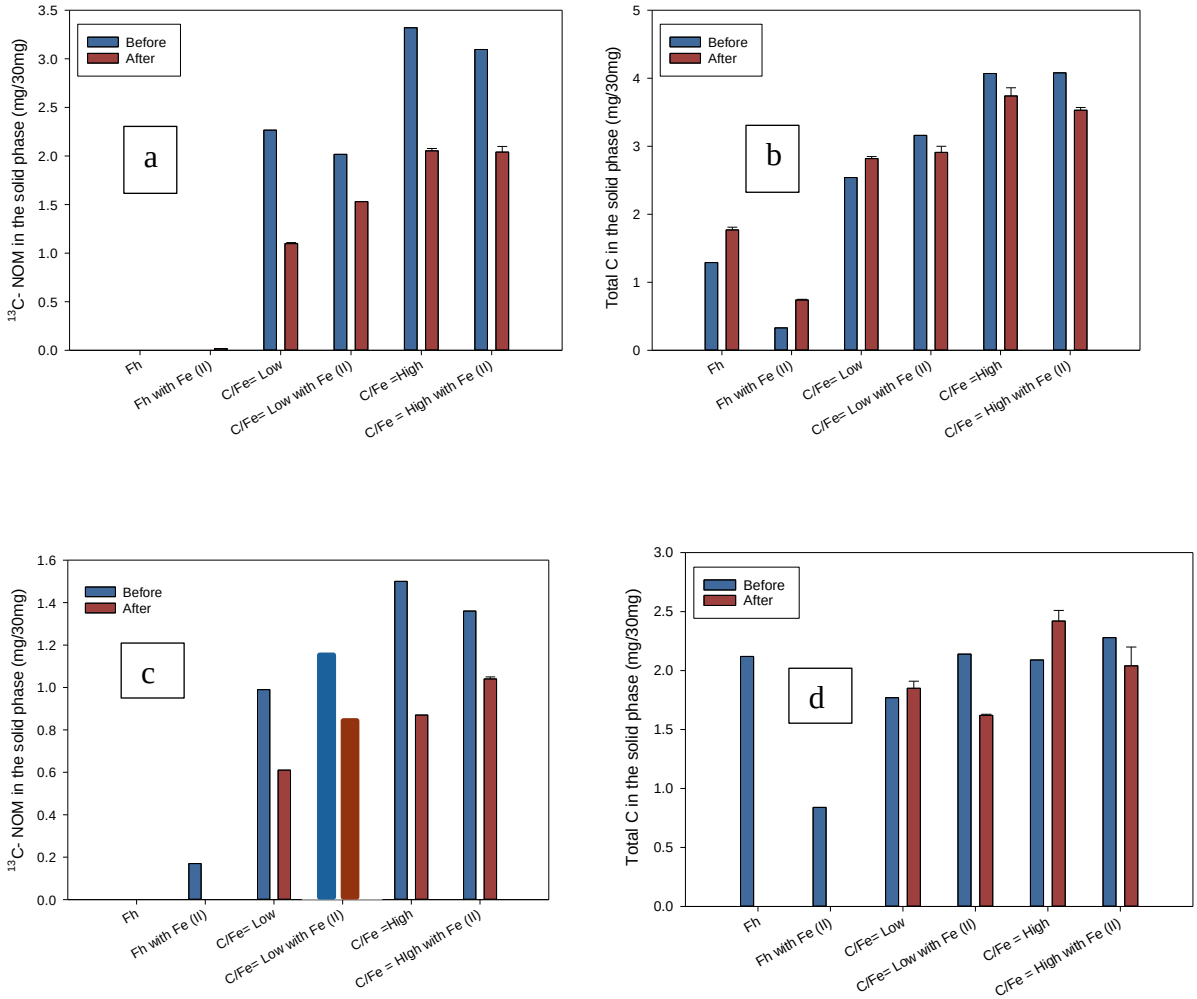

Figure 4.1: Added ^{13}C-NOM (mg 30g^{-1}) and Total C (mg 30g^{-1}) in the Fresh (a, b) and Aged (c, d) sample before and after biotic incubation.

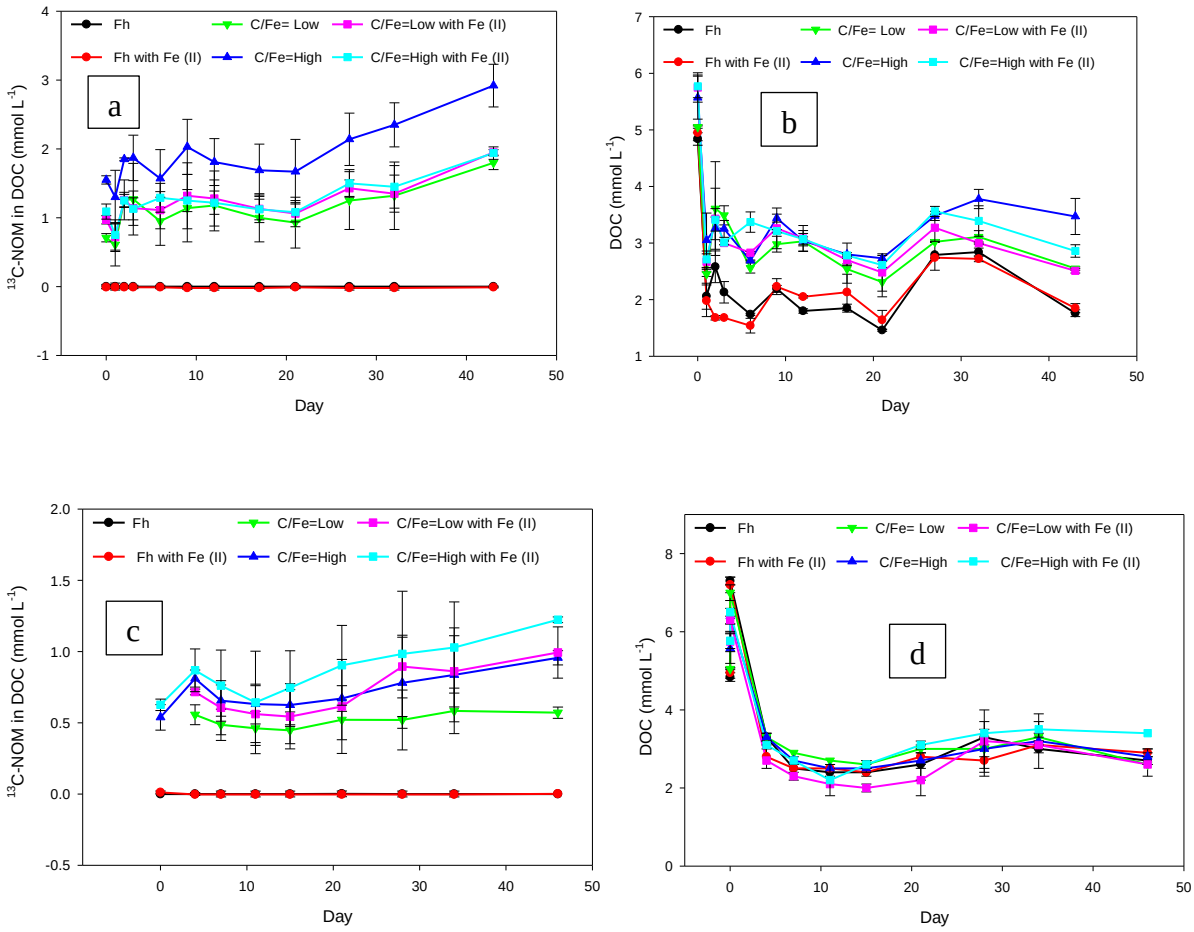

Figure 4.2: Added ^{13}C-NOM in DOC and total DOC in Fresh (a, b) and Aged (c, d) biotic reactors.

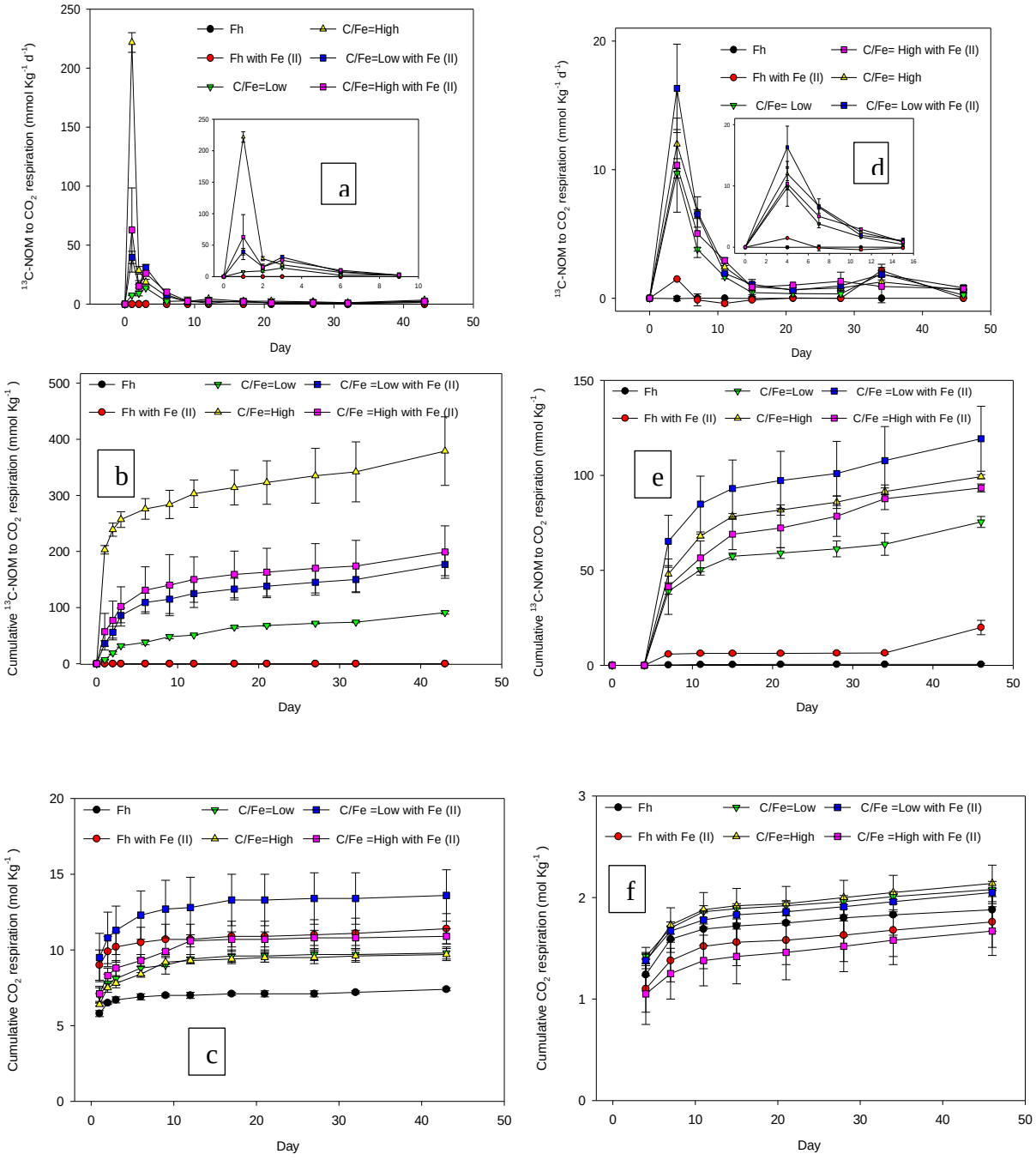

Figure 4.3: Added ^{13}C-NOM mineralization as CO_2 -C, cumulative ^{13}C-NOM and Cumulative CO_2 respiration from the Fresh (a, b, c) and Aged (d, e, f) biotic reactors, respectively.

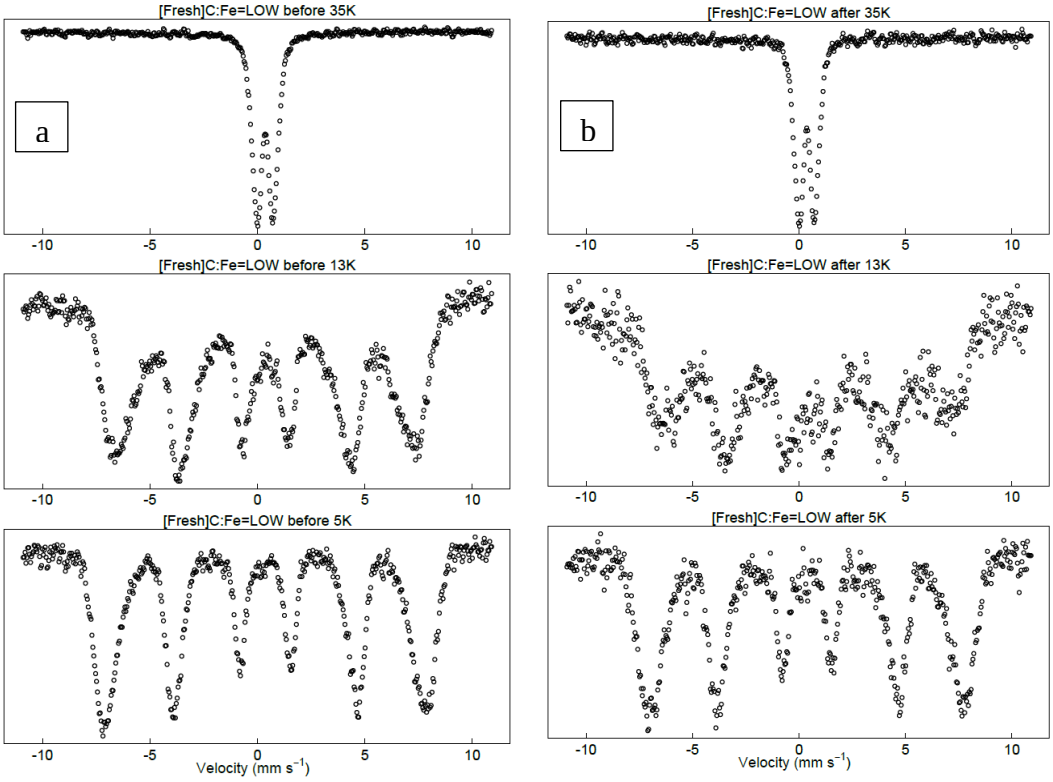
[Fresh]C:Fe=LOW before 35K
a
[Fresh]C:Fe=LOW after 35K
b
[Fresh]C:Fe=LOW before 13K
[Fresh]C:Fe=LOW after 13K
[Fresh]C:Fe=LOW before 5K
[Fresh]C:Fe=LOW after 5K
-10
-5
0
5
10
Velocity (mm s^{-1})

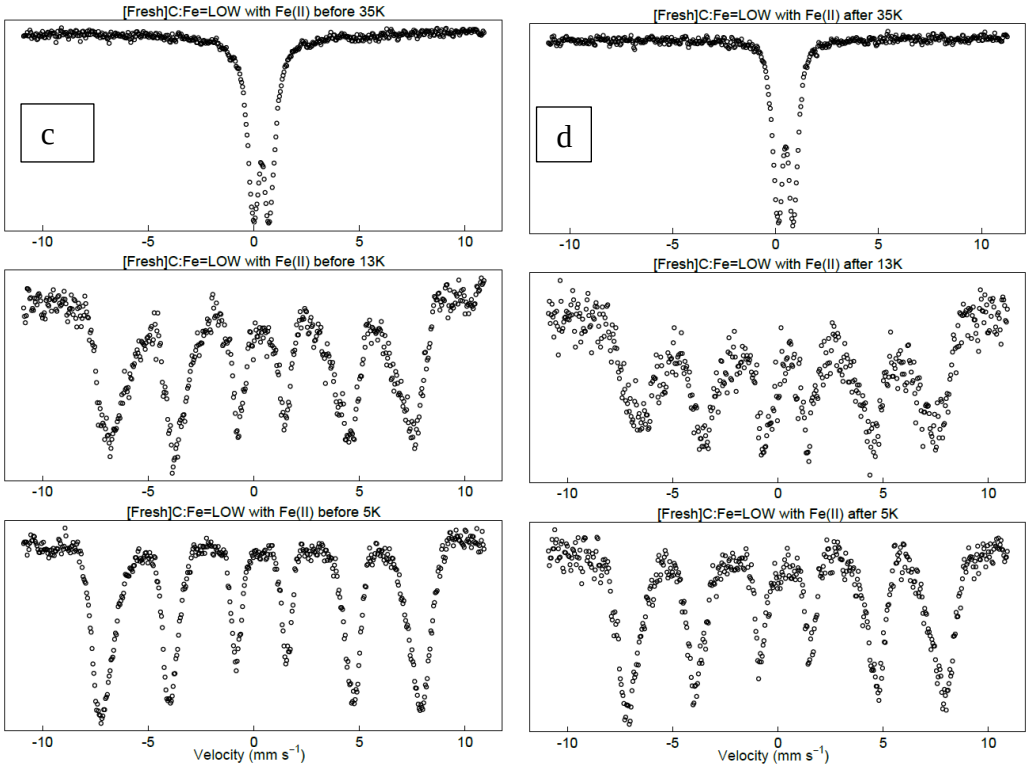
[Fresh]C:Fe=LOW with Fe(II) before 35K
c
[Fresh]C:Fe=LOW with Fe(II) after 35K
d
[Fresh]C:Fe=LOW with Fe(II) before 13K
[Fresh]C:Fe=LOW with Fe(II) after 13K
[Fresh]C:Fe=LOW with Fe(II) before 5K
[Fresh]C:Fe=LOW with Fe(II) after 5K
-10
-5
0
5
10
Velocity (mm s^{-1})

Figure 4.4: Mössbauer spectra (at 35K, 13K, and 5K) of before and after incubation solids of Fresh Low C/Fe unreacted (a,b) and Fe(II) reacted (c,d) coprecipitates.

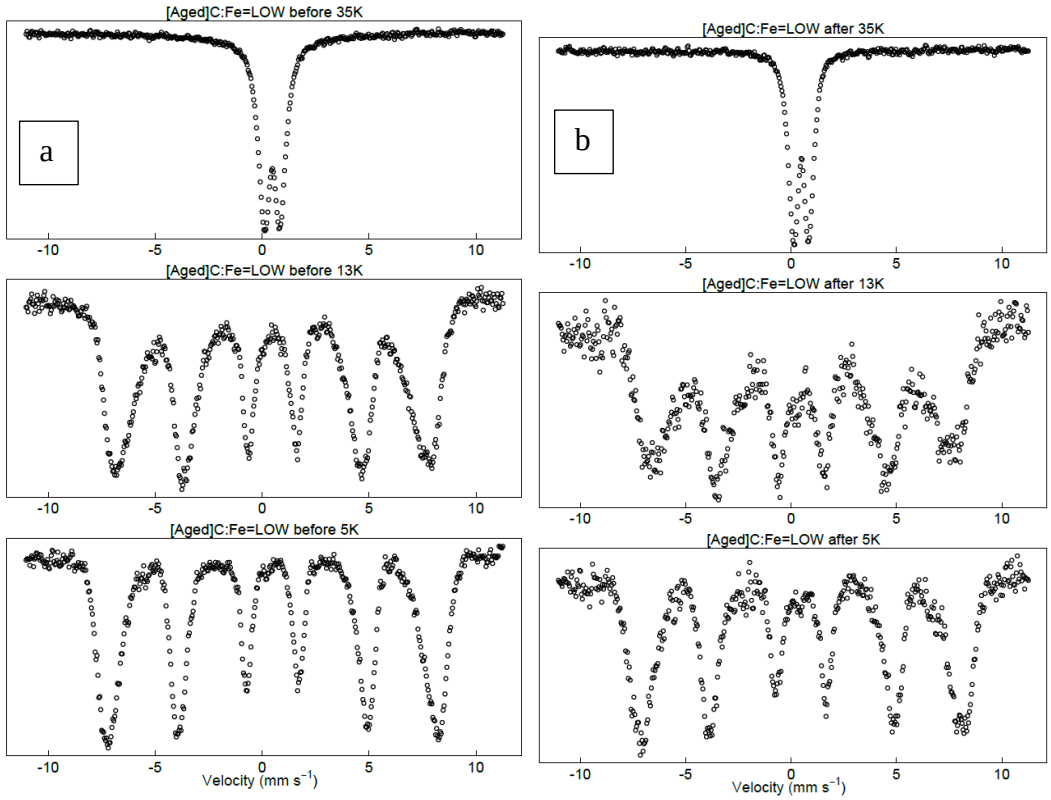
[Aged]C:Fe=LOW before 35K
a
[Aged]C:Fe=LOW after 35K
b
[Aged]C:Fe=LOW before 13K
[Aged]C:Fe=LOW after 13K
[Aged]C:Fe=LOW before 5K
[Aged]C:Fe=LOW after 5K
-10
-5
0
5
10
Velocity (mm s^{-1})

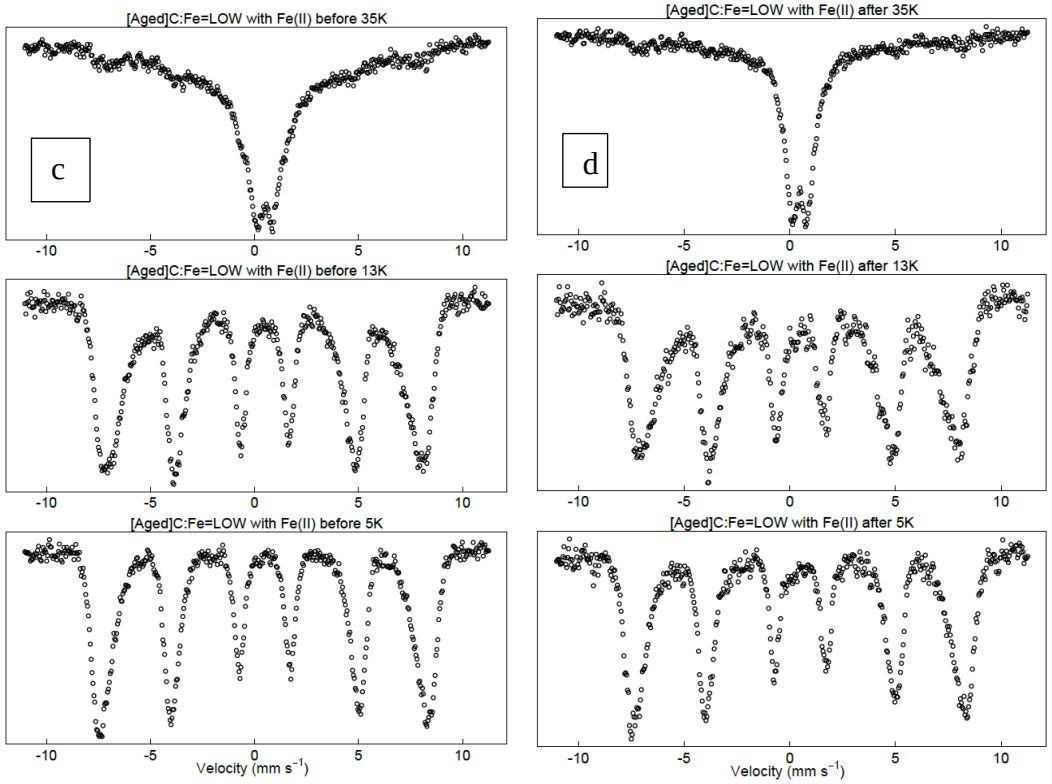
[Aged]C:Fe=LOW with Fe(II) before 35K
c
[Aged]C:Fe=LOW with Fe(II) after 35K
d
[Aged]C:Fe=LOW with Fe(II) before 13K
[Aged]C:Fe=LOW with Fe(II) after 13K
[Aged]C:Fe=LOW with Fe(II) before 5K
[Aged]C:Fe=LOW with Fe(II) after 5K
-10
-5
0
5
10
Velocity (mm s^{-1})

Figure 4.5: Mössbauer spectra (at 35K, 13K, and 5K) of before and after incubation solids of Aged Low C/Fe unreacted (a,b) and Fe(II) reacted (c,d) coprecipitates.

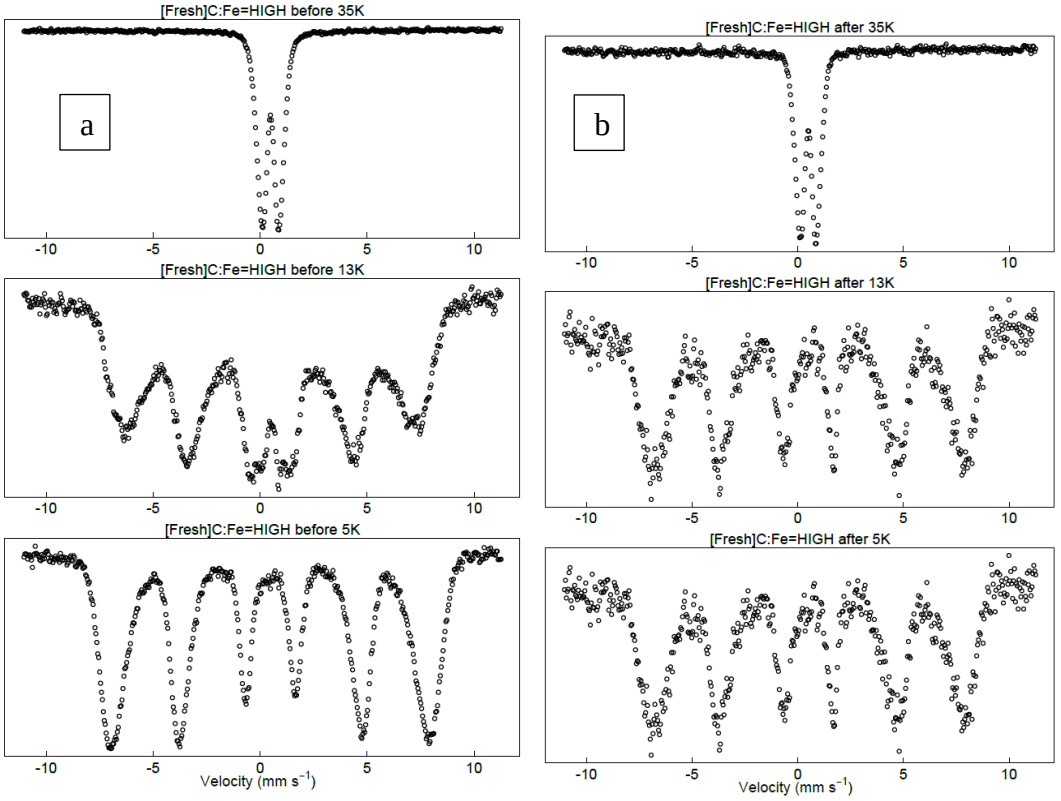
[Fresh]C:Fe=HIGH before 35K
a
[Fresh]C:Fe=HIGH after 35K
b
[Fresh]C:Fe=HIGH before 13K
[Fresh]C:Fe=HIGH after 13K
[Fresh]C:Fe=HIGH before 5K
[Fresh]C:Fe=HIGH after 5K
-10
-5
0
5
10
Velocity (mm s^{-1})

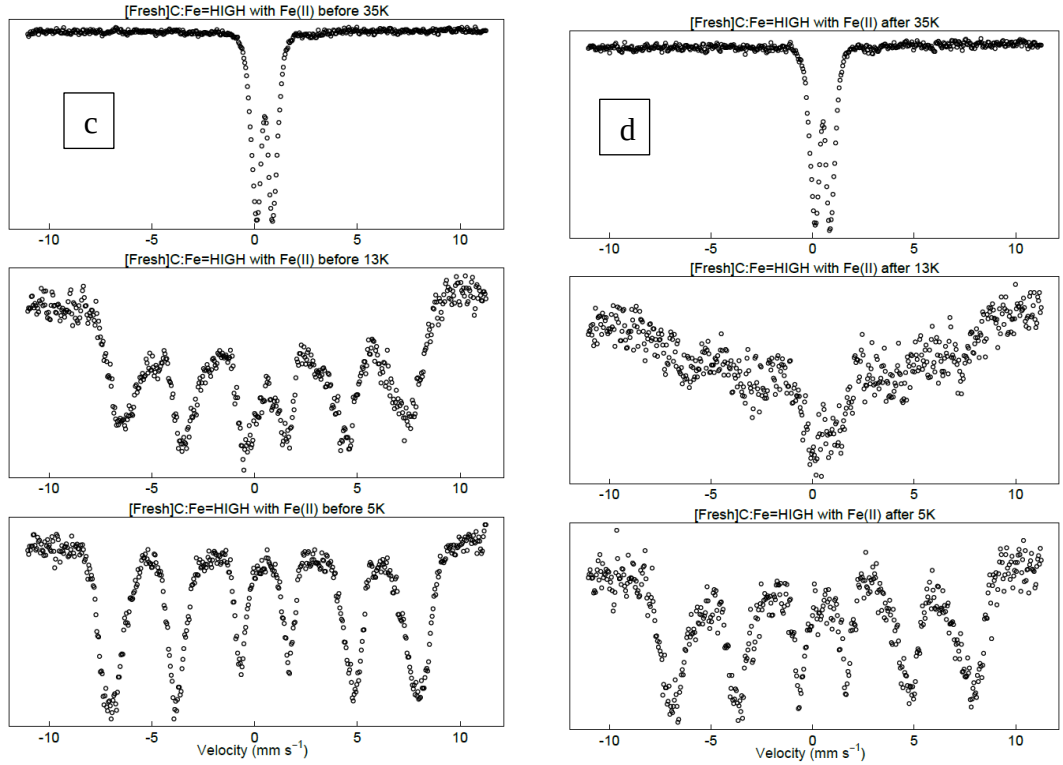
[Fresh]C:Fe=HIGH with Fe(II) before 35K
c
[Fresh]C:Fe=HIGH with Fe(II) after 35K
d
[Fresh]C:Fe=HIGH with Fe(II) before 13K
[Fresh]C:Fe=HIGH with Fe(II) after 13K
[Fresh]C:Fe=HIGH with Fe(II) before 5K
[Fresh]C:Fe=HIGH with Fe(II) after 5K
-10
-5
0
5
10
Velocity (mm s^{-1})

Figure 4.6: Mössbauer spectra (at 35K, 13K, and 5K) of before and after incubation solids of Fresh High C/Fe unreacted (a,b) and Fe(II) reacted (c,d) coprecipitates.

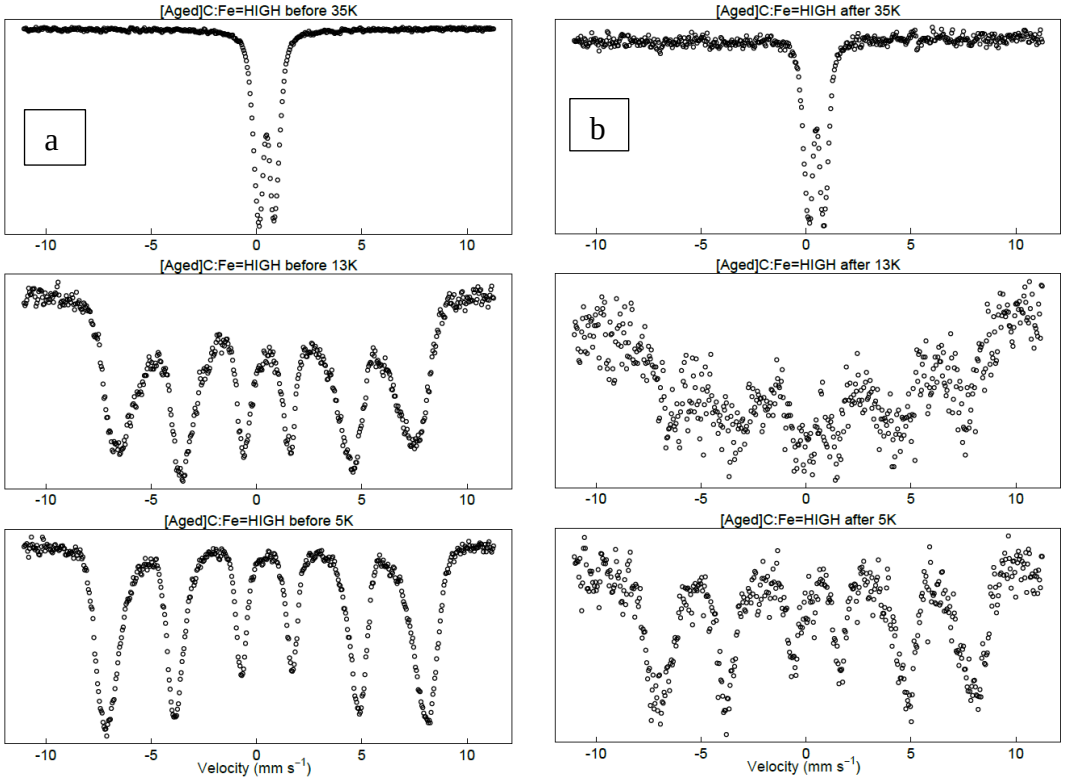
[Aged]C:Fe=HIGH before 35K
a
[Aged]C:Fe=HIGH after 35K
b
[Aged]C:Fe=HIGH before 13K
[Aged]C:Fe=HIGH after 13K
[Aged]C:Fe=HIGH before 5K
[Aged]C:Fe=HIGH after 5K
-10
-5
0
5
10
Velocity (mm s^{-1})

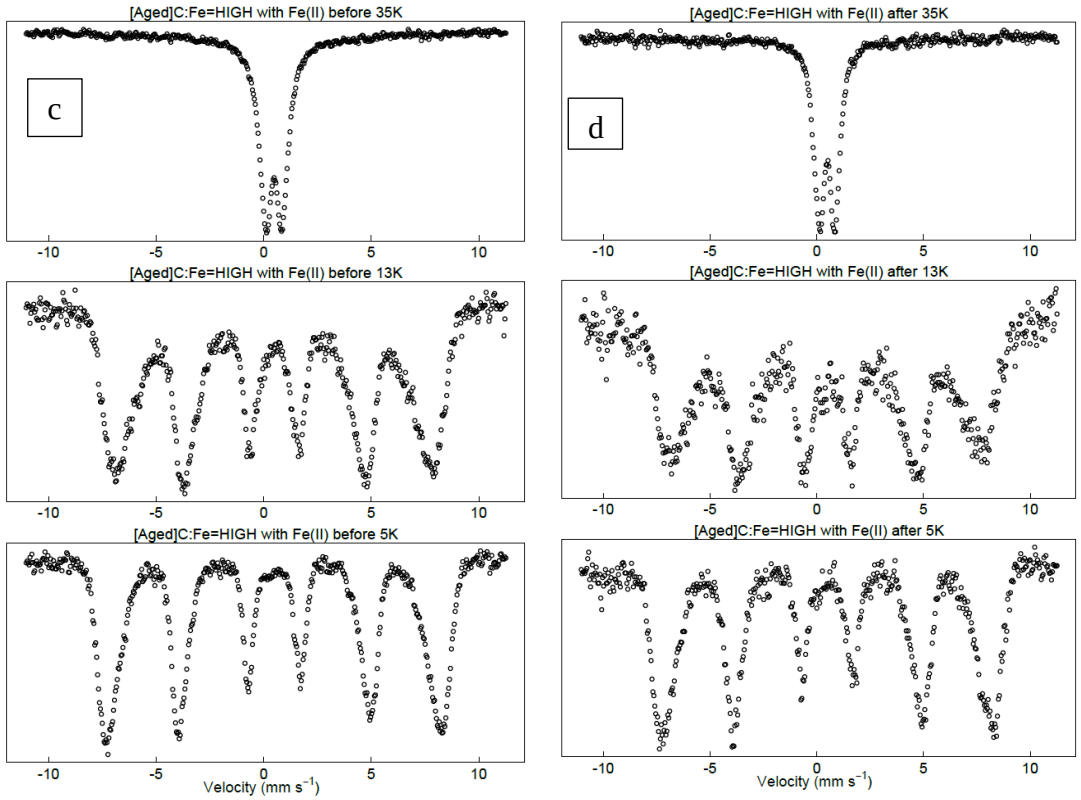
[Aged]C:Fe=HIGH with Fe(II) before 35K
c
[Aged]C:Fe=HIGH with Fe(II) after 35K
d
[Aged]C:Fe=HIGH with Fe(II) before 13K
[Aged]C:Fe=HIGH with Fe(II) after 13K
[Aged]C:Fe=HIGH with Fe(II) before 5K
[Aged]C:Fe=HIGH with Fe(II) after 5K
-10
-5
0
5
10
Velocity (mm s^{-1})

Figure 4.7: Mössbauer spectra (at 35K, 13K, and 5K) of before and after incubation solids of Aged High C/Fe unreacted (a,b) and Fe(II) reacted (c,d) coprecipitates.

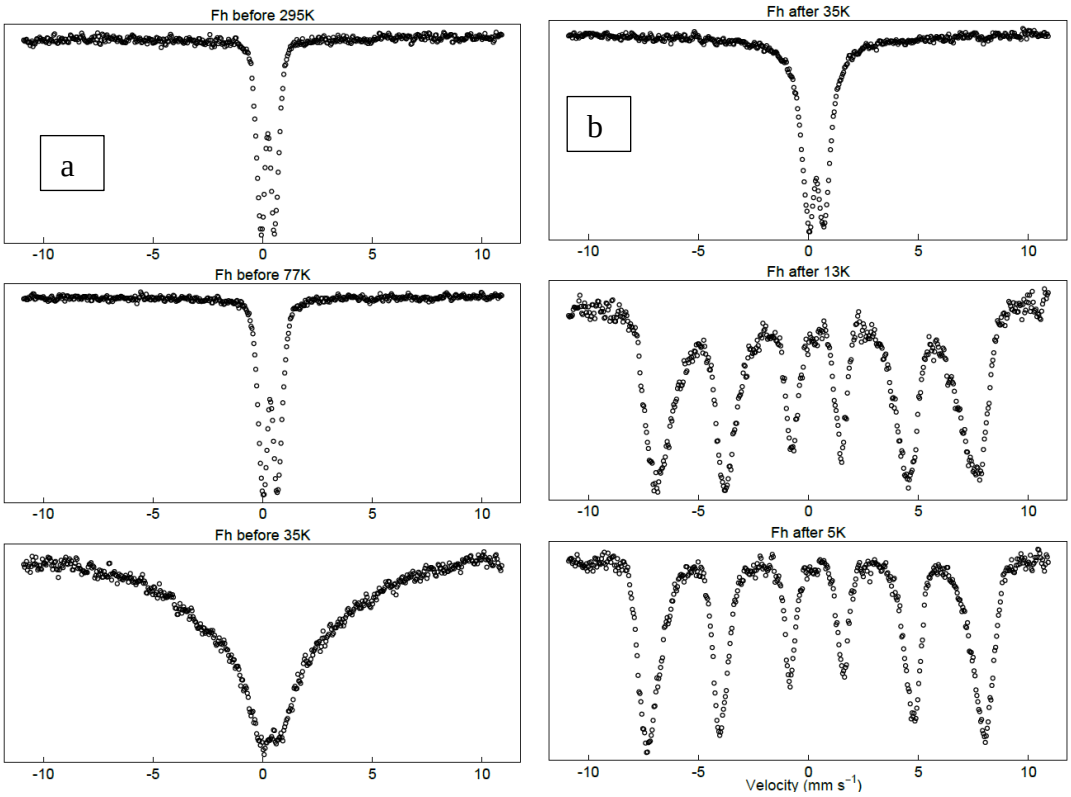

Figure 4.8: Mössbauer spectra (at 35K, 13K, and 5K) of before (a) and after(b) incubation solids of Fresh Fh.

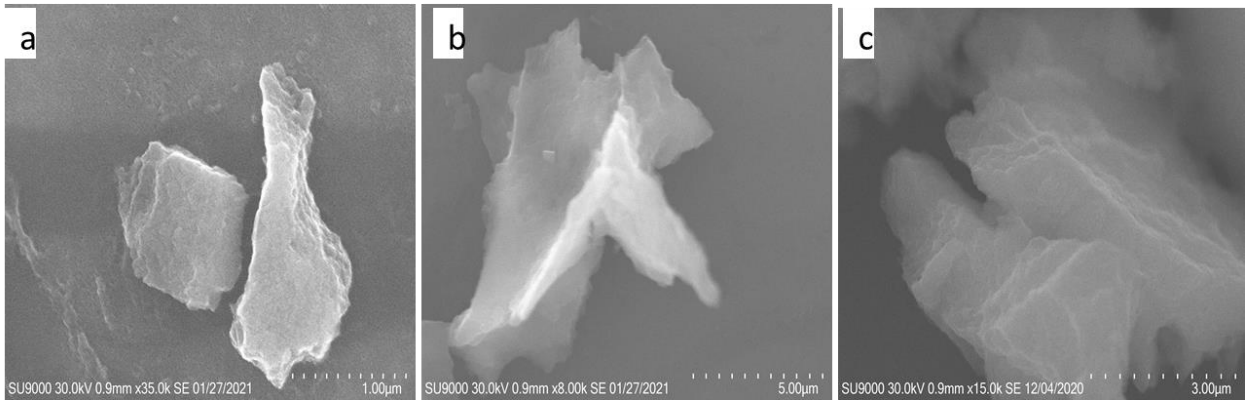

Figure 4.9: STEM image of Fresh Low C/Fe molar coprecipitates before (a,b) and after (c) incubation.

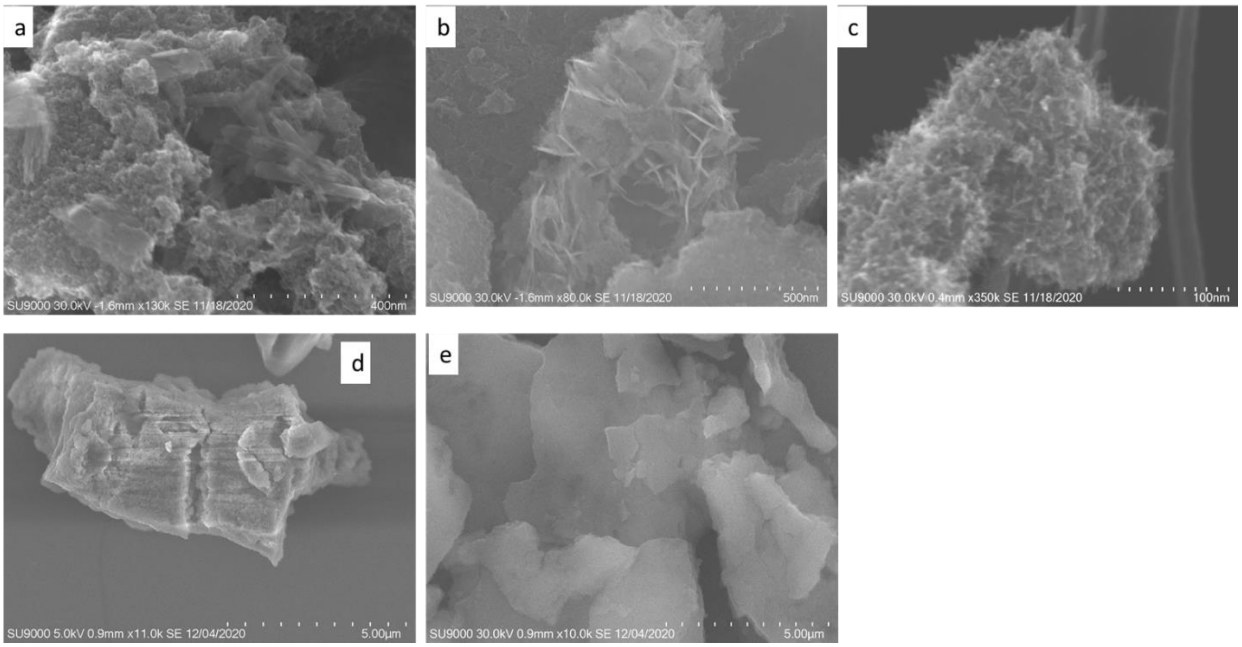

Figure 4.10: STEM image of Fresh Low C/Fe with Fe(II) reacted coprecipitates before (a-c) and after (d, e) incubation.

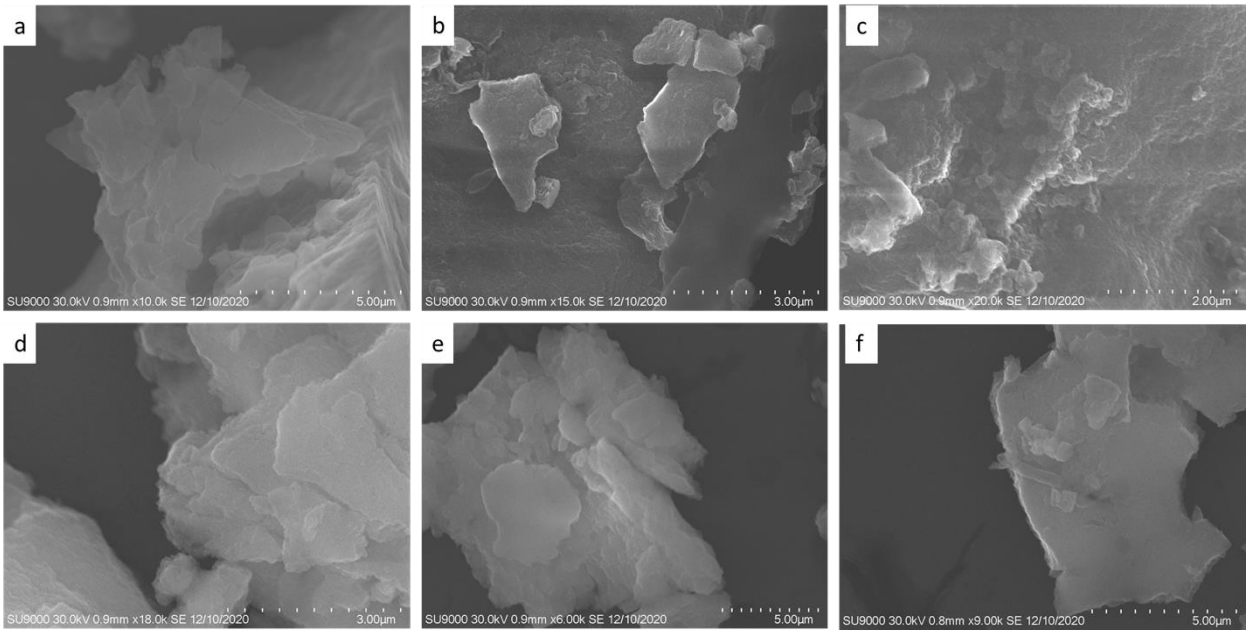

Figure 4.11: STEM image of Aged Low C/Fe with Fe(II) reacted coprecipitates before (a-c) and after (d-f) incubation.

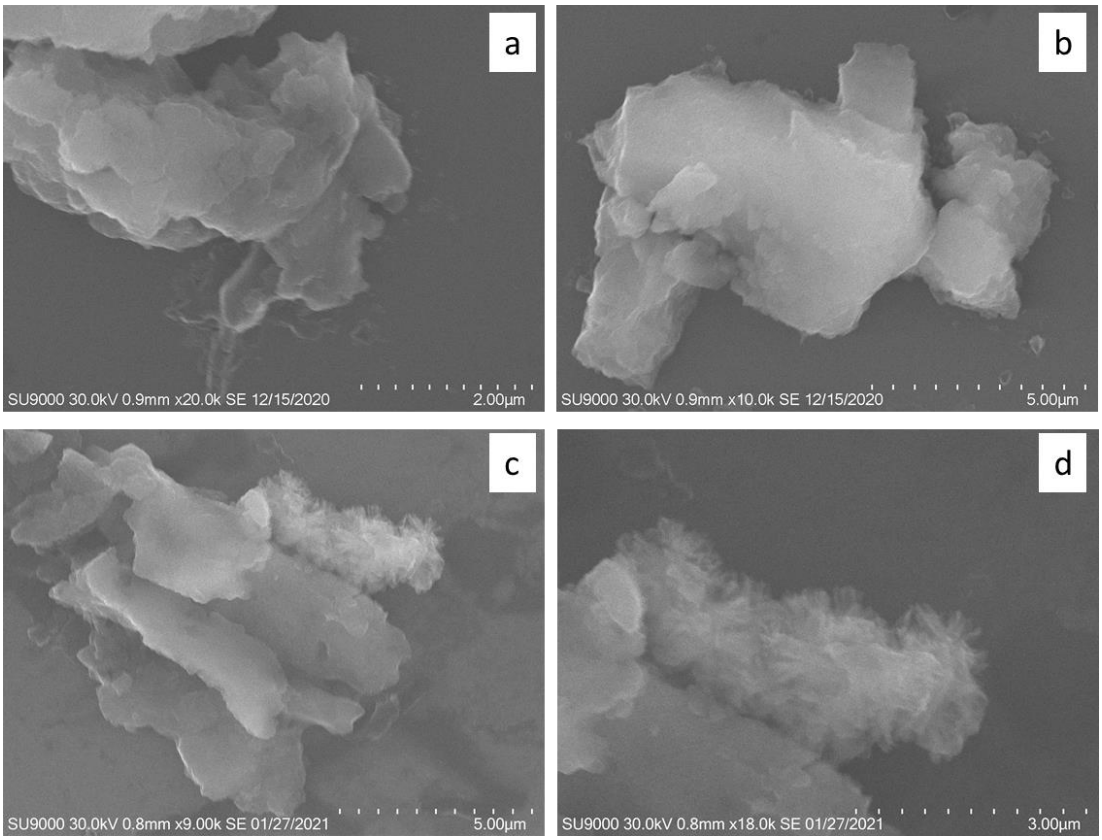

Figure 4.12: STEM image of Fresh High C/Fe coprecipitates before (a,b) and after (c,d) incubation.

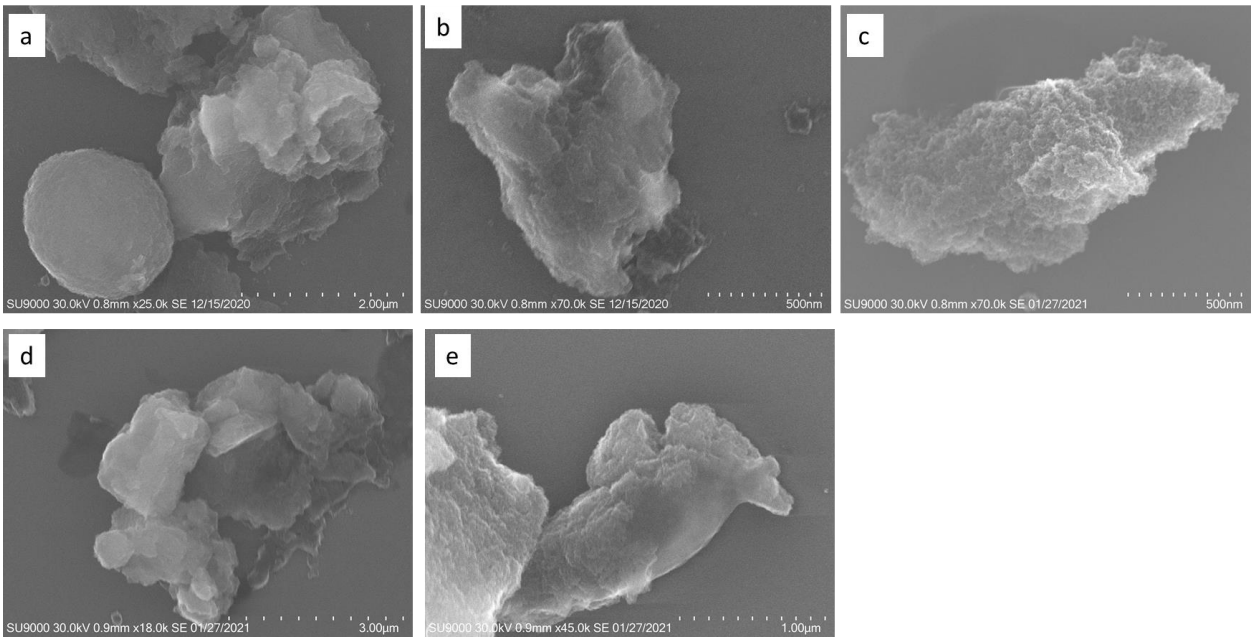

Figure 4.13: STEM image of Fresh High C/Fe with Fe(II) reacted coprecipitates before (a,b) and after (c-e) incubation.

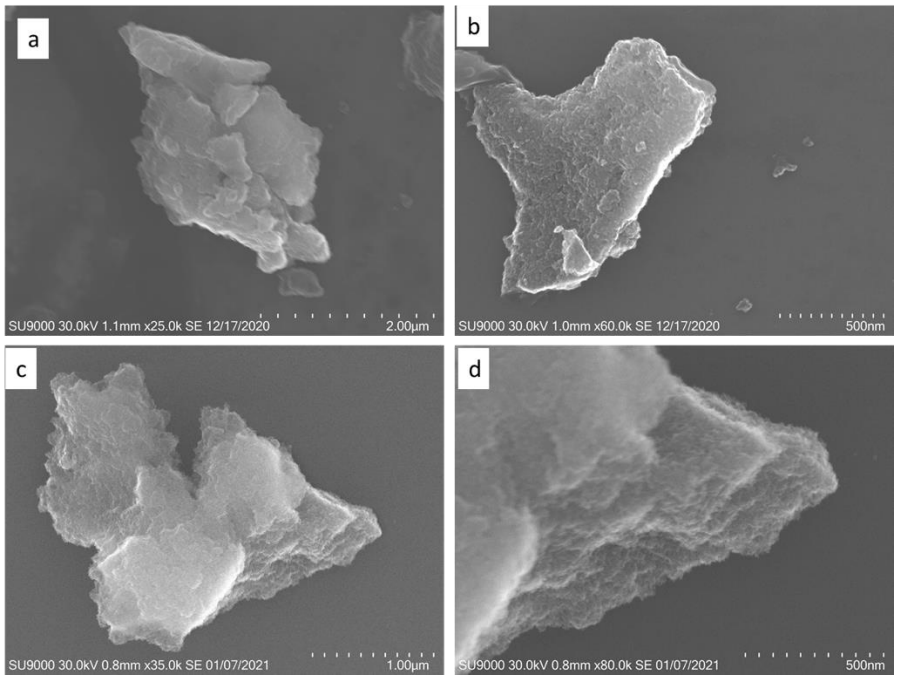

Figure 4.14: STEM image of Aged High C/Fe before (a,b) and after (c,d) incubation.

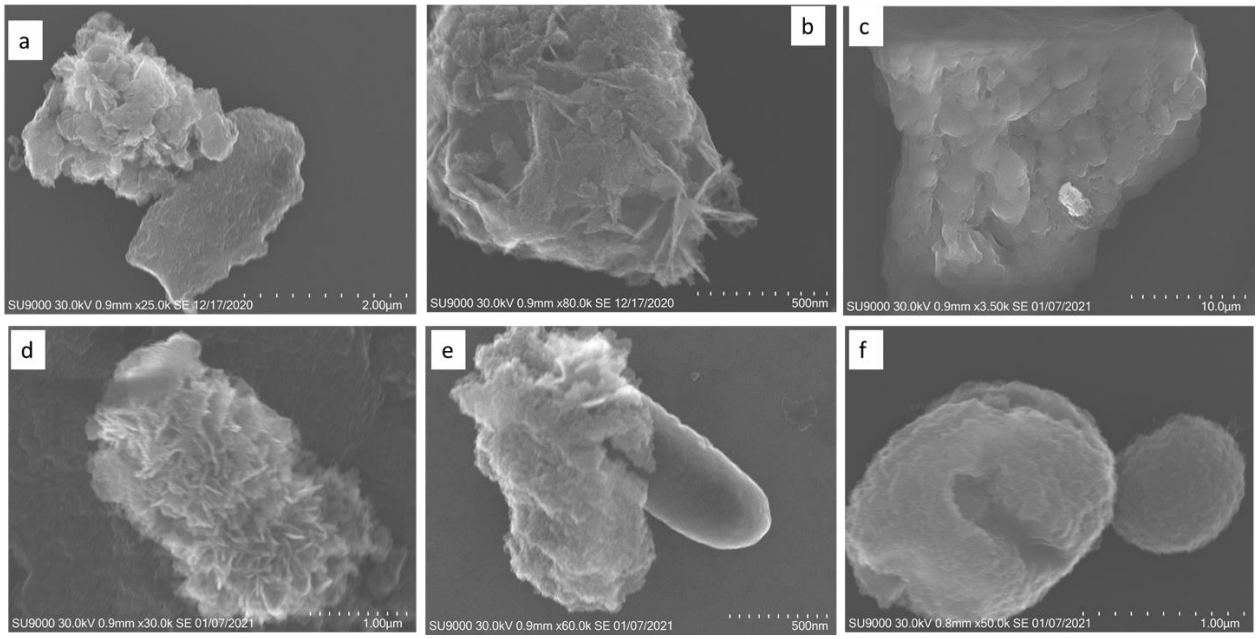

Figure 4.15: STEM image of Aged High C/Fe with Fe(II) reacted coprecipitates before (a,b) and after (c-f) incubation.

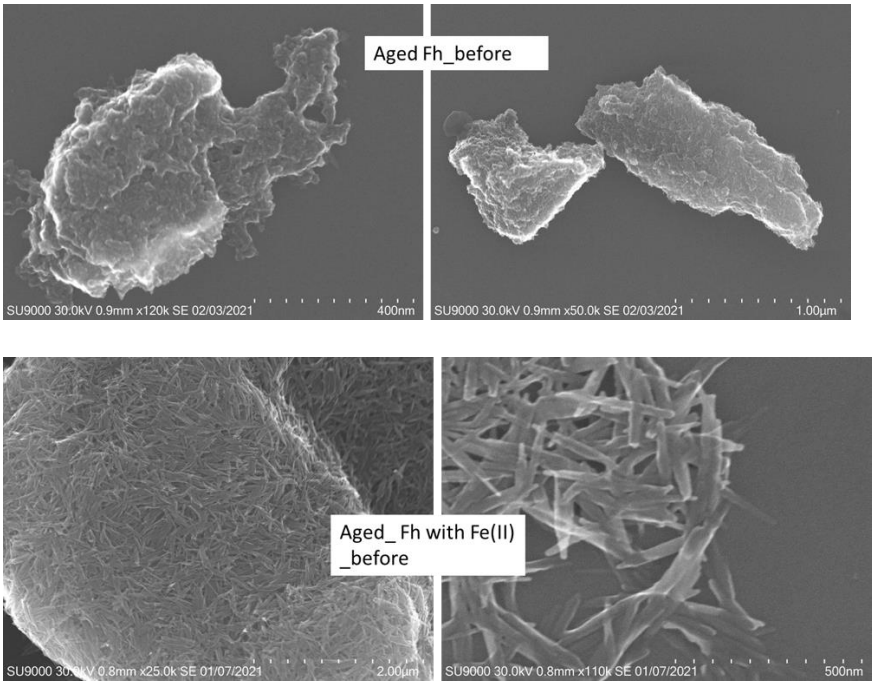

Figure 4.16: STEM image of Aged Fh mineral before and after reacted with Fe(II).

Table 4.1: Change in C/Fe molar ratio of the Fe(II) reacted and unreacted coprecipitates after 1d (Fresh) and 14d (Aged). The initial C/Fe indicates the synthesised C/Fe molar ratio of the coprecipitates.

Treatment	**Initial C/Fe**	**C/Fe After reaction**	
		Fresh	Aged
Low C/Fe	0.8	0.9	0.5
Low C/Fe with Fe(II)	0.8	1.0	0.5
High C/Fe	1.8	1.8	0.7
High C/Fe with Fe(II)	1.8	1.7	0.7

CHAPTER 5

CONCLUSION

Summary

This work shows new evidence regarding the change in the Ferrihydrite-Natural organic matter (Fh-NOM) coprecipitates following reaction with Fe(II) and its impact on the stability of the associated organic matter (OM). In this work, the bioavailability of organic carbon (OC) from the Fe(II) reacted Fh-NOM has been measured. To demonstrate the effect of Fe(II) reaction on the Fh-NOM coprecipitate and its impact on the bioavailability of OC, I conducted laboratory studies using synthesized Fh-NOM coprecipitates. Along with that I also measured the bioavailability of OC from the naturally occurring bacteriogenic iron(oxyhydrr)oxides (BIOS) and also the release of associated heavy metals (appendix).

In the first experiment, I measured the bioavailability of OC from Ferrihydrite-Suwannee river natural organic matter (Fh-SRNOM) with a C/Fe molar ratio of 1.2 reacted with Fe(II) for 1, 7, and 14 days. I found that the reaction with Fe(II) decreased the bioavailability of OC relative to unreacted controls, but primarily in the freshly Fe(II) reacted samples (1 day). I separately assessed the thermodynamic stability of the OC in the 1 day reacted coprecipitates, but found no discernable difference from the controls. In this experiment labeled lactate was added to ensure the growth of the microbial community and all the solid sample sorbed a small amount of added lactate regardless of the treatments. This raised a question regarding the impact of Fe(II) reaction on the coprecipitates crystallinity of structure. The microbial community used the added lactate for the first few days but after that, they continued using the coprecipitate C as their food source.

In the 2nd experiment, I further investigated the impact of the Fe(II) reaction of the coprecipitates crystallinity and structure, I focused on changes in the Fh-NOM coprecipitates occurring during the reaction with Fe(II). I conducted a 2nd laboratory experiment where this time Ferrihydrite-Natural organic matter (Fh-NOM) coprecipitates were synthesized using an isotopically-labeled NOM (^{13}C) and then reacted with Fe(II) for 1 and 14 days. Here I found that reaction with Fe(II) drove localized increases in Fh crystallinity without complete mineral transformation in the low C/Fe molar coprecipitate after 1 day reaction. This process also resulted in the partial release of coprecipitated C. This localized change in crystallinity also occurred in the high C/Fe molar ratio coprecipitate when they lost a substantial amount of coprecipitated C after reacting with Fe(II) during longer reaction time (i.e. in our study 14days). This study also demonstrated that the coprecipitated OM composition can be exchanged readily with OC from the media.

In the third experiment, I measured the bioavailability of the OM in the Fh-NOM coprecipitates studied in the 2nd experiment. Here I found that during the microbial incubation assay, the Fe(II) reacted coprecipitate lost less OM than the unreacted coprecipitate with again the freshly reacted (1 day) coprecipitates retaining the most of their initial coprecipitated C. The result also suggested that a small amount of coprecipitated was mineralized as CO_2 and most of the released coprecipitated C remained in the solution. This could result from the continuous interaction between the released coprecipitated C and the solid surface making the C unavailable for the microbial inoculum to use as a food source. In addition, the crystallinity of the Fe(II) reacted coprecipitates decreased during the incubation, likely because of the sorption of OC from the solution.

A fourth experiment was conducted and partially analyzed (Appendix A) to compare the bioavailability of the C from the synthesized coprecipitates with natural coprecipitates. In this experiment, I collected some bacteriogenic iron (oxyhydr)oxides (BIOS), which contained OM, and conducted a similar microbial incubation to evaluate the OM bioavailability. I found that the BIOS OC was retained better than the synthesized Fh-NOM coprecipitates OC. Further, I found that the BIOS sorbed less OC from the solution than the coprecipitate and did not change crystallinity or crystal morphology during the incubation. Finally, I also measured the release of heavy metals during the aerobic microbial incubation and found of the initial metals in the BIOS, 10% of the Zn and 4% of the Cu released, whereas the release of other heavy metals such as Ni, Pb, Cr, As, Al were less than 1% of the original abundances.

Environmental implications

Due to the increasing atmospheric CO_2 concentration and growing concern regarding climate change, the stabilization of C in the soil is receiving increasing interest. Among different C stabilization mechanisms, the association of OM with minerals is considered a key mechanism reducing the amount of microbial decomposition. The high abundance of Iron oxide minerals especially short ranged ordered (SRO) Ferrihydrite (Fh) mineral and its ability to adsorb dissolved organic matter (DOM) introduced a general assumption that Fh mineral stabilizes C in the soil. But the redox sensitivity of the iron oxide minerals and multiplicity of interaction among the Fe(III) in the mineral and Fe(II) in the solution can have a significant impact on the mineral associated OM. Although there have been detailed studies conducted regarding the dissimilatory iron reduction under reducing conditions and the resulting impact on the associated C, a few studies have been conducted regarding the bioavailability of iron mineral associated C under aerobic conditions. Moreover, there have been no studies conducted to assess the bioavailability of C from

the iron oxide mineral-organic matter associations after reacting with Fe(II). Therefore, this study introduces a new insight into the stability of C in the soil.

Overall, my study provides further understanding of how complex and dynamic the interaction of iron mineral -organic matter association with Fe(II) can be. This complex interaction can impact the stabilization of C in soil. My study demonstrated that under anoxic conditions the interaction of Fe(II) with the Fe(III) minerals can cause localized morphological changes and increase the crystallinity of the Fh minerals. This process can result in the release of associated C from the coprecipitate and also change the C composition in the coprecipitate by exchanging C with the surrounding C sources. Later should these coprecipitates become subjected to oxic conditions they are likely to protect the mineral associated C from microbial degradation better than non-Fe(II) reacted coprecipitates. This finding will help us understand how the C stabilization potential of soil might change when exposed to redox dynamics. Moreover, our study also suggests the crystallinity of Fe(II) reacted Fh-NOM coprecipitates decreases after microbial incubation. Although our study was conducted in a liquid media instead of dry conditions, if a similar situation prevails in the soil then this decreasing crystallinity i.e. increasing the surface area of the Fh-NOM coprecipitate can have an impact on other biogeochemical processes occurring in the soil such as heavy metal or nutrient cycling.

REFERENCES

Adhikari, D., Dunham-Cheatham, S. M., Wordofa, D. N., Verburg, P., Poulson, S. R., & Yang, Y. (2019). Aerobic respiration of mineral-bound organic carbon in a soil. *Science of the Total Environment, 651*, 1253-1260.

Adhikari, D., Poulson, S. R., Sumaila, S., Dynes, J. J., McBeth, J. M., & Yang, Y. (2016). Asynchronous reductive release of iron and organic carbon from hematite–humic acid complexes. *Chemical Geology, 430*, 13-20.

Ascenso, L., d'Amore, F., Carvalho, A., & Bezzo, F. (2018). Assessing multiple biomass-feedstock in the optimization of power and fuel supply chains for sustainable mobility. *Chemical Engineering Research and Design, 131*, 127-143.

Berquó, T. S., Banerjee, S. K., Ford, R. G., Penn, R. L., & Pichler, T. (2007). High crystallinity Si-ferrihydrite: An insight into its Néel temperature and size dependence of magnetic properties. *Journal of Geophysical Research: Solid Earth, 112*(B2).

Berquó, T. S., Erbs, J. J., Lindquist, A., Penn, R. L., & Banerjee, S. K. (2009). Effects of magnetic interactions in antiferromagnetic ferrihydrite particles. *Journal of Physics: Condensed Matter, 21*(17), 176005.

Boland, D. D., Collins, R. N., Miller, C. J., Glover, C. J., & Waite, T. D. (2014). Effect of solution and solid-phase conditions on the Fe (II)-accelerated transformation of ferrihydrite to lepidocrocite and goethite. *Environmental science & technology, 48*(10), 5477-5485.

Bruun, A.-M., Finster, K., Gunnlaugsson, H. P., N∅ rnberg, P., & Friedrich, M. W. (2010). A comprehensive investigation on iron cycling in a freshwater seep including microscopy, cultivation and molecular community analysis. *Geomicrobiology Journal, 27*(1), 15-34.

Bussan, A. L., & Strathmann, T. J. (2007). Influence of organic ligands on the reduction of polyhalogenated alkanes by iron (II). *Environmental science & technology, 41*(19), 6740-6747.

Catalano, J. G., Fenter, P., Park, C., Zhang, Z., & Rosso, K. M. (2010). Structure and oxidation state of hematite surfaces reacted with aqueous Fe (II) at acidic and neutral pH. *Geochimica et Cosmochimica Acta, 74*(5), 1498-1512.

Chan, C. S., De Stasio, G., Welch, S. A., Girasole, M., Frazer, B. H., Nesterova, M. V., Fakra, S., & Banfield, J. F. (2004). Microbial polysaccharides template assembly of nanocrystal fibers. *science, 303*(5664), 1656-1658.

Chan, C. S., Fakra, S. C., Edwards, D. C., Emerson, D., & Banfield, J. F. (2009). Iron oxyhydroxide mineralization on microbial extracellular polysaccharides. *Geochimica et Cosmochimica Acta, 73*(13), 3807-3818.

Chen, C., Dynes, J. J., Wang, J., & Sparks, D. L. (2014). Properties of Fe-organic matter associations via coprecipitation versus adsorption. *Environmental science & technology, 48*(23), 13751-13759.

Chen, C., Hall, S. J., Coward, E., & Thompson, A. (2020). Iron-mediated organic matter decomposition in humid soils can counteract protection. *Nature communications, 11*(1), 1-13.

Chen, C., Kukkadapu, R., & Sparks, D. L. (2015). Influence of Coprecipitated Organic Matter on Fe2+ (aq)-Catalyzed Transformation of Ferrihydrite: Implications for Carbon Dynamics. *Environmental science & technology, 49*(18), 10927-10936.

Chen, C., & Sparks, D. L. (2018). Fe (II)-induced mineral transformation of ferrihydrite–organic matter adsorption and co-precipitation complexes in the absence and presence of As (III). *ACS Earth and Space Chemistry, 2*(11), 1095-1101.

Cheng, L., Zhu, J., Chen, G., Zheng, X., Oh, N. H., Rufty, T., Richter, D. d., & Hu, S. (2010). Atmospheric CO2 enrichment facilitates cation release from soil. *Ecology Letters, 13*(3), 284-291.

Chesworth, W. (2007). *Encyclopedia of soil science*. Springer Science & Business Media.

Christensen, B. T. (1996). Carbon in primary and secondary organomineral complexes. In *Structure and organic matter storage in agricultural soils* (Vol. 27, pp. 97-165). CRC Press Boca Raton, FL.

Ciais, P., Sabine, C., Bala, G., Bopp, L., Brovkin, V., Canadell, J., Chhabra, A., DeFries, R., Galloway, J., & Heimann, M. (2013). Climate change 2013: the physical science basis. Contribution of Working Group I to the Fifth Assessment Report of the Intergovernmental Panel on Climate Change. *K., Tignor, M., Allen, SK, Boschung, J., Nauels, A., Xia, Y., Bex, V., Midgley, PM, Eds*.

Cismasu, A. C., Michel, F. M., Tcaciuc, A. P., Tyliszczak, T., & Brown Jr, G. E. (2011). Composition and structural aspects of naturally occurring ferrihydrite. *Comptes Rendus Geoscience, 343*(2-3), 210-218.

Coleman, D., & Elliot, E. (1988). Let the soil work for us. *Ecol Bull, 39*, 23-32.

Compositions, E. Stable Isotopic Ratios of IHSS Samples. *IHSS-Natural Organic Matter Research*.

Cornell, R., & Schneider, W. (1989). Formation of goethite from ferrihydrite at physiological pH under the influence of cysteine. *Polyhedron, 8*(2), 149-155.

Cornell, R. M., & Schwertmann, U. (2003). *The iron oxides: structure, properties, reactions, occurrences and uses*. John Wiley & Sons.

Coughlin, B. R., & Stone, A. T. (1995). Nonreversible adsorption of divalent metal ions (MnII, CoII, NiII, CuII, and PbII) onto goethite: effects of acidification, FeII addition, and picolinic acid addition. *Environmental science & technology, 29*(9), 2445-2455.

Daugherty, E. E., Gilbert, B., Nico, P. S., & Borch, T. (2017). Complexation and redox buffering of iron (II) by dissolved organic matter. *Environmental science & technology, 51*(19), 11096-11104.

De-Campos, A. B., Huang, C.-h., & Johnston, C. T. (2012). Biogeochemistry of terrestrial soils as influenced by short-term flooding. *Biogeochemistry, 111*(1), 239-252.

Druschel, G. K., Emerson, D., Sutka, R., Suchecki, P., & Luther III, G. W. (2008). Low-oxygen and chemical kinetic constraints on the geochemical niche of neutrophilic iron (II) oxidizing microorganisms. *Geochimica et Cosmochimica Acta, 72*(14), 3358-3370.

Dubinsky, E. A., Silver, W. L., & Firestone, M. K. (2010). Tropical forest soil microbial communities couple iron and carbon biogeochemistry. *Ecology, 91*(9), 2604-2612.

Duckworth, O. W., Holmström, S. J., Peña, J., & Sposito, G. (2009). Biogeochemistry of iron oxidation in a circumneutral freshwater habitat. *Chemical Geology, 260*(3-4), 149-158.

Edwards, A. P., & Bremner, J. (1967). Microaggregates in soils 1. *Journal of Soil Science, 18*(1), 64-73.

Elliott, E. (1986). Aggregate structure and carbon, nitrogen, and phosphorus in native and cultivated soils. *Soil Science Society of America Journal, 50*(3), 627-633.

Emerson, D. (2019). Biogenic iron dust: a novel approach to ocean iron fertilization as a means of large scale removal of carbon dioxide from the atmosphere. *Frontiers in Marine Science, 6*, 22.

Emerson, D., Fleming, E. J., & McBeth, J. M. (2010). Iron-oxidizing bacteria: an environmental and genomic perspective. *Annual review of microbiology, 64*, 561-583.

Emerson, D., & Revsbech, N. P. (1994). Investigation of an iron-oxidizing microbial mat community located near Aarhus, Denmark: field studies. *Applied and environmental microbiology, 60*(11), 4022.

Emerson, D., & Weiss, J. V. (2004). Bacterial iron oxidation in circumneutral freshwater habitats: findings from the field and the laboratory. *Geomicrobiology Journal, 21*(6), 405-414.

Eusterhues, K., Neidhardt, J., Hädrich, A., Küsel, K., & Totsche, K. U. (2014a, 2014/06/01). Biodegradation of ferrihydrite-associated organic matter. *Biogeochemistry, 119*(1), 45-50. https://doi.org/10.1007/s10533-013-9943-0

Eusterhues, K., Neidhardt, J., Hädrich, A., Küsel, K., & Totsche, K. U. (2014b). Biodegradation of ferrihydrite-associated organic matter. *Biogeochemistry, 119*(1-3), 45-50.

Eusterhues, K., Rumpel, C., Kleber, M., & Kögel-Knabner, I. (2003). Stabilisation of soil organic matter by interactions with minerals as revealed by mineral dissolution and oxidative degradation. *Organic geochemistry, 34*(12), 1591-1600.

Eusterhues, K., Wagner, F. E., Häusler, W., Hanzlik, M., Knicker, H., Totsche, K. U., Kögel-Knabner, I., & Schwertmann, U. (2008). Characterization of ferrihydrite-soil organic matter coprecipitates by X-ray diffraction and Mossbauer spectroscopy. *Environmental science & technology, 42*(21), 7891-7897.

Feller, C., & Beare, M. (1997). Physical control of soil organic matter dynamics in the tropics. *Geoderma, 79*(1-4), 69-116.

Ferris, F. (2005). Biogeochemical properties of bacteriogenic iron oxides. *Geomicrobiology Journal, 22*(3-4), 79-85.

Ferris, F., Tazaki, K., & Fyfe, W. (1989). Iron oxides in acid mine drainage environments and their association with bacteria. *Chemical Geology, 74*(3-4), 321-330.

Fleming, E. J., Cetinić, I., Chan, C. S., King, D. W., & Emerson, D. (2014). Ecological succession among iron-oxidizing bacteria. *The ISME journal, 8*(4), 804-815.

Flemming, H.-C., & Wingender, J. (2010). The biofilm matrix. *Nature Reviews Microbiology, 8*(9), 623-633.

Fontaine, S., Barot, S., Barré, P., Bdioui, N., Mary, B., & Rumpel, C. (2007). Stability of organic carbon in deep soil layers controlled by fresh carbon supply. *Nature, 450*(7167), 277-280.

Fontaine, S., Mariotti, A., & Abbadie, L. (2003). The priming effect of organic matter: a question of microbial competition? *Soil Biology and Biochemistry, 35*(6), 837-843.

Fortin, D., & Langley, S. (2005). Formation and occurrence of biogenic iron-rich minerals. *Earth-Science Reviews, 72*(1-2), 1-19.

Franke, C., Kissel, C., Robin, E., Bonté, P., & Lagroix, F. (2009). Magnetic particle characterization in the Seine river system: Implications for the determination of natural versus anthropogenic input. *Geochemistry, Geophysics, Geosystems, 10*(8).

Géhin, A., Greneche, J.-M., Tournassat, C., Brendle, J., Rancourt, D. G., & Charlet, L. (2007). Reversible surface-sorption-induced electron-transfer oxidation of Fe (II) at reactive sites on a synthetic clay mineral. *Geochimica et Cosmochimica Acta, 71*(4), 863-876.

Geiss, C. E., Egli, R., & Zanner, C. W. (2008). Direct estimates of pedogenic magnetite as a tool to reconstruct past climates from buried soils. *Journal of Geophysical Research: Solid Earth, 113*(B11).

Gentsch, N., Mikutta, R., Shibistova, O., Wild, B., Schnecker, J., Richter, A., Urich, T., Gittel, A., Šantrůčková, H., & Bárta, J. (2015). Properties and bioavailability of particulate and mineral-associated organic matter in A rctic permafrost soils, L ower K olyma R egion, R ussia. *European Journal of Soil Science, 66*(4), 722-734.

Ginn, B. R., Habteselassie, M. Y., Meile, C., & Thompson, A. (2014). Effects of sample storage on microbial Fe-reduction in tropical rainforest soils. *Soil Biology and Biochemistry, 68*, 44-51.

Gorski, C. A., & Scherer, M. M. (2011). Fe2+ sorption at the Fe oxide-water interface: A revised conceptual framework. In *Aquatic Redox Chemistry* (pp. 315-343). ACS Publications.

Grybos, M., Davranche, M., Gruau, G., & Petitjean, P. (2007). Is trace metal release in wetland soils controlled by organic matter mobility or Fe-oxyhydroxides reduction? *Journal of Colloid and Interface Science, 314*(2), 490-501.

Grybos, M., Davranche, M., Gruau, G., Petitjean, P., & Pédrot, M. (2009). Increasing pH drives organic matter solubilization from wetland soils under reducing conditions. *Geoderma, 154*(1-2), 13-19.

Haaijer, S. C., Harhangi, H. R., Meijerink, B. B., Strous, M., Pol, A., Smolders, A. J., Verwegen, K., Jetten, M. S., & Den Camp, H. J. O. (2008). Bacteria associated with iron seeps in a sulfur-rich, neutral pH, freshwater ecosystem. *The ISME journal, 2*(12), 1231-1242.

Hall, S. J., Berhe, A. A., & Thompson, A. (2018). Order from disorder: do soil organic matter composition and turnover co-vary with iron phase crystallinity? *Biogeochemistry, 140*(1), 93-110.

Hammel, K. E., Kapich, A. N., Jensen Jr, K. A., & Ryan, Z. C. (2002). Reactive oxygen species as agents of wood decay by fungi. *Enzyme and microbial technology, 30*(4), 445-453.

Hansel, C. M., Benner, S. G., & Fendorf, S. (2005). Competing Fe (II)-induced mineralization pathways of ferrihydrite. *Environmental science & technology, 39*(18), 7147-7153.

Hansel, C. M., Benner, S. G., Neiss, J., Dohnalkova, A., Kukkadapu, R. K., & Fendorf, S. (2003). Secondary mineralization pathways induced by dissimilatory iron reduction of ferrihydrite under advective flow. *Geochimica et Cosmochimica Acta, 67*(16), 2977-2992.

Hassink, J. (1997). The capacity of soils to preserve organic C and N by their association with clay and silt particles. *Plant and soil, 191*(1), 77-87.

Henneberry, Y. K., Kraus, T. E., Nico, P. S., & Horwath, W. R. (2012). Structural stability of coprecipitated natural organic matter and ferric iron under reducing conditions. *Organic geochemistry, 48*, 81-89.

Hiemstra, T. (2015). Formation, stability, and solubility of metal oxide nanoparticles: Surface entropy, enthalpy, and free energy of ferrihydrite. *Geochimica et Cosmochimica Acta, 158*, 179-198.

Hiemstra, T. (2018). Surface structure controlling nanoparticle behavior: magnetism of ferrihydrite, magnetite, and maghemite. *Environmental Science: Nano, 5*(3), 752-764.

Hiemstra, T., Mendez, J. C., & Li, J. (2019). Evolution of the reactive surface area of ferrihydrite: time, pH, and temperature dependency of growth by Ostwald ripening. *Environmental Science: Nano, 6*(3), 820-833.

Hochella, M. F., Lower, S. K., Maurice, P. A., Penn, R. L., Sahai, N., Sparks, D. L., & Twining, B. S. (2008). Nanominerals, mineral nanoparticles, and earth systems. *science, 319*(5870), 1631-1635.

Huang, W., & Hall, S. J. (2017). Elevated moisture stimulates carbon loss from mineral soils by releasing protected organic matter. *Nature communications, 8*(1), 1-10.

Jambor, J. L., & Dutrizac, J. E. (1998). Occurrence and constitution of natural and synthetic ferrihydrite, a widespread iron oxyhydroxide. *Chemical reviews, 98*(7), 2549-2586.

James, R., & Ferris, F. (2004). Evidence for microbial-mediated iron oxidation at a neutrophilic groundwater spring. *Chemical Geology, 212*(3-4), 301-311.

Jang, J.-H., Dempsey, B. A., Catchen, G. L., & Burgos, W. D. (2003). Effects of Zn (II), Cu (II), Mn (II), Fe (II), NO3−, or SO42− at pH 6.5 and 8.5 on transformations of hydrous ferric oxide (HFO) as evidenced by Mössbauer spectroscopy. *Colloids and Surfaces A: Physicochemical and Engineering Aspects, 221*(1-3), 55-68.

Jastrow, J. (1996). Soil aggregate formation and the accrual of particulate and mineral-associated organic matter. *Soil Biology and Biochemistry, 28*(4-5), 665-676.

Jeon, B.-H., Dempsey, B. A., & Burgos, W. D. (2003). Kinetics and mechanisms for reactions of Fe (II) with iron (III) oxides. *Environmental science & technology, 37*(15), 3309-3315.

Jiang, W., Cai, Q., Xu, W., Yang, M., Cai, Y., Dionysiou, D. D., & O'Shea, K. E. (2014). Cr (VI) adsorption and reduction by humic acid coated on magnetite. *Environmental science & technology, 48*(14), 8078-8085.

Jones, A. M., Collins, R. N., Rose, J., & Waite, T. D. (2009). The effect of silica and natural organic matter on the Fe (II)-catalysed transformation and reactivity of Fe (III) minerals. *Geochimica et Cosmochimica Acta, 73*(15), 4409-4422.

Jones, D., & Edwards, A. (1998). Influence of sorption on the biological utilization of two simple carbon substrates. *Soil Biology and Biochemistry, 30*(14), 1895-1902.

Kaiser, K., & Guggenberger, G. (2000). The role of DOM sorption to mineral surfaces in the preservation of organic matter in soils. *Organic geochemistry, 31*(7-8), 711-725.

Kaiser, K., & Guggenberger, G. (2003). Mineral surfaces and soil organic matter. *European Journal of Soil Science, 54*(2), 219-236.

Kaiser, K., & Guggenberger, G. (2007). Sorptive stabilization of organic matter by microporous goethite: sorption into small pores vs. surface complexation. *European Journal of Soil Science, 58*(1), 45-59.

Kalbitz, K., Schwesig, D., Rethemeyer, J., & Matzner, E. (2005). Stabilization of dissolved organic matter by sorption to the mineral soil. *Soil Biology and Biochemistry, 37*(7), 1319-1331.

Kappler, A., Bryce, C., Mansor, M., Lueder, U., Byrne, J. M., & Swanner, E. D. (2021). An evolving view on biogeochemical cycling of iron. *Nature Reviews Microbiology*, 1-15.

Kassim, J., Baird, T., & Fryer, J. (1982). Electron microscope studies of iron corrosion products in water at room temperature. *Corrosion science, 22*(2), 147-158.

Katoh, M., Murase, J., Hayashi, M., Matsuya, K., & Kimura, M. (2004). Nutrient leaching from the plow layer by water percolation and accumulation in the subsoil in an irrigated paddy field. *Soil science and plant nutrition, 50*(5), 721-729.

Katsoyiannis, I. A., Althoff, H. W., Bartel, H., & Jekel, M. (2006). The effect of groundwater composition on uranium (VI) sorption onto bacteriogenic iron oxides. *Water research, 40*(19), 3646-3652.

Keil, R. G., Tsamakis, E., Fuh, C. B., Giddings, J. C., & Hedges, J. I. (1994). Mineralogical and textural controls on the organic composition of coastal marine sediments: Hydrodynamic separation using SPLITT-fractionation. *Geochimica et Cosmochimica Acta, 58*(2), 879-893.

Kellerman, A. M., Guillemette, F. o., Podgorski, D. C., Aiken, G. R., Butler, K. D., & Spencer, R. G. (2018). Unifying concepts linking dissolved organic matter composition to persistence in aquatic ecosystems. *Environmental science & technology, 52*(5), 2538-2548.

Kennedy, C., Scott, S., & Ferris, F. (2003). Characterization of bacteriogenic iron oxide deposits from Axial Volcano, Juan de Fuca Ridge, northeast Pacific Ocean. *Geomicrobiology Journal, 20*(3), 199-214.

Kikuchi, S., Kashiwabara, T., Shibuya, T., & Takahashi, Y. (2019). Molecular-scale insights into differences in the adsorption of cesium and selenium on biogenic and abiogenic ferrihydrite. *Geochimica et Cosmochimica Acta, 251*, 1-14.

Kim, S., Kramer, R. W., & Hatcher, P. G. (2003). Graphical method for analysis of ultrahigh-resolution broadband mass spectra of natural organic matter, the van Krevelen diagram. *Analytical chemistry, 75*(20), 5336-5344.

Kleber, M., Bourg, I. C., Coward, E. K., Hansel, C. M., Myneni, S. C., & Nunan, N. (2021). Dynamic interactions at the mineral–organic matter interface. *Nature Reviews Earth & Environment*, 1-20.

Kleber, M., Eusterhues, K., Keiluweit, M., Mikutta, C., Mikutta, R., & Nico, P. S. (2015). Mineral–organic associations: formation, properties, and relevance in soil environments. *Advances in agronomy, 130*, 1-140.

Koch, B. P., & Dittmar, T. (2006). From mass to structure: An aromaticity index for high-resolution mass data of natural organic matter. *Rapid communications in mass spectrometry, 20*(5), 926-932.

Kögel-Knabner, I., Guggenberger, G., Kleber, M., Kandeler, E., Kalbitz, K., Scheu, S., Eusterhues, K., & Leinweber, P. (2008). Organo-mineral associations in temperate soils: Integrating biology, mineralogy, and organic matter chemistry. *Journal of Plant Nutrition and Soil Science, 171*(1), 61-82.

Kukkadapu, R. K., Zachara, J. M., Fredrickson, J. K., Smith, S. C., Dohnalkova, A. C., & Russell, C. K. (2003). Transformation of 2-line ferrihydrite to 6-line ferrihydrite under oxic and anoxic conditions. *American Mineralogist, 88*(11-12), 1903-1914.

Ladd, J., Amato, M., & Oades, J. (1985). Decomposition of plant material in Australian soils. III. Residual organic and microbial biomass C and N from isotope-labelled legume material and soil organic matter, decomposing under field conditions. *Soil Research, 23*(4), 603-611.

Lal, R. (2004). Soil carbon sequestration impacts on global climate change and food security. *science, 304*(5677), 1623-1627.

Lal, R. (2008). Carbon sequestration. *Philosophical Transactions of the Royal Society B: Biological Sciences, 363*(1492), 815-830.

Lalonde, K., Mucci, A., Ouellet, A., & Gélinas, Y. (2012). Preservation of organic matter in sediments promoted by iron. *Nature, 483*(7388), 198-200.

Langley, S., Gault, A. G., Ibrahim, A., Takahashi, Y., Renaud, R., Fortin, D., Clark, I. D., & Ferris, F. G. (2009). Sorption of strontium onto bacteriogenic iron oxides. *Environmental science & technology, 43*(4), 1008-1014.

Larese-Casanova, P., & Scherer, M. M. (2007). Fe (II) sorption on hematite: New insights based on spectroscopic measurements. *Environmental science & technology, 41*(2), 471-477.

Lehmann, J., & Kleber, M. (2015). The contentious nature of soil organic matter. *Nature, 528*(7580), 60-68.

Li, D., Nielsen, M. H., Lee, J. R., Frandsen, C., Banfield, J. F., & De Yoreo, J. J. (2012). Direction-specific interactions control crystal growth by oriented attachment. *science, 336*(6084), 1014-1018.

Lipson, D. A., Jha, M., Raab, T. K., & Oechel, W. C. (2010). Reduction of iron (III) and humic substances plays a major role in anaerobic respiration in an Arctic peat soil. *Journal of Geophysical Research: Biogeosciences, 115*(G4).

Liu, C., Zhu, Z., Li, F., Liu, T., Liao, C., Lee, J.-J., Shih, K., Tao, L., & Wu, Y. (2016). Fe (II)-induced phase transformation of ferrihydrite: The inhibition effects and stabilization of divalent metal cations. *Chemical Geology, 444*, 110-119.

Liu, H., Guo, H., Li, P., & Wei, Y. (2008). The transformation of ferrihydrite in the presence of trace Fe (II): the effect of the anionic media. *Journal of Solid State Chemistry, 181*(10), 2666-2671.

Marín-Spiotta, E., Gruley, K., Crawford, J., Atkinson, E., Miesel, J., Greene, S., Cardona-Correa, C., & Spencer, R. (2014). Paradigm shifts in soil organic matter research affect interpretations of aquatic carbon cycling: transcending disciplinary and ecosystem boundaries. *Biogeochemistry, 117*(2), 279-297.

Mayer, L. M. (1994). Relationships between mineral surfaces and organic carbon concentrations in soils and sediments. *Chemical Geology, 114*(3-4), 347-363.

McGhee, I., Sannino, F., Gianfreda, L., & Burns, R. G. (1999). Bioavailability of 2, 4-D sorbed to a chlorite-like complex. *Chemosphere*, *39*(2), 285-291.

Melton, E. D., Swanner, E. D., Behrens, S., Schmidt, C., & Kappler, A. (2014). The interplay of microbially mediated and abiotic reactions in the biogeochemical Fe cycle. *Nature Reviews Microbiology*, *12*(12), 797-808.

Michel, F. M., Barrón, V., Torrent, J., Morales, M. P., Serna, C. J., Boily, J.-F., Liu, Q., Ambrosini, A., Cismasu, A. C., & Brown, G. E. (2010). Ordered ferrimagnetic form of ferrihydrite reveals links among structure, composition, and magnetism. *Proceedings of the National Academy of Sciences*, *107*(7), 2787-2792.

Michel, F. M., Ehm, L., Antao, S. M., Lee, P. L., Chupas, P. J., Liu, G., Strongin, D. R., Schoonen, M. A., Phillips, B. L., & Parise, J. B. (2007). The structure of ferrihydrite, a nanocrystalline material. *science*, *316*(5832), 1726-1729.

Mikutta, C. (2011). X-ray absorption spectroscopy study on the effect of hydroxybenzoic acids on the formation and structure of ferrihydrite. *Geochimica et Cosmochimica Acta*, *75*(18), 5122-5139.

Mikutta, C., Mikutta, R., Bonneville, S., Wagner, F., Voegelin, A., Christl, I., & Kretzschmar, R. (2008). Synthetic coprecipitates of exopolysaccharides and ferrihydrite. Part I: Characterization. *Geochimica et Cosmochimica Acta*, *72*(4), 1111-1127.

Mikutta, R., Kleber, M., Torn, M. S., & Jahn, R. (2006). Stabilization of soil organic matter: association with minerals or chemical recalcitrance? *Biogeochemistry*, *77*(1), 25-56.

Mikutta, R., Lorenz, D., Guggenberger, G., Haumaier, L., & Freund, A. (2014). Properties and reactivity of Fe-organic matter associations formed by coprecipitation versus adsorption: Clues from arsenate batch adsorption. *Geochimica et Cosmochimica Acta*, *144*, 258-276.

Mikutta, R., Mikutta, C., Kalbitz, K., Scheel, T., Kaiser, K., & Jahn, R. (2007). Biodegradation of forest floor organic matter bound to minerals via different binding mechanisms. *Geochimica et Cosmochimica Acta*, *71*(10), 2569-2590.

Morgan, J. J., & Stumm, W. (1996). *Aquatic chemistry: chemical equilibria and rates in natural waters*. Wiley.

Muehe, E. M., Adaktylou, I. J., Obst, M., Zeitvogel, F., Behrens, S., Planer-Friedrich, B., Kraemer, U., & Kappler, A. (2013). Organic carbon and reducing conditions lead to

cadmium immobilization by secondary Fe mineral formation in a pH-neutral soil. *Environmental science & technology, 47*(23), 13430-13439.

Navrotsky, A., Mazeina, L., & Majzlan, J. (2008). Size-driven structural and thermodynamic complexity in iron oxides. *science, 319*(5870), 1635-1638.

Neubauer, S. C., Toledo-Durán, G. E., Emerson, D., & Megonigal, J. P. (2007). Returning to their roots: iron-oxidizing bacteria enhance short-term plaque formation in the wetland-plant rhizosphere. *Geomicrobiology Journal, 24*(1), 65-73.

Newcomb, C. J., Qafoku, N. P., Grate, J. W., Bailey, V. L., & De Yoreo, J. J. (2017). Developing a molecular picture of soil organic matter–mineral interactions by quantifying organo–mineral binding. *Nature communications, 8*(1), 1-8.

Notini, L., Latta, D. E., Neumann, A., Pearce, C. I., Sassi, M., N'Diaye, A. T., Rosso, K. M., & Scherer, M. M. (2018). The role of defects in Fe (II)–goethite electron transfer. *Environmental science & technology, 52*(5), 2751-2759.

Oades, J. (1988). The retention of organic matter in soils. *Biogeochemistry, 5*(1), 35-70.

Pan, W., Kan, J., Inamdar, S., Chen, C., & Sparks, D. (2016). Dissimilatory microbial iron reduction release DOC (dissolved organic carbon) from carbon-ferrihydrite association. *Soil Biology and Biochemistry, 103*, 232-240.

Parks, G. A. (1965). The isoelectric points of solid oxides, solid hydroxides, and aqueous hydroxo complex systems. *Chemical reviews, 65*(2), 177-198.

Pasakarnis, T., McCormick, M. L., Parkin, G. F., Thompson, A., & Scherer, M. M. Fe II aq–Fe III oxide electron transfer and Fe exchange: effect of organic carbon. *transformation, 33*, 34.

Pasakarnis, T. S. (2013). Effects of carbon during Fe(II)-catalyzed Fe oxide recrystallization: implications for Fe and carbon cycling. *Ph.D. Dissertation, University of Iowa, Iowa City, IA,*

Pedersen, H. D., Postma, D., Jakobsen, R., & Larsen, O. (2005). Fast transformation of iron oxyhydroxides by the catalytic action of aqueous Fe (II). *Geochimica et Cosmochimica Acta, 69*(16), 3967-3977.

Picard, A., Kappler, A., Schmid, G., Quaroni, L., & Obst, M. (2015). Experimental diagenesis of organo-mineral structures formed by microaerophilic Fe (II)-oxidizing bacteria. *Nature communications, 6*(1), 1-8.

Plante, A. F., Fernández, J. M., & Leifeld, J. (2009). Application of thermal analysis techniques in soil science. *Geoderma, 153*(1-2), 1-10.

Pokrovsky, O., & Schott, J. (2002). Iron colloids/organic matter associated transport of major and trace elements in small boreal rivers and their estuaries (NW Russia). *Chemical Geology, 190*(1-4), 141-179.

Porras, R., Pries, C. H., Torn, M., & Nico, P. (2018). Synthetic iron (hydr) oxide-glucose associations in subsurface soil: effects on decomposability of mineral associated carbon. *Science of the Total Environment, 613*, 342-351.

Posth, N. R., Huelin, S., Konhauser, K. O., & Kappler, A. (2010). Size, density and composition of cell–mineral aggregates formed during anoxygenic phototrophic Fe (II) oxidation: impact on modern and ancient environments. *Geochimica et Cosmochimica Acta, 74*(12), 3476-3493.

Rasmussen, C., Heckman, K., Wieder, W. R., Keiluweit, M., Lawrence, C. R., Berhe, A. A., Blankinship, J. C., Crow, S. E., Druhan, J. L., & Pries, C. E. H. (2018). Beyond clay: towards an improved set of variables for predicting soil organic matter content. *Biogeochemistry, 137*(3), 297-306.

Riedel, T., Zak, D., Biester, H., & Dittmar, T. (2013). Iron traps terrestrially derived dissolved organic matter at redox interfaces. *Proceedings of the National Academy of Sciences, 110*(25), 10101-10105.

Roden, E. E., & Wetzel, R. G. (1996). Organic carbon oxidation and suppression of methane production by microbial Fe (III) oxide reduction in vegetated and unvegetated freshwater wetland sediments. *Limnology and Oceanography, 41*(8), 1733-1748.

Royer, R. A., Burgos, W. D., Fisher, A. S., Jeon, B.-H., Unz, R. F., & Dempsey, B. A. (2002). Enhancement of hematite bioreduction by natural organic matter. *Environmental science & technology, 36*(13), 2897-2904.

Royer, R. A., Burgos, W. D., Fisher, A. S., Unz, R. F., & Dempsey, B. A. (2002). Enhancement of biological reduction of hematite by electron shuttling and Fe (II) complexation. *Environmental science & technology, 36*(9), 1939-1946.

Šantl-Temkiv, T., Finster, K., Dittmar, T., Hansen, B. M., Thyrhaug, R., Nielsen, N. W., & Karlson, U. G. (2013). Hailstones: a window into the microbial and chemical inventory of a storm cloud. *PloS one*, *8*(1), e53550.

Schmid, G., Zeitvogel, F., Hao, L., Ingino, P., Floetenmeyer, M., Stierhof, Y. D., Schroeppel, B., Burkhardt, C. J., Kappler, A., & Obst, M. (2014). 3-D analysis of bacterial cell-(iron) mineral aggregates formed during Fe (II) oxidation by the nitrate-reducing Acidovorax sp. strain BoFeN1 using complementary microscopy tomography approaches. *Geobiology*, *12*(4), 340-361.

Schmidt, M. W., Torn, M. S., Abiven, S., Dittmar, T., Guggenberger, G., Janssens, I. A., Kleber, M., Kögel-Knabner, I., Lehmann, J., & Manning, D. A. (2011). Persistence of soil organic matter as an ecosystem property. *Nature*, *478*(7367), 49-56.

Schwertmann, U., & Cornell, R. M. (2008). *Iron oxides in the laboratory: preparation and characterization*. John Wiley & Sons.

Schwertmann, U., & Murad, E. (1983). Effect of pH on the formation of goethite and hematite from ferrihydrite. *Clays and Clay Minerals*, *31*(4), 277-284.

Schwertmann, U., & Taylor, R. M. (1989). Iron oxides. *Minerals in soil environments*, *1*, 379-438.

Schwertmann, U., & Thalmann, H. (1976). The influence of [Fe (II)],[Si], and pH on the formation of lepidocrocite and ferrihydrite during oxidation of aqueous FeCl 2 solutions. *Clay minerals*, *11*(3), 189-200.

Schwertmann, U., Wagner, F., & Knicker, H. (2005). Ferrihydrite–humic associations: magnetic hyperfine interactions. *Soil Science Society of America Journal*, *69*(4), 1009-1015.

Sheng, A., Liu, J., Li, X., Qafoku, O., Collins, R. N., Jones, A. M., Pearce, C. I., Wang, C., Ni, J., & Lu, A. (2020). Labile Fe (III) from sorbed Fe (II) oxidation is the key intermediate in Fe (II)-catalyzed ferrihydrite transformation. *Geochimica et Cosmochimica Acta*, *272*, 105-120.

Singh, N., Megharaj, M., Gates, W. P., Churchman, G., Anderson, J., Kookana, R. S., Naidu, R., Chen, Z., Slade, P. G., & Sethunathan, N. (2003). Bioavailability of an organophosphorus pesticide, fenamiphos, sorbed on an organo clay. *Journal of agricultural and food chemistry*, *51*(9), 2653-2658.

Sørensen, J., & Thorling, L. (1991). Stimulation by lepidocrocite (7-FeOOH) of Fe (II)-dependent nitrite reduction. *Geochimica et Cosmochimica Acta, 55*(5), 1289-1294.

Sowers, T. D., Harrington, J. M., Polizzotto, M. L., & Duckworth, O. W. (2017). Sorption of arsenic to biogenic iron (oxyhydr) oxides produced in circumneutral environments. *Geochimica et Cosmochimica Acta, 198*, 194-207.

Sowers, T. D., Holden, K. L., Coward, E. K., & Sparks, D. L. (2019). Dissolved Organic Matter Sorption and Molecular Fractionation by Naturally Occurring Bacteriogenic Iron (Oxyhydr) oxides. *Environmental science & technology, 53*(8), 4295-4304.

Sowers, T. D., Holden, K. L., Coward, E. K., & Sparks, D. L. (2019, Apr 16). Dissolved Organic Matter Sorption and Molecular Fractionation by Naturally Occurring Bacteriogenic Iron (Oxyhydr)oxides. *Environ Sci Technol, 53*(8), 4295-4304. https://doi.org/10.1021/acs.est.9b00540

Sowers, T. D., Stuckey, J. W., & Sparks, D. L. (2018). The synergistic effect of calcium on organic carbon sequestration to ferrihydrite. *Geochemical transactions, 19*(1), 4.

Stevenson, F. J. (1994). *Humus chemistry: genesis, composition, reactions*. John Wiley & Sons.

Swanner, E. D., Nell, R. M., & Templeton, A. S. (2011). Ralstonia species mediate Fe-oxidation in circumneutral, metal-rich subsurface fluids of Henderson mine, CO. *Chemical Geology, 284*(3-4), 339-350.

ThomasArrigo, L. K., Byrne, J. M., Kappler, A., & Kretzschmar, R. (2018). Impact of organic matter on iron (II)-catalyzed mineral transformations in ferrihydrite–organic matter coprecipitates. *Environmental science & technology, 52*(21), 12316-12326.

ThomasArrigo, L. K., Kaegi, R., & Kretzschmar, R. (2019). Ferrihydrite growth and transformation in the presence of ferrous iron and model organic ligands. *Environmental science & technology, 53*(23), 13636-13647.

ThomasArrigo, L. K., Mikutta, C., Byrne, J., Kappler, A., & Kretzschmar, R. (2017). Iron (II)-catalyzed Iron atom exchange and mineralogical changes in Iron-rich organic freshwater Flocs: an Iron isotope tracer study. *Environmental science & technology, 51*(12), 6897-6907.

Thompson, A., Chadwick, O. A., Rancourt, D. G., & Chorover, J. (2006). Iron-oxide crystallinity increases during soil redox oscillations. *Geochimica et Cosmochimica Acta, 70*(7), 1710-1727.

Thompson, A., Rancourt, D. G., Chadwick, O. A., & Chorover, J. (2011). Iron solid-phase differentiation along a redox gradient in basaltic soils. *Geochimica et Cosmochimica Acta, 75*(1), 119-133.

Tisdall, J. M., & OADES, J. M. (1982). Organic matter and water-stable aggregates in soils. *Journal of Soil Science, 33*(2), 141-163.

Toner, B. M., Berquó, T. S., Michel, F. M., Sorensen, J. V., Templeton, A. S., & Edwards, K. J. (2012). Mineralogy of iron microbial mats from Loihi Seamount. *Frontiers in microbiology, 3*, 118.

Torn, M. S., Trumbore, S. E., Chadwick, O. A., Vitousek, P. M., & Hendricks, D. M. (1997). Mineral control of soil organic carbon storage and turnover. *Nature, 389*(6647), 170.

Totsche, K. U., Amelung, W., Gerzabek, M. H., Guggenberger, G., Klumpp, E., Knief, C., Lehndorff, E., Mikutta, R., Peth, S., & Prechtel, A. (2018). Microaggregates in soils. *Journal of Plant Nutrition and Soil Science, 181*(1), 104-136.

Tronc, E., Belleville, P., Jolivet, J. P., & Livage, J. (1992). Transformation of ferric hydroxide into spinel by iron (II) adsorption. *Langmuir, 8*(1), 313-319.

Wagai, R., & Mayer, L. M. (2007). Sorptive stabilization of organic matter in soils by hydrous iron oxides. *Geochimica et Cosmochimica Acta, 71*(1), 25-35.

Weiss, J. V., Emerson, D., Backer, S. M., & Megonigal, J. P. (2003). Enumeration of Fe (II)-oxidizing and Fe (III)-reducing bacteria in the root zone of wetland plants: implications for a rhizosphere iron cycle. *Biogeochemistry, 64*(1), 77-96.

Weiss, J. V., Emerson, D., & Megonigal, J. P. (2004). Geochemical control of microbial Fe (III) reduction potential in wetlands: comparison of the rhizosphere to non-rhizosphere soil. *FEMS microbiology ecology, 48*(1), 89-100.

Weiss, J. V., Rentz, J. A., Plaia, T., Neubauer, S. C., Merrill-Floyd, M., Lilburn, T., Bradburne, C., Megonigal, J. P., & Emerson, D. (2007). Characterization of neutrophilic Fe (II)-oxidizing bacteria isolated from the rhizosphere of wetland plants and description of Ferritrophicum radicicola gen. nov. sp. nov., and Sideroxydans paludicola sp. nov. *Geomicrobiology Journal, 24*(7-8), 559-570.

Whitaker, A. H., Austin, R. E., Holden, K. L., Jones, J. L., Michel, F. M., Peak, D., Thompson, A., & Duckworth, O. W. (2021). The structure of natural biogenic iron (oxyhydr) oxides formed in circumneutral pH environments. *Geochimica et Cosmochimica Acta, 308*, 237-255.

Whitaker, A. H., & Duckworth, O. W. (2018). Cu, Pb, and Zn sorption to biogenic iron (oxyhydr) oxides formed in circumneutral environments. *Soil Systems, 2*(2), 18.

Whitaker, A. H., Peña, J., Amor, M., & Duckworth, O. W. (2018). Cr (VI) uptake and reduction by biogenic iron (oxyhydr) oxides. *Environmental Science: Processes & Impacts, 20*(7), 1056-1068.

Wild, B., Schnecker, J., Alves, R. J. E., Barsukov, P., Bárta, J., Čapek, P., Gentsch, N., Gittel, A., Guggenberger, G., & Lashchinskiy, N. (2014). Input of easily available organic C and N stimulates microbial decomposition of soil organic matter in arctic permafrost soil. *Soil Biology and Biochemistry, 75*, 143-151.

Williams, A. G., & Scherer, M. M. (2004). Spectroscopic evidence for Fe (II)− Fe (III) electron transfer at the iron oxide− water interface. *Environmental science & technology, 38*(18), 4782-4790.

Wood, P. M. (1994). Pathways for production of Fenton's reagent by wood-rotting fungi. *FEMS Microbiology Reviews, 13*(2-3), 313-320.

Zhou, Z. (2018). *Fe (II)-catalyzed transformation of ferrihydrite associated with natural organic matter*. The University of Iowa.

Zhou, Z., Latta, D. E., Noor, N., Thompson, A., Borch, T., & Scherer, M. M. (2018). Fe (II)-catalyzed transformation of organic matter–ferrihydrite coprecipitates: a closer look using Fe isotopes. *Environmental science & technology*, *52*(19), 11142-11150.

Zhou, Z., Latta, D. E., & Scherer, M. M. (2021). Natural organic matter inhibits Ni stabilization during Fe (II)-catalyzed ferrihydrite transformation. *Science of the Total Environment, 755*, 142612.

APPENDIX A

Bioavailability of organic matter in bacteriogenic iron(oxyhydr)oxides (BIOS) and the release of heavy metals.

Noor, N., and A. Thompson. To be submitted to the Soil Science Society of America Journal.

ABSTRACT

Bacteriogenic iron(oxyhydr)oxides (BIOS) are common in soil redox transition conditions and quiescent waterways and are well known to retain dissolve organic matter and heavy metals in these environments. However, our understanding of the bioavailability of BIOS associated organic matter and heavy metals are limited. In this study, we have conducted a microbial incubation study under aerobic conditions using soil microbial inoculum. We have also included C/Fe coprecipitate and Fh as a control for comparison with BIOS. We found that the BIOS lost 27% of its initial C whereas 56% of the C was lost from the coprecipitate. Moreover, we have added 1mM ^{13}C labeled Na-lactate in the reactors and found that sorption of Na lactate in the coprecipitate and Fh was higher than the BIOS. 9.2±2.5% and 8.2± 3% added Na lactate was sorbed on the coprecipitate and Fh, respectively, whereas 3.9±0.4% was sorbed on the BIOS. 30% of the C from the BIOS was released during the incubation and around 0.04 to 10% of heavy metal release were observed. Among the heavy metals, the maximum release of Zn (10%) was observed following Cu (4.4%). Along with that we have used the scanning transmission electron microscopy technique to observe the morphological change in the BIOS, coprecipitate and Fh before and after incubation. The BIOS and coprecipitate did not show any morphological change after incubation, but the Fh transformed into goethite during incubation.

INTRODUCTION

Bacteriogenic iron(oxyhydr)oxides (BIOS) are composites of intact or partly degraded remains bacterial cells mixed with poorly ordered iron(oxyhydr)oxides minerals (Ferris, 2005). They can be produced in aerobic surface water (Duckworth et al., 2009; Emerson & Weiss, 2004; Ferris, 2005) where chemical or bacterial oxidation of Fe^{2+} to Fe^{3+} follows hydrolysis resulting in

precipitation in association with bacterial cells (Ferris, 2005) and/ or in the suboxic zone [i.e. ~5–50 µM O_2 (Druschel et al., 2008)] of a redox gradient where high concentrations of Fe^{2+} containing water intersects with oxygenated water creating an environment where iron-oxidizing bacteria can outcompete abiotic Fe^{2+} oxidation reactions (Druschel et al., 2008; Ferris, 2005; Whitaker & Duckworth, 2018). BIOS usually prevail in quiescent waterways and oxygen-limited sediments (Tyler D Sowers et al., 2019), groundwater seeps (Bruun et al., 2010; Fleming et al., 2014; James & Ferris, 2004), springs (Emerson & Revsbech, 1994), mines (Chan et al., 2004; Swanner et al., 2011), wetland soils (Emerson & Weiss, 2004; Weiss et al., 2004), and also in the rhizosphere (Neubauer et al., 2007; Weiss et al., 2003; Weiss et al., 2007).

Due to the broad distribution and reactive surface properties of natural iron(oxyhydr)oxides, they have a high affinity to sorb dissolve organic matter (DOM). BIOS also has a preferential sorption tendency towards aromatic and carboxylic C compounds (Tyler D Sowers et al., 2019). Moreover, they tend to sorb the dissolve metals (Morgan & Stumm, 1996) or toxicants (Whitaker et al., 2018) present in the aquatic environment. BIOS have been found as a good adsorbent of As(III), As(V), U(VI), Sr(II), Pb(II), Cu(II), Zn(II) (Bussan & Strathmann, 2007; Katsoyiannis et al., 2006; Langley et al., 2009; Sowers et al., 2017). BIOS are embedded in a biofilm matrix (Flemming & Wingender, 2010) which can impact their reactivity. The biofilm contains bacteria, Fe oxidizing and reducing organisms (Emerson et al., 2010; Toner et al., 2012), cell-derived organic matter (Chan et al., 2004; Chan et al., 2009; Ferris et al., 1989; Kennedy et al., 2003) which can directly bind metals. Along with that their sorption ability to DOM can also impact the surface charge properties which can ultimately impact the retention ability of heavy metals, contaminants, and toxicants. Therefore, the release of organic matter can impact the associated metals and their biogeochemistry. The sorption-desorption ability of the BIOS along

with the reductive release of heavy metals were analyzed previously. But there is little information available regarding the bioavailability of C and the release of heavy metal under aerobic conditions.

Due to their short range ordered (SRO) structure, BIOS has been compared with two-line ferrihydrite (2LFh) in terms of their ability to retain metals and contaminants (Emerson et al., 2010). However, relative to 2LFh, BIOS have a smaller crystal size, and more negative charges (Duckworth et al., 2009; Sowers et al., 2017). Studies have also shown that BIOS are more resistant to crystal transformation than synthesized Fh (Picard et al., 2015; Toner et al., 2012). The adsorption and incorporation of organic matter into biogenic Fh can also enhance its hydrophobicity (Fortin & Langley, 2005). For example, BIOS has been found to sorb half as much DOM as 2LFh (Tyler D Sowers et al., 2019), but as much as eightfold higher amounts of heavy metals (Katsoyiannis et al., 2006; Sowers et al., 2017). However, the bioavailability of OM in BIOS has not been measured.

Thus, we designed a study to measure the bioavailability of organic matter from the BIOS and also assessed the release of heavy metals during OM decomposition. We coupled this with parallel incubations of a Fh-NOM coprecipitate with a similar C/Fe ratio as the BIOS. In addition to tracking the loss of C and mineralization OM to CO_2, we tracked changes in the morphology and crystallinity of the BIOS using scanning transmission electron microscopy and Mössbauer spectroscopy.

MATERIALS AND METHODS

Sample collection and characterization

Iron flocks were collected in November 2020, 24 h after a heavy rainfall event from a shallow natural wetland connected to a low-flow shallow stream in Whitehall forest (Leech wetland; 33°52'48.69"N, 83°21'36.67"W, Athens, Georgia; Figure 9). Samples were collected carefully using a syringe without disturbing the underlying soil in several 50-ml polypropylene falcon tubes. All the samples were collected from the same location and the tubes were filled to the top with the wetland water to eliminate air space. Samples were transported to the laboratory on dry ice, where they were immediately centrifuged at 10,000g for 10 min. The supernatant was then decanted and all the samples were pooled into a 50-ml centrifuge tube in an anoxic glovebox (97% N_2, 3%H_2). A 40-mL aliquot of anoxic 18.2MΩ (nanopure) water was added and mixed with the sample using vortex shaking to homogenize the samples. The BIOS samples were centrifuged for a final time at 10,000g for 10 min., the supernatant decanted (Whitaker et al., 2018) and a small amount of nanopure water was added to make a slurry. A subsample was separated to measure the moisture content and elemental composition of the slurry. The samples were preserved in the -20°C freezer before further experimental analysis. Moisture content was measured by taking a small amount of sample (wet mass basis) and oven drying it at 70°C for 24h and calculating the dry mass per cent. The pH of the sample was 7.1 after collection. The pH, Temperature, Eh, dissolved O_2 concentration and conductivity of the wetland water was 6.5, 17.0°C, -33.1 mV, 9.60 mg L^{-1}, 25.8 µs cm^{-1}, respectively. Total C, ^{13}C isotope and N content of the BIOS was measured on the freeze-dried sample and analyzed using a CHNS element analyzer. Total Fe, As, Na, Ca, Mg, Al, K, Cr, Cu, Zn, Pb, Ni, Cd, Mn, P, Si content of the sample was analyzed by dissolving the solid sample in concentrated HCl and HNO_3 acids

following filtration through a 0.22 μm polyvinylidene fluoride filter via inductively coupled plasma mass spectrometry (ICP-MS) (Whitaker et al., 2018). The X-ray diffraction (XRD), Mössbauer spectroscopy and Scanning transmission electron microscopy (STEM) image analysis was also done to get an overall idea about the mineralogical composition of the sample along with its morphological appearance.

Ferrihydrite (Fh) and Fh-C coprecipitates synthesis

In this study natural BIOS were compared with synthesized Fh and Fh-C coprecipitates. In previous studies, Fh was preferred as a control (Tyler D Sowers et al., 2019; Whitaker & Duckworth, 2018; Whitaker et al., 2018) or coprecipitates prepared from a particular type of C compound were used (ThomasArrigo et al., 2017). Our understanding of BIOS indicates that it will have more similarities in activity with Fh-C coprecipitates than with Fh, but either way, we have used both coprecipitate and Fh as a control. To prepare Fh-C coprecipitates, dissolved natural organic matter (DOC) was extracted from a fresh litter sample of the O horizon from the same location where BIOS were sampled to maintain similarity in organic matter type. Collected fresh litter samples were mixed with DI water and continuously shaken for 24h at a 1:2 (w/v) ratio. The mixture was centrifuged at 20,000 g for 20 min and suspension was then pressure filtered through a 0.45 μm polyvinylidene fluoride membrane filter (Chen et al., 2014; Chen et al., 2015). The DOC concentration of the stock solution was measured by Shimadzu TOC-500 analyzers and later diluted with ultrapure 18.2 MΩ deionized water (DI) water to achieve the required concentration to prepare the coprecipitates.

Freshly extracted DOC was used to prepare Fh-C coprecipitates with a C/Fe molar ratio of 0.5 following the methods described by Chen et al (Chen et al., 2014). The C/Fe molar ratio of 0.5 was chosen as the C/Fe molar ratio of the collected BIOS was 0.58. Briefly, $Fe(NO_3).9H_2O$ was

mixed with DOC stock solution containing the required amount of C to achieve the required C/Fe ratio under vigorous stirring. The pH of the suspension was raised from ~2.0 to 7 by slowly adding 0.1 M KOH.

2LFh was synthesized following (Schwertmann & Cornell, 2008) where $Fe(NO_3).9H_2O$ was dissolved in ultrapure 18.2 MΩ water and pH were adjusted at 7 using 1M KOH. Synthesized Fh and C/Fe coprecipitate was centrifuged at 10,000rpm for 10 minutes and washed twice using 18.2 MΩ ultrapure water and stored in the 4°C refrigerators and used within days after preparation.

Microbial inoculum collection

Soil microbial inoculum was obtained from the soil in the same area as the BIOS was collected to approximate a microbial community that might also be exposed to the BIOS in the natural system. Freshly collected soil from the top 10 cm was shaken in a 4 mM $CaCl_2$ solution for 24 h and passed through 5μm filters (Eusterhues et al., 2014b). A small portion of that filtrate was added to Luria broth (LB) media and incubated for 12 h at 25°C to achieve the most active cells. The resulting incubated solution was centrifuged at 3000 rpm for 10 min, and the supernatant was discarded. The microbial enrichments were then washed with 18.2 MΩ ultrapure water twice to remove the remaining LB media and resuspended in a small amount of selective media containing 0.5 g KH_2PO_4, 1.0 g $NaSO_4$, 2.0 g NH_4Cl, 0.5 mM $CaCl_2$, 0.1 mM $MgSO_4$, and 1 mM ^{13}C-Na lactate (per Liter basis).

Incubation experiment set up and sample collection

The incubation study was conducted in 125-ml opaque serum bottles containing 30-mg of BIOS and 50-ml of selective media containing 0.5 g KH_2PO_4, 1.0 g $NaSO_4$, 2.0 g NH_4Cl, 0.5 mM $CaCl_2$, 0.1 mM $MgSO_4$, and 1 mM ^{13}C-Na lactate (per Liter basis) (Ginn et al., 2014). The soil microbial inoculum was added at a rate of $2x10^8$ cells ml^{-1}. Two separate sets of reactors with a

similar set-up were also included where the BIOS was replaced with Fh and Fh-C coprecipitates. These treatments were named as "BIOS/Fh/Coprecipitate + Na-lactate + Inoculum". Along with that, three sets of controls such as (i) BIOS + Without Na-lactate + Inoculum (ii) BIOS + Only media (where no Na-lactate or microbial inoculum added in the media) (iii) Media with Lactate and Inoculum (No solid samples added). All the vials were seal capped with butyl rubber stoppers and continuously shaken on a rotatory shaker at 20°C. The experiment was conducted for 9 days in total. Sampling was done every 24 h for the first 5 days then every other day for the next 4 days. During each sampling, 3.5-ml of gas sample was collected for CO_2 measurement and 25-ml for $^{13}CO_2$ measurement. Gas samples were stored in pre-evacuated sealed sterile vials and analyzed within 2 to 3 days. At the same time, 5ml solution was collected and filtered through a 0.22 µm polyvinylidene fluoride filter for DOC, pH and heavy metal analysis. After each sampling, the vials were uncapped for at least 6 hrs and left under a laminar hood on the rotatory shaker to ensure the mixing of atmospheric O_2 in the reactors and avoid the buildup of anoxic conditions. At the end of the incubation experiment, the solid samples were collected, washed twice with 18.2 MΩ ultrapure water and stored at -20 °C for future analysis. The experiment was conducted with two replicates of each treatment.

Solid sample characterization

The before and after incubation, solid samples were analyzed using Mössbauer spectroscopy and Scanning transmission electron microscopy (STEM). Mössbauer spectra were collected using 50-mCi ^{57}Co/Rh source at 5 K, 13 K, and 35 K. Solid samples were washed twice with ultrapure water by suspending the samples in ~ 5 ml of water, gently shaking the samples, and then centrifuging them at 10,000 rpm for 10 min. The supernatants were then poured off, the pelleted samples were mounted in a nylon o-ring, sealed between two pieces of Kapton tape, and

immediately frozen at −20 °C. Mössbauer spectra were analyzed using Recoil software and spectra fitting was done using Voigt-based fitting (VBF) as described elsewhere (Thompson et al., 2011). The STEM image was obtained using an ultrahigh resolution scanning transmission electron microscopy (STEM-Hitachi SU 9000EA) with a resolution of 0.4 nm operating at 30 kV. The solid sample slurry was placed on a silica chip and dried overnight before analysis. A secondary electron (SE) detector was used for collecting the images and EDS spectra were recorded with Oxford Ultim Extreme software. X-ray diffraction spectra of the initial BIOS sample was collected using the Bruker D8-Advance XRD system. The sample was scanned at a speed of 0.1 sec/step, with an increment of 0.01 deg/ step and 2 theta range (10 to 80) was used.

Sample analysis calculations

The per cent contribution of added ^{13}C labelled Na -lactate from the solution media to the solid samples after incubation study (P ^{13}C Na- lactate in solid) was calculated using a two-way source mixing model.

$$P^{13}C_{\text{Na lactate}}\text{in solid} = \frac{x[13C]\ \text{after} - x[13C]_{Fh}}{x[13C]_{DOC} - x[13C]_{Fh}} * 100$$

where, $x[13C]$ after and $x[13C]_{Fh}$ are atom fraction of ^{13}C isotope in the coprecipitates after incubation and ^{13}C content of the Fh, respectively; $x[13C]_{DOC}$ is the initial atom fraction of added ^{13}C Na -lactate. The C content of the solids after incubation was calculated by subtracting the amount of labelled Na-lactate sorbed on the solid after incubation.

The amount of DOC from the BIOS or Coprecipitate was calculated by subtracting the "Media with Na-lactate+ Inoculum" reactors from the "BIOS/Coprecipitate+ Na-lactate+ Inoculum. Later the amount of C released in each sampling time was added along with the amount remained in the solution at the end of the experiment to get the total amount of C released. The per cent C released from the solid was then calculated using the initial C content of the BIOS/Coprecipitate.

RESULTS

Characterization of BIOS synthesized Fh and C/Fe coprecipitates

Scanning transmission electron microscopy image (STEM) of collected BIOS, synthesized 2LFh, and coprecipitate are shown in Figures 6 and 8. The morphology of BIOS particles comprises a ragged morphology along with some rounded particles with particles sizes ranged from approximately 50 to 200 nm (Figure A. 6). Many particles also have a sheath or tube-like morphology that is characteristic of iron (oxyhydr)oxide that has been produced by Fe(II)-oxidizing bacteria (i.e., BIOS). This morphology is similar to what has previously been reported (Duckworth et al., 2009; Ferris, 2005; Haaijer et al., 2008; Posth et al., 2010; T. D. Sowers et al., 2019; Whitaker et al., 2021; Whitaker & Duckworth, 2018). In contrast, the synthesized Fh, and Fh-NOM coprecipitates both had rounded aggregates with jagged edges. After incubation, we did not observe any substantial morphological changes in the BIOS (Figure A.7) or the Fh-NOM coprecipitate (Figure A.8), but the Fh exhibited substantial transformation to needle-like structures, resembling goethite.

The elemental composition of BIOS, along with total Fe, C content of the Fh and coprecipitate are shown in Table 1. The BIOS samples were predominantly composed of Fe (781 mg g^{-1} solid) and C (98 mg g^{-1}solid), which gave the BIOS a C/Fe molar ratio of 0.6. The BIOS contained significant Si (X mg g-1 solid) and Ca (56 mg g^{-1} solid) as well as lower concentrations of Cu, As, Cr, Pb, Ni, Cd, Zn, Mn, P, Ca, Mg, and Na (ranging from 0.2 – 13 mg g^{-1}solid). The Fe content of the synthesized Fh was in line with other reported values (Michel et al., 2010). We synthesized the Fh-NOM to match the C/Fe ratio of the BIOS (0.58), but during the synthesis and washing some loss of Fe and C occurred, resulting in a coprecipitate with C/Fe ratio of 0.3. This decrease in C/Fe ratio than target C/Fe ratio is not unusual and some decrease in C/Fe ratio during

the synthesis process is expected especially when the ratio is at the lower end (ThomasArrigo et al., 2017). The X-ray diffraction pattern for BIOS showed (Figure A.9) similarities with amorphous Fh XRD pattern along with some sharp peaks indicating silica structure.

Change in C content

After incubation, the Fh-NOM coprecipitate lost more C (56% of initial) than the BIOS (27% of initial), whereas the Fh gained C from the incubation media (Figure A.1). A similar C loss occurred across all BIOS incubation controls (i.e., those without added microbial inoculum or without added lactate) suggesting this loss is not governed by the microbial inoculum. The % contribution of added lactate in the solid after incubation suggest that the C/Fe coprecipitate and Fh gained or sorbed higher amount of C from the Lactate than the BIOS. The BIOS sorbed 3.9±0.4% whereas the C/Fe coprecipitate and Fh sorbed 9.2±2.5% and 8.2±3%, respectively.

Dissolved organic matter, mineralization of CO_2-C and heavy metal release

The dissolved organic carbon (DOC) content increased for the first 120 hrs of the incubation and then decreased for all treatments (Figure A.3) and was higher in the BIOS than in the other treatments. Based on analysis of the solid phases, ~30% of the initial C was lost from the BIOS during the 216 hrs of incubation time, whereas 20% was lost from the coprecipitate.

The addition of lactate increased the total CO_2-C respiration from the BIOS reactors and the highest amount of CO_2-C respired was from the BIOS reactor with lactate and inoculum (182 mg g^{-1} CO_2-C), whereas the reactor without the added lactate respired 57 mg g^{-1} CO_2-C (Figure 4 and 5). The addition of lactate may have increased the activity of the microbes in the BIOS itself, which may have resulted in this higher emission of CO_2. The maximum CO_2 released from the BIOS reactor with lactate and inoculum was at day 1 of incubation.

In our experiment we have used labeled lactate to differentiate the CO_2-C respiration from the lactate and the CO_2-C respiration from the BIOS. The labeled $^{13}CO_2$ sample analysis is not complete yet and will be included in future preparations of this data. The total CO_2-C respiration from the C/Fe coprecipitate was 10 mg g^{-1} CO_2-C and from Fh containing reactor it was 15 mg g^{-1} CO_2-C.

The release of heavy metal from the BIOS during microbial incubation under aerobic condition was measured and presented in Figure A.5. Around 0.04 – 10% of the heavy metal present in the BIOS was released over time. The maximum amount of Zn i.e. 10% from the BIOS was released. Around 4.35 % of Cu was released. The amount of Ni, Pb, Cr, As and Al was 0.075%, 0.047%, 0.042%, 0.6%, 0.68%, respectively.

FIGURES AND TABLES

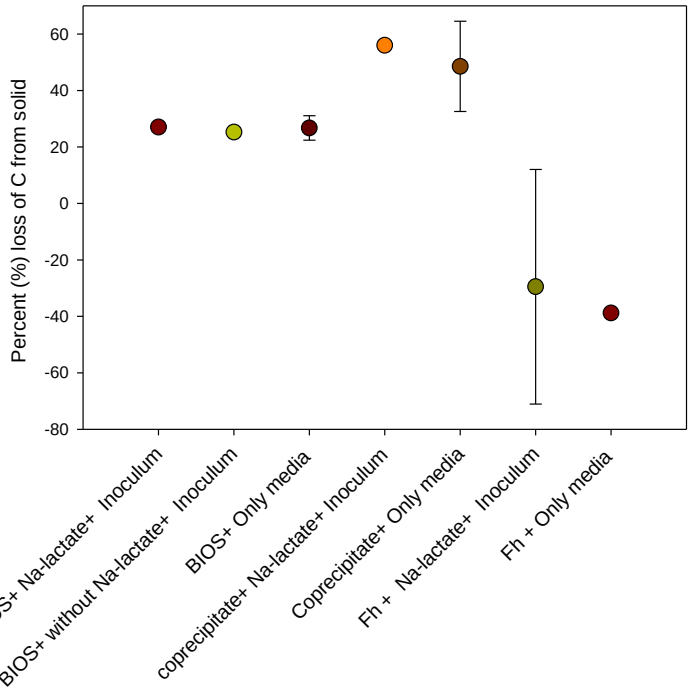

Figure A.1: Percent (%) loss of carbon from the solid during incubation. This calculation was done based on the amount of C present in the solids before incubation and the amount of C left after incubation. The effect of labeled added C was also considered during the calculation.

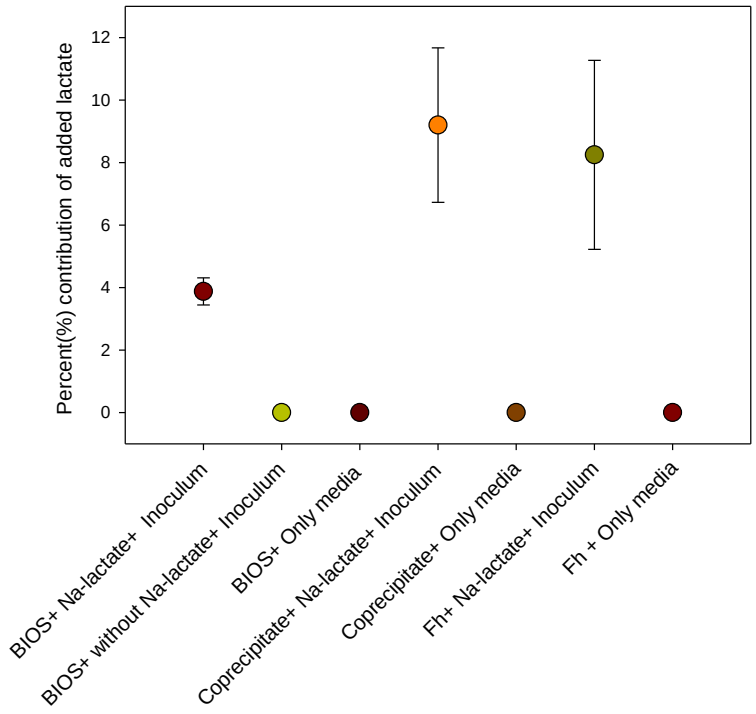

Figure A.2: Percent (%) contribution of added lactate to the solid during incubation i.e. the percentage of added lactate sorbed to the solids after incubation. The use of ^{13}C labeled lactate ensured that this C came from only lactate.

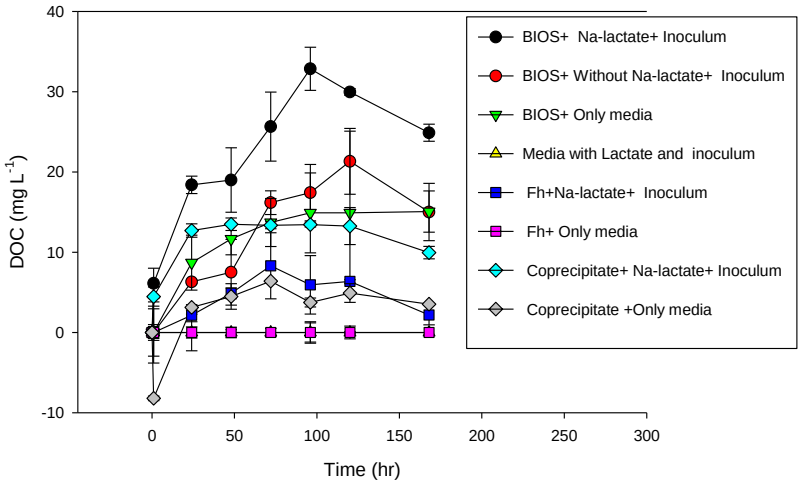

Figure A.3: Dissolved organic carbon concentration (DOC) during the microbial incubation.

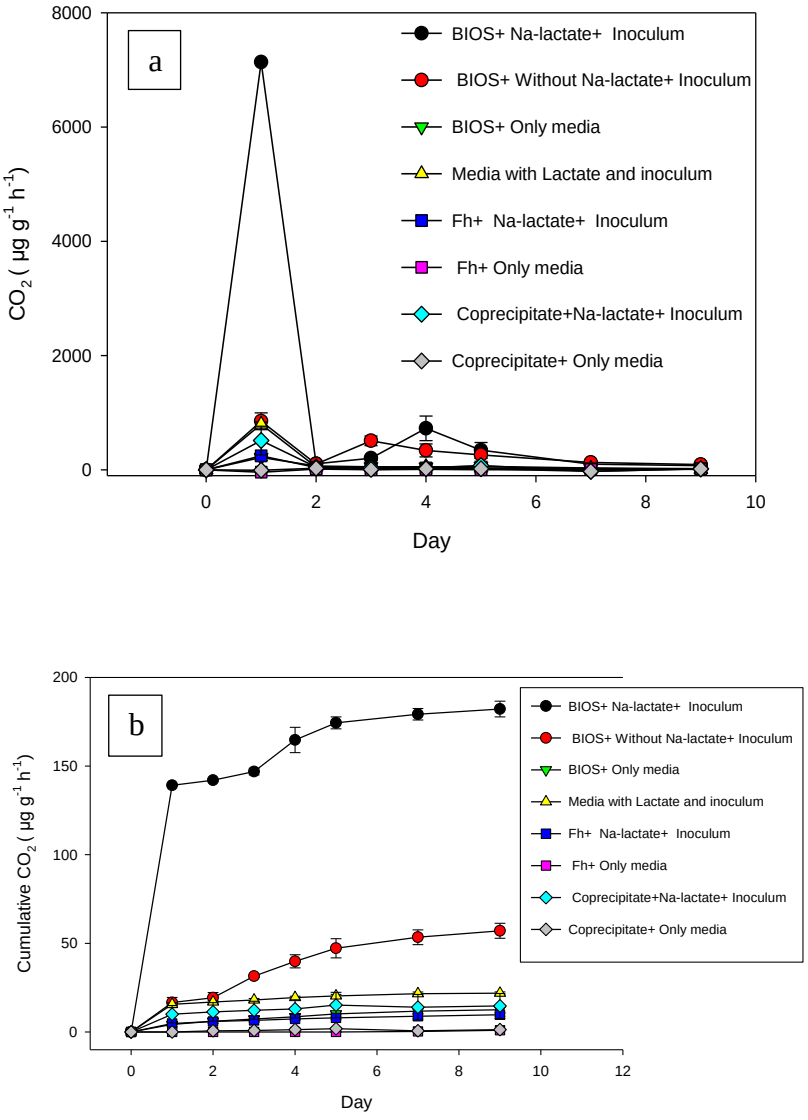

Figure A.4: (a) CO_2 mineralization over time and (b) cumulative CO_2 mineralization.

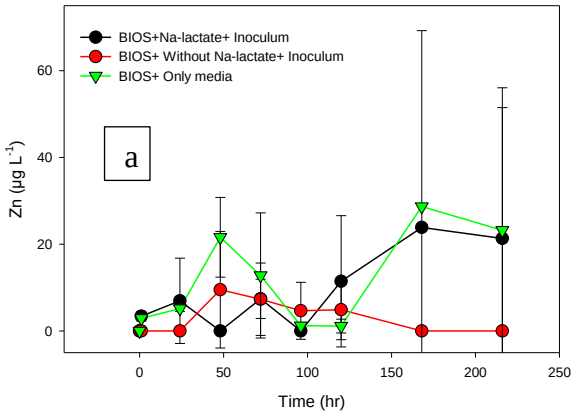
BIOS+Na-lactate+ Inoculum
BIOS+ Without Na-lactate+ Inoculum
BIOS+ Only media
a
Zn (µg L-1)
Time (hr)

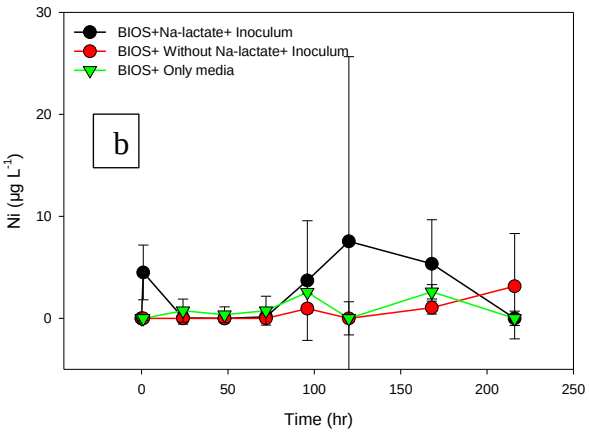
BIOS+Na-lactate+ Inoculum
BIOS+ Without Na-lactate+ Inoculum
BIOS+ Only media
b
Ni (µg L-1)
Time (hr)

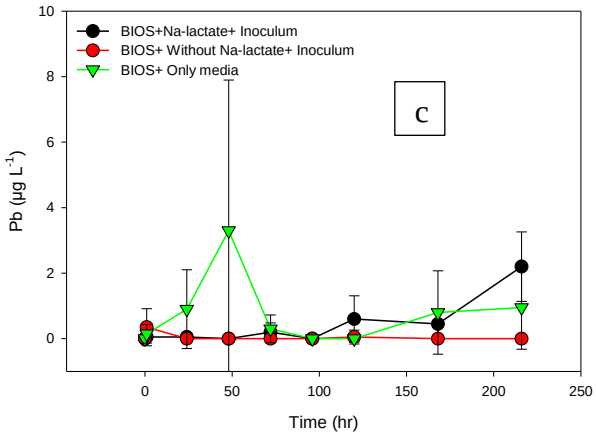
BIOS+Na-lactate+ Inoculum
BIOS+ Without Na-lactate+ Inoculum
BIOS+ Only media
c
Pb (µg L-1)
Time (hr)

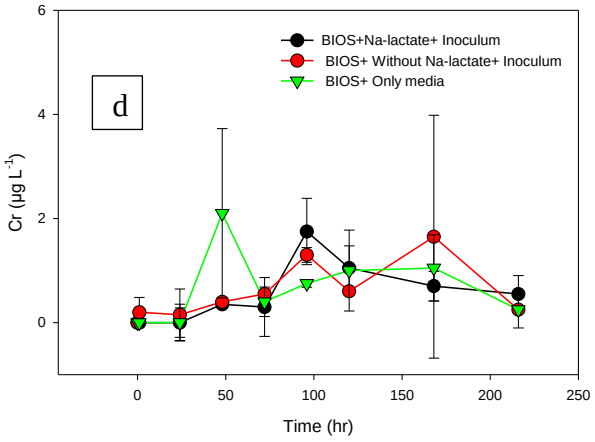
BIOS+Na-lactate+ Inoculum
BIOS+ Without Na-lactate+ Inoculum
BIOS+ Only media
d
Cr (µg L-1)
Time (hr)

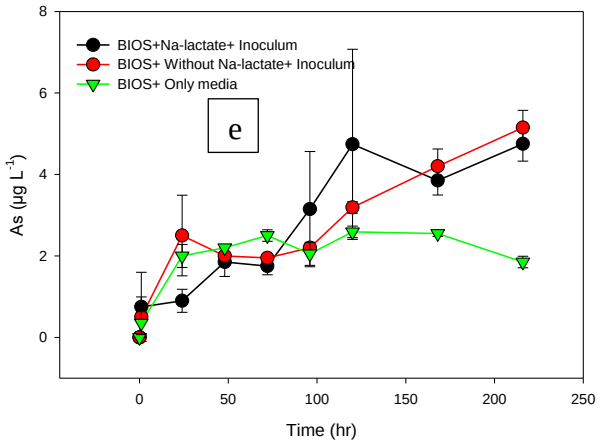
BIOS+Na-lactate+ Inoculum
BIOS+ Without Na-lactate+ Inoculum
BIOS+ Only media
e
As (µg L-1)
Time (hr)

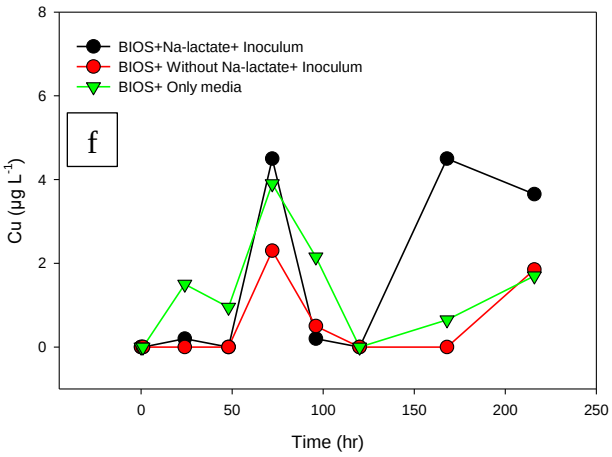
BIOS+Na-lactate+ Inoculum
BIOS+ Without Na-lactate+ Inoculum
BIOS+ Only media
f
Cu (µg L-1)
Time (hr)

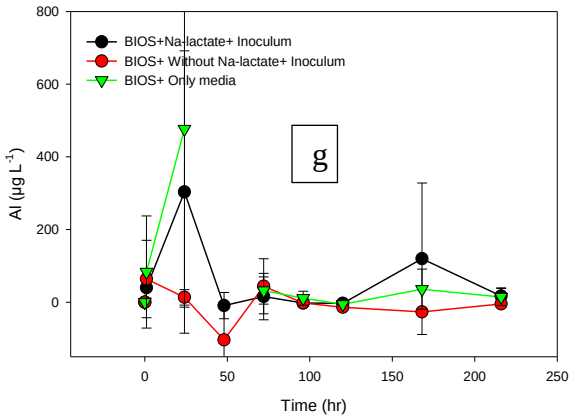

Figure A.5: Aqueous concentrations of (a) Zn (b) Ni (c) Pb (d) Cr (e) As (f) Cu and (g) Al during the microbial incubation.

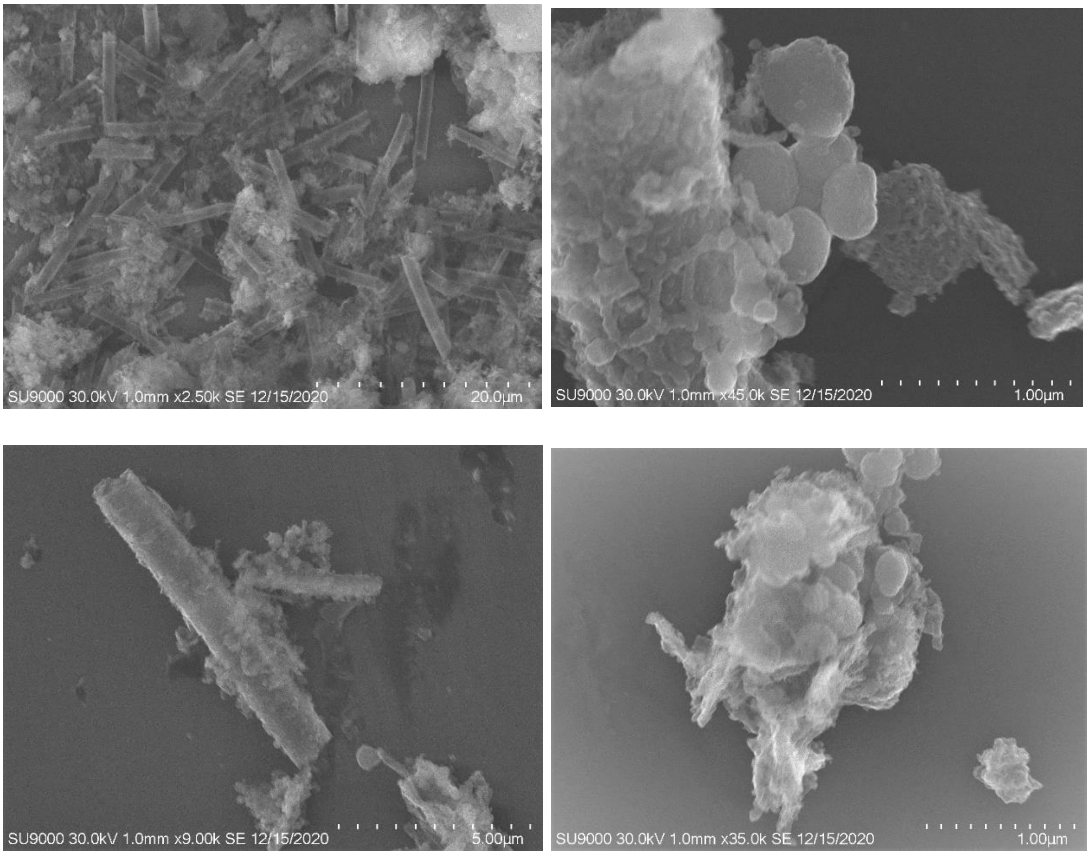

Figure A.6: Scanning transmission electron microscopy image of BIOS before incubation.

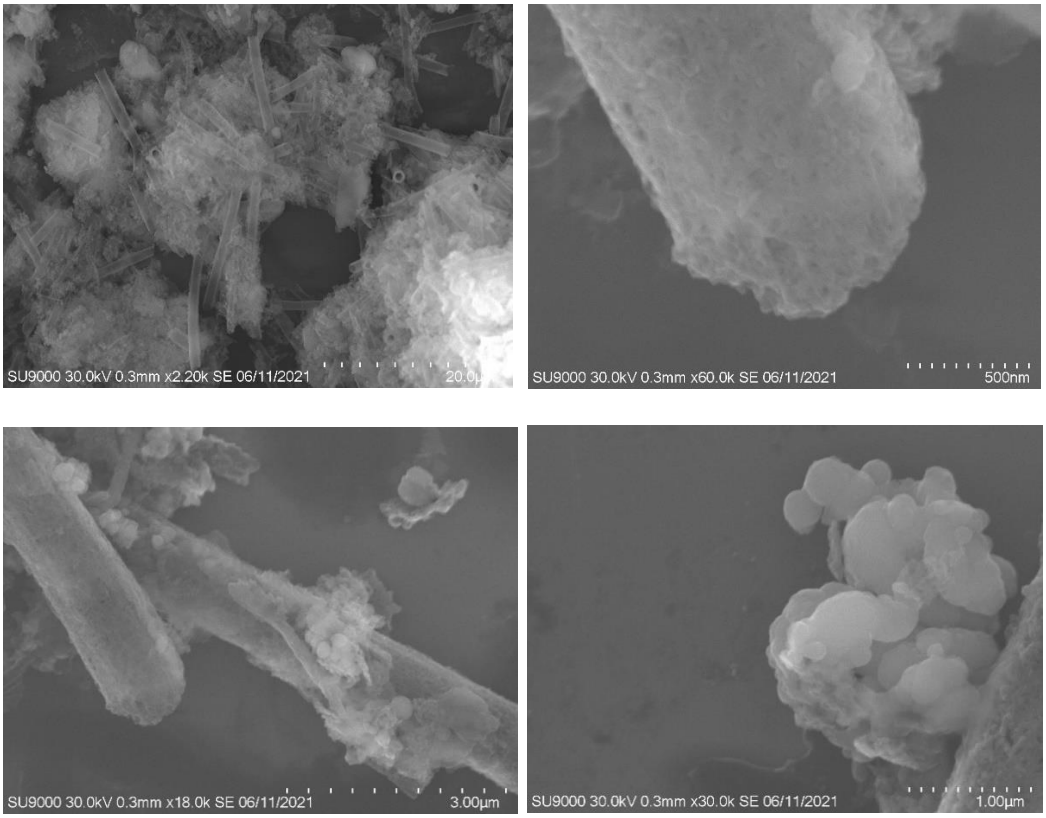

Figure A.7: Scanning transmission electron microscopy image of BIOS after incubation

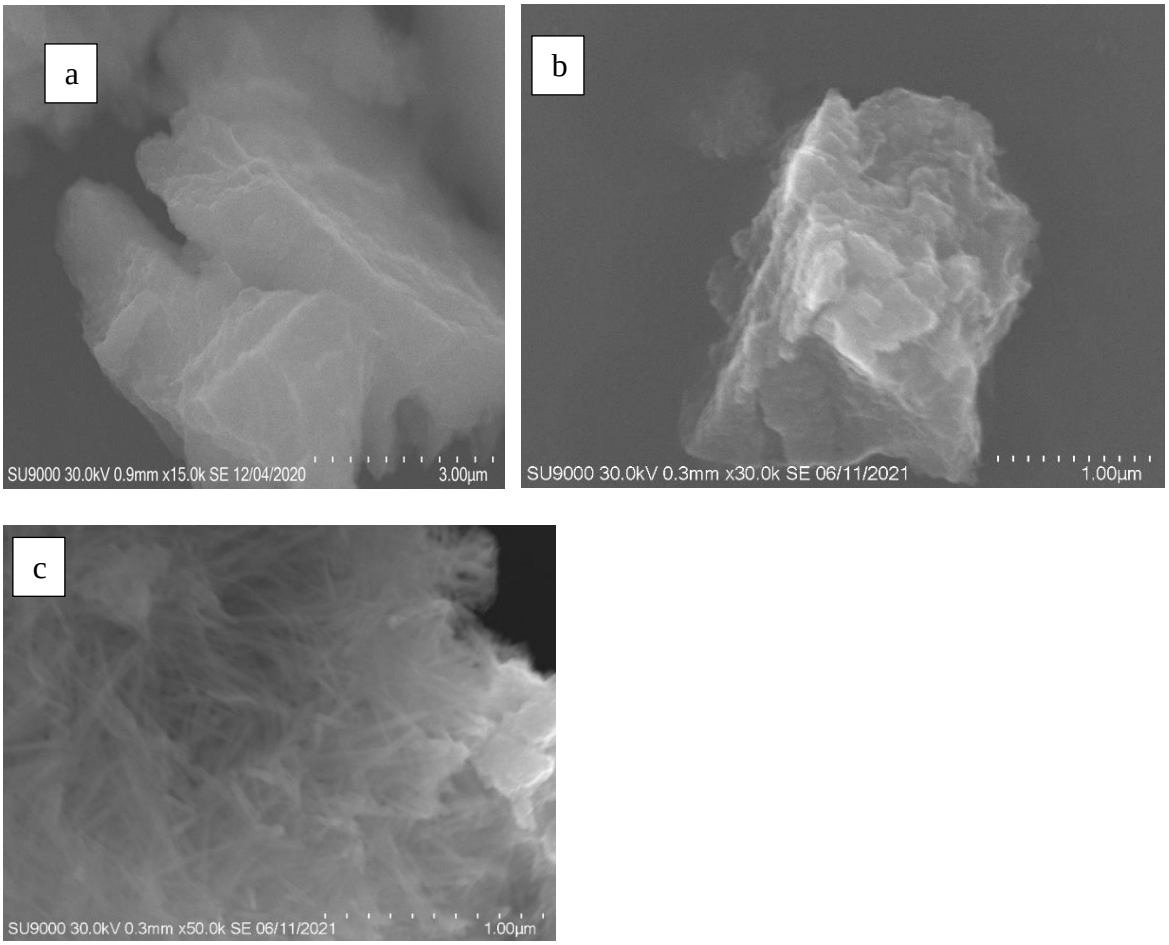

Figure A.8: Scanning transmission electron microscopy image of coprecipitate (a) before and (b) after incubation as well as (c) Fh treatment after incubation, illustrating the formation of new crystal structures.

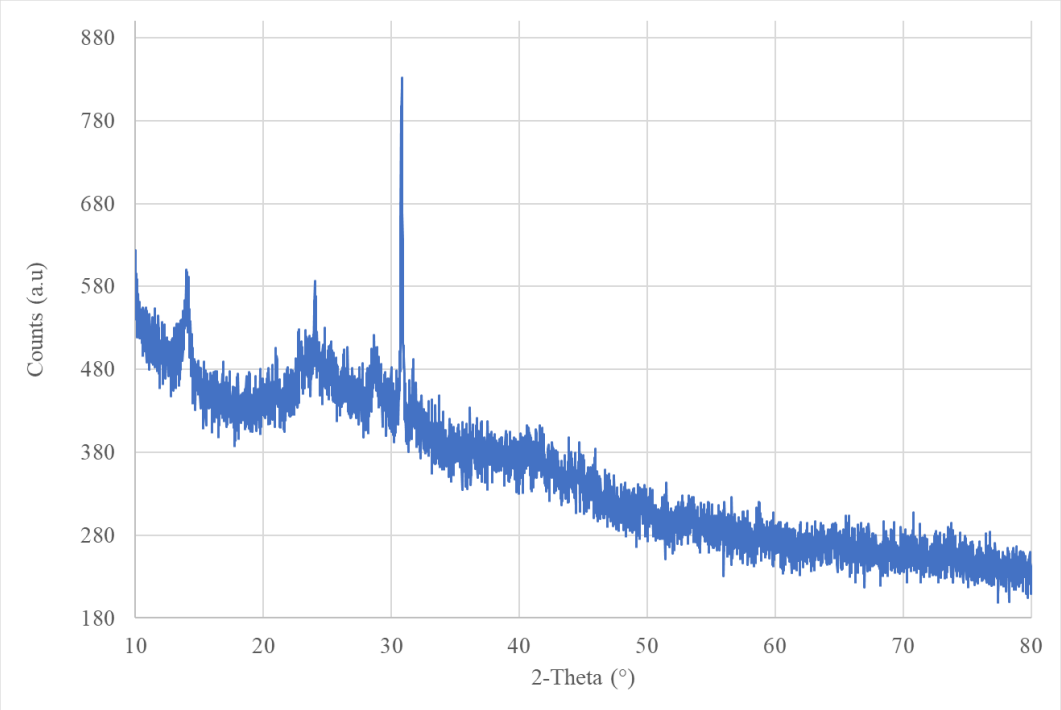

Figure A.9: X-ray diffraction pattern of collected BIOS.

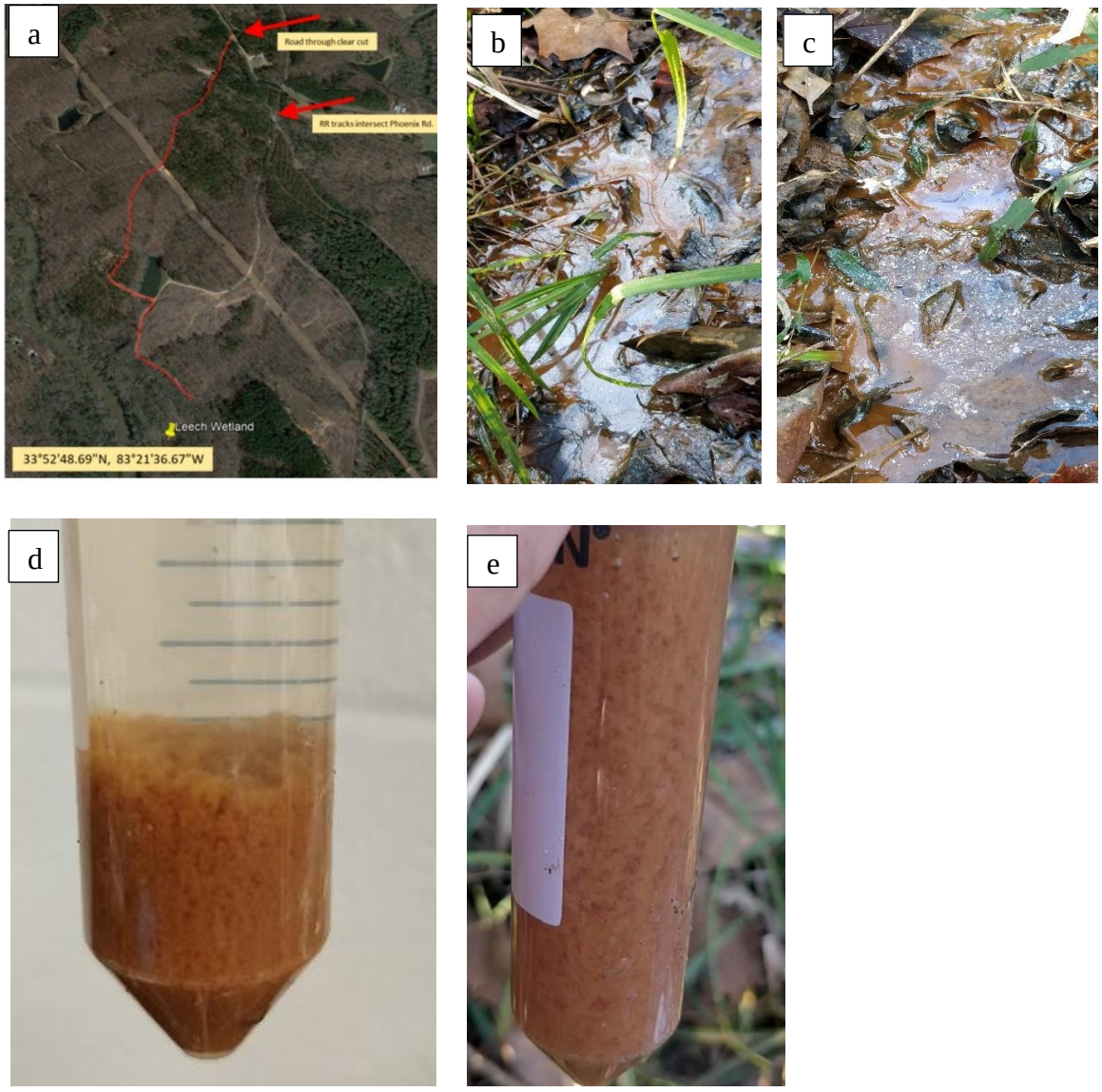

Figure A.10: (a) GPS map of the sampling site where the yellow pinpointing out the exact position. (b, c) the iron containing flocks in the wetland from where the sampling occurred. (d, e) collected sample in the tube.

Table A.1: Elemental composition of the BIOS and synthesized coprecipitates, Ferrihydrite.

Sample	Element	Initial (mg g^{-1})	C/Fe ratio
BIOS	C	98	0.58
	^{13}C	1.1	
	Na	5.9	
	Mg	7.0	
	Al	13	
	K	5.9	
	Ca	56	
	Fe	781	
	Zn	0.3	
	Cd	6.5	
	Ni	5.4	
	Pb	2.8	
	Cr	2.2	
	As	0.9	
	Cu	0.2	
	Mn	1.7	
	P	3.0	
	Si	510	
Fh	C	28	0.1
	^{13}C	0.3	
	Fe	791	
Coprecipitate	C	60	0.3
	Atom%^{13}C	1.07	
	Fe	1029	

APPENDIX B

SUPPLEMENTAL INFORMATION OF CHAPTER 3

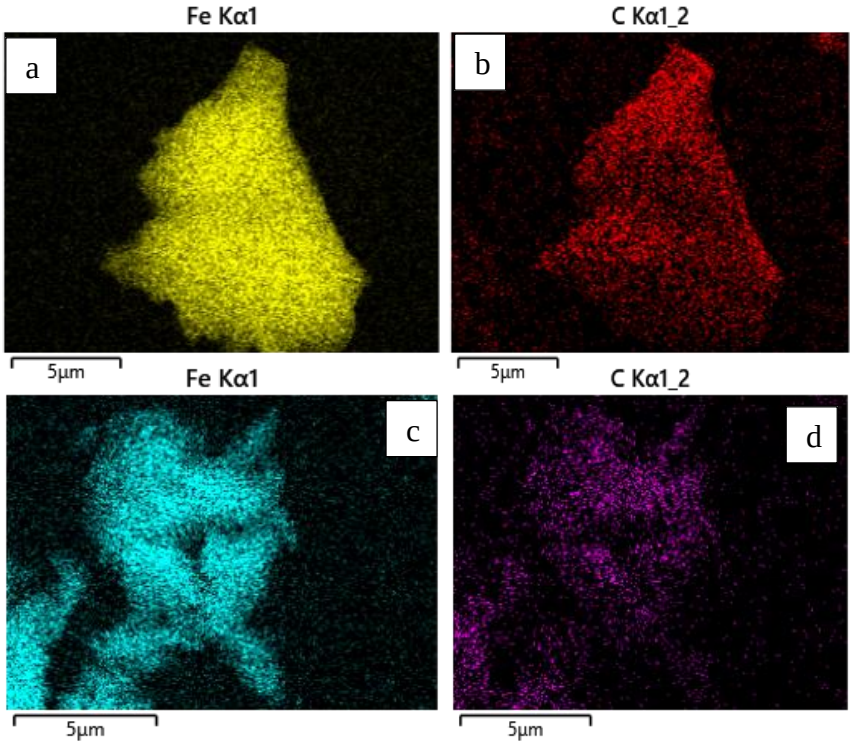

Figure B.1: EDS mapping of results of Fresh Low unreacted (a-b) and reacted coprecipitate with Fe (II) (c, d).

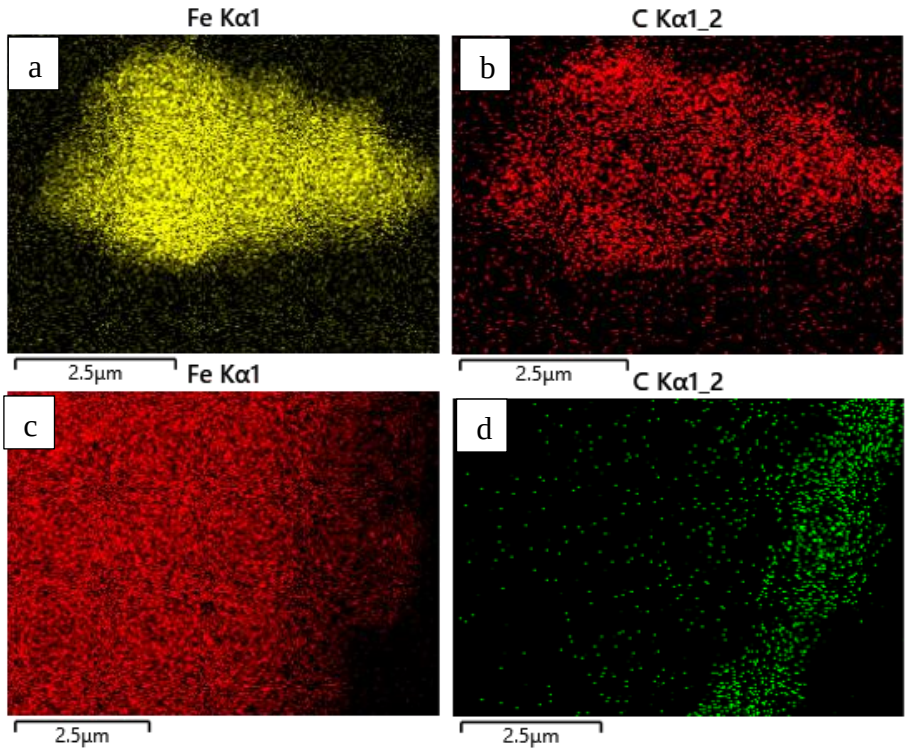

Figure B.2: EDS mapping of results of Aged Low unreacted (a, b) and reacted coprecipitate with Fe (II) (c, d).

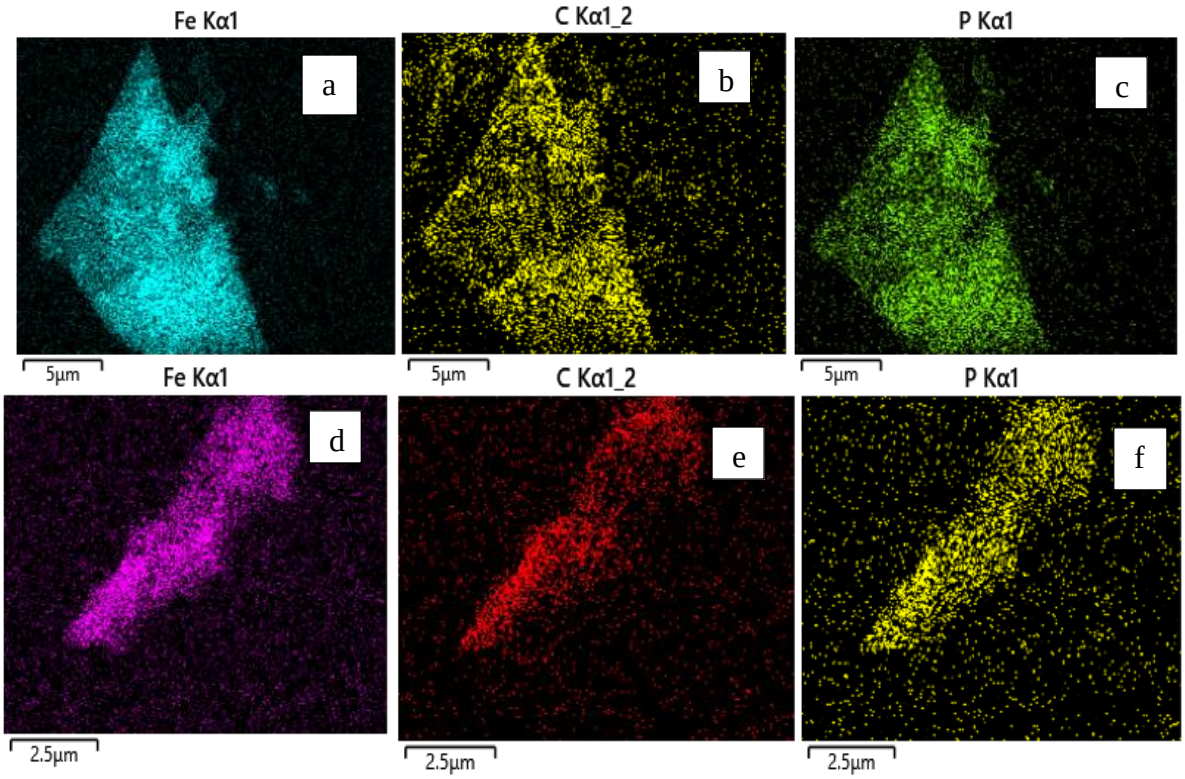

Figure B.3: EDS mapping of results of Fresh High unreacted (a-c) and reacted coprecipitate with Fe(II) (d-f).

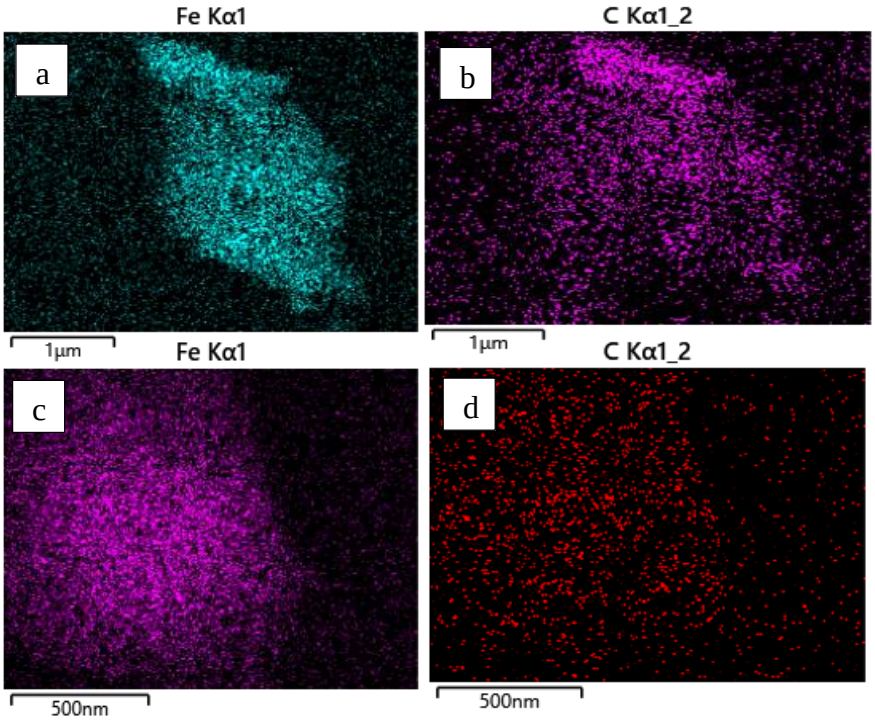

Figure B.4: EDS mapping of results of Aged High unreacted (a, b) and reacted coprecipitate with Fe(II) (c, d).

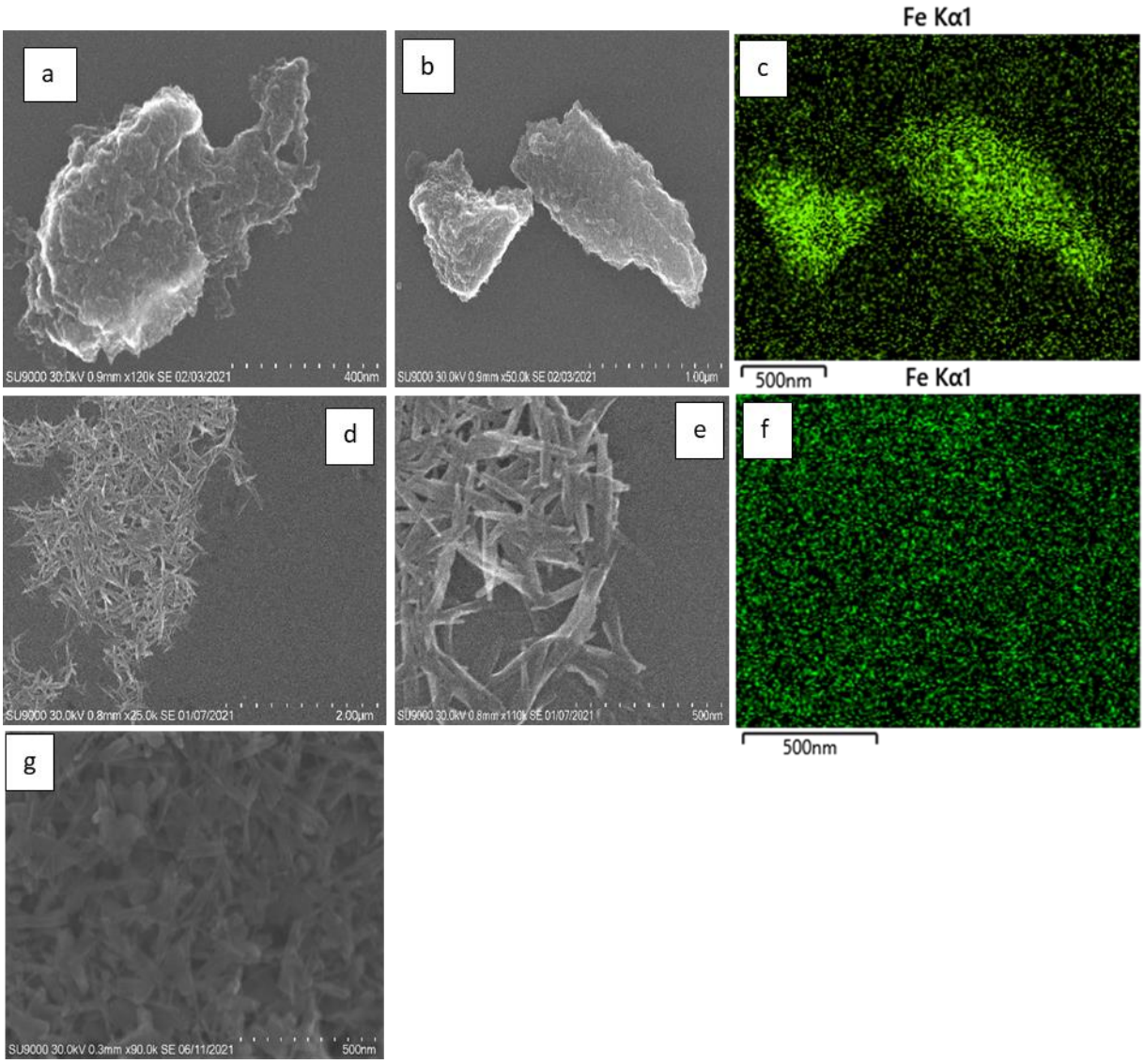

Figure B.5: STEM image of Aged unreacted (a-c) and Fe(II) reacted (d-f) Fh. (g) Fresh Fe(II) reacted Fh.

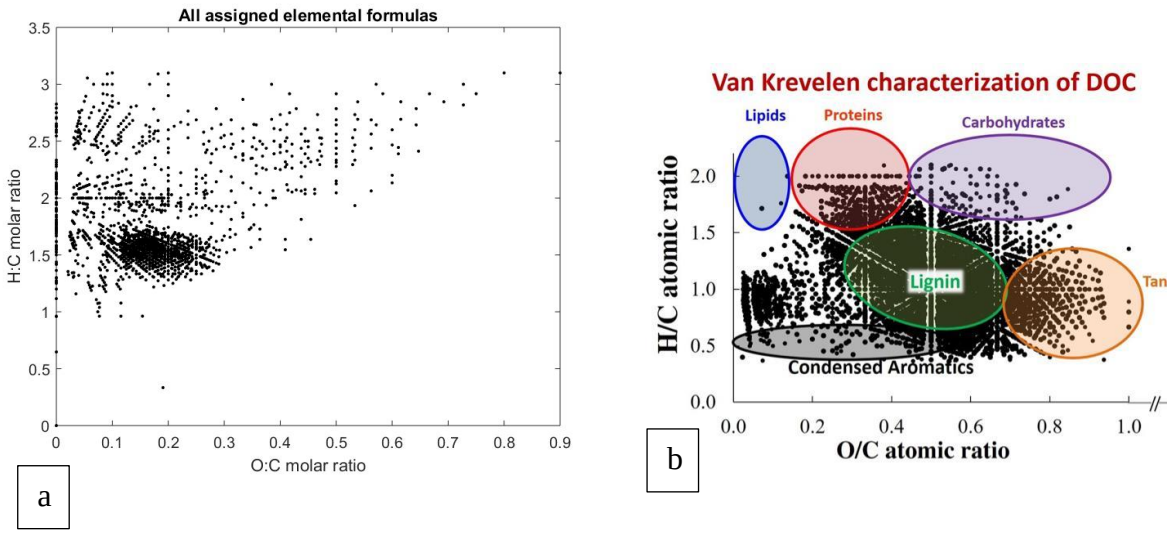

Figure B.6: Van Krevelen space diagram (VKD) of the ^{13}C-DOM used as a C source for preparing the coprecipitate from FTICR analysis. (b) Van Krevelen diagram of DOC from an Arctic stream. Image Source: Dr. Rose Cory (University of Michigan). This image was used to compare our Van Krevelen diagram.

Table B.1: Magnetic susceptibility of the Fh mineral and Fh-NOM coprecipitates

	Sample name	**Magnetic susceptibility (10^{-8} m^3Kg^{-1})**
Fresh	Fh	164
	Fh with Fe (II)	5674
	C/Fe =Low	106
	C/Fe =Low with Fe(II)	204
	C/Fe =High	-48
	C/Fe =High with 1.8+Fe(II)	17
Aged	Fh	98
	Fh with Fe(II)	63
	C/Fe =Low	100
	C/Fe =Low with Fe(II)	197
	C/Fe =High	28
	C/Fe =High with 1.8+Fe(II)	62

APPENDIX C

SUPPLEMENTAL INFORMATION OF CHAPTER 4

Table C.1: Total C and added ^{13}C-NOM content of the solids before and after incubation study (mg /30mg unit) for Fresh samples. The same treatment names indicating replications.

Treatment	Total C (before)	Total C (after)	Added ^{13}C-NOM (before)	Added ^{13}C-NOM (after)	% loss of added ^{13}C-NOM
Fh	1.29	1.79	0.00	0.00	0
Fh	1.29	1.74	0.00	0.00	0
Fh with Fe (II)	0.33	0.75	0.00	0.00	0
Fh with Fe (II)	0.33	0.73	0.00	0.00	0
C/Fe= Low	2.54	2.84	2.27	1.11	51
C/Fe =Low	2.54	2.80	2.27	1.09	52
C/Fe= Low with Fe (II)	3.16	2.85	2.02	1.53	24
C/Fe = Low with Fe (II)	3.16	2.98	2.02	1.53	24
C/Fe =High	4.07	3.66	3.32	2.07	38
C/Fe = High	4.07	3.83	3.32	2.04	39
C/Fe = High with Fe (II)	4.09	3.56	3.10	2.00	35
C/Fe = High with Fe (II)	4.09	3.51	3.10	2.08	33
Without the presence of inoculum					
C/Fe = Low	2.54	2.62	2.27	1.17	48
C/Fe = Low with Fe (II)	3.16	2.61	2.02	1.68	17
C/Fe = High	4.07	3.47	3.32	2.29	31
C/Fe= High with Fe (II)	4.09	3.15	3.10	2.28	27
Fh	1.29	1.58	0.00	0.00	0
Fh with Fe(II)	0.33	0.49	0.00	0.02	0

Table C.2: Total C and added ^{13}C-NOM content of the solids before and after incubation study (mg/30mg unit) for **Aged samples**. The same treatment names indicating replications.

Treatment	Total C (before)	Total C (after)	Added ^{13}C-NOM (before)	Added ^{13}C-NOM (after)	% loss of added ^{13}C-NOM
Fh	2.12	bdl	0.00	bdl	bdl
Fh	2.12	bdl	0.00	bdl	bdl
Fh with Fe (II)	0.84	bdl	-	bdl	bdl
Fh with Fe (II)	0.84	bdl	-	bdl	bdl
C/Fe= Low	1.77	1.81	0.99	0.62	38
C/Fe= Low	1.77	1.90	0.99	0.61	38
C/Fe= Low with Fe (II)	2.14	1.63	1.00	0.73	26
C/Fe = Low with Fe (II)	2.14	1.61	1.01	0.73	28
C/Fe =High	2.09	2.48	1.50	0.87	42
C/Fe = High	2.09	2.36	1.50	0.87	42
C/Fe = High with Fe (II)	2.28	2.16	1.36	1.03	24
C/Fe = High with Fe (II)	2.28	1.93	1.36	1.04	23
Without the presence of inoculum					
C/Fe = Low	1.77	1.97	0.99	0.67	33
C/Fe = Low with Fe (II)	2.14	1.68	1.07	0.73	32
C/Fe = High	2.09	2.33	1.50	0.95	37
C/Fe= High with Fe (II)	2.28	2.29	1.36	1.17	14
Fh	2.12	bdl	0.00	bdl	bdl
Fh with Fe(II)	0.84	bdl	-	bdl	bdl

bdl= Below detection limit.

Table C.3: per cent contribution of added ^{13}C-NOM released as DOC and CO_2-C (% of solid ^{13}C-NOM initially present in the solids) in Fresh and Aged reactors.

Treatment	^{13}C NOM in DOC		^{13}C-NOM in CO_2	
	Fresh	**Aged**	**Fresh**	**Aged**
C/Fe= Low	34	38	1.4	2.8
C/Fe= Low	36	31	1.5	3.0
C/Fe= Low with Fe(II)	41	49	3.4	5.1
C/Fe = Low with Fe(II)	45	54	2.9	4.2
C/Fe =High	40	33	3.6	2.5
C/Fe = High	40	38	4.6	2.6
C/Fe = High with Fe(II)	29	50	1.9	2.7
C/Fe = High with Fe(II)	29	46	2.7	2.7
Without microbial inoculum				
C/Fe = Low	36	41	2.2	1.1
C/Fe = Low with Fe(II)	42	59	6.9	1.5
C/Fe = High	38	41	3.2	0.7
C/Fe= High with Fe(II)	29	59	4.9	1.0

Table C.4: Mass balance calculation for added ^{13}C-NOM in each Fresh reactor. The calculation has been done based on 30mg solid in 55ml solution basis.

Before					After			
Treatment	**C in solid (mg/30 mg)**	**Solution (mg/55ml)**	**Total C**		**C in solid (mg/30mg)**	**C released in solution (mg/55ml)**	**Mineralized CO_2-C (mg/30mg)**	**Total C**
Fh	0	0	0.0		0.00	0	0	0.0
Fh	0	0	0.0		0.00	0	0	0.0
Fh with Fe (II)	0.00	0	0.0		0.02	-0.01	0	0.0
Fh with Fe (II)	0.00	0	0.0		0.02	-0.01	0	0.0
C/Fe= Low	2.27	0	2.3		1.11	0.78	0.03	1.9
C/Fe =Low	2.27	0	2.3		1.09	0.82	0.03	1.9
C/Fe= Low with Fe (II)	2.02	0	2.0		1.53	1.33	0.12	3.0
C/Fe = Low with Fe (II)	2.02	0	2.0		1.53	1.34	0.15	3.0
C/Fe =High	3.32	0	3.3		2.07	0.83	0.07	3.0
C/Fe = High	3.32	0	3.3		2.04	0.91	0.06	3.0
C/Fe = High with Fe (II)	3.10	0	3.1		2.00	0.89	0.06	2.9
C/Fe = High with Fe (II)	3.10	0	3.1		2.08	0.89	0.08	3.1
Without the presence of inoculum								
C/Fe = Low	2.27	0	2.3		1.17	0.82	0.05	2.0
C/Fe = Low with Fe (II)	2.02	0	2.0		1.68	1.25	0.11	3.0
C/Fe = High	3.32	0	3.3		2.29	0.85	0.14	3.3
C/Fe= High with Fe (II)	3.10	0	3.1		2.28	0.90	0.15	3.3

Table C.5: Mass balance calculation for added ^{13}C-NOM in each Aged reactor. The calculation has been done based on 30mg solid in 55ml solution basis.

Before					After			
Treatment	**C in solid (mg/30 mg)**	**Solution (mg/55ml)**	**Total C**		**C in solid (mg/30mg)**	**C released in solution (mg/55ml)**	**Mineralized CO_2-C (mg/30mg)**	**Total C**
Fh	0.00	0	0.0		bdl	0.00	0.00	0.0
Fh	0.00	0	0.0		bdl	0.00	0.00	0.0
Fh with Fe (II)	0.17	0	0.2		bdl	0.00	0.01	0.0
Fh with Fe (II)	0.17	0	0.2		bdl	0.00	0.00	0.0
C/Fe= Low	0.99	0	1.0		0.62	0.37	0.03	1.0
C/Fe= Low	0.99	0	1.0		0.61	0.30	0.03	0.9
C/Fe= Low with Fe (II)	1.0	0	1.0		0.73	0.49	0.04	1.2
C/Fe = Low with Fe (II)	1.01	0	1.0		0.73	0.56	0.04	1.3
C/Fe =High	1.50	0	1.5		0.87	0.49	0.05	1.4
C/Fe = High	1.50	0	1.5		0.87	0.55	0.04	1.5
C/Fe = High with Fe (II)	1.36	0	1.4		1.03	0.68	0.04	1.8
C/Fe = High with Fe (II)	1.36	0	1.4		1.04	0.62	0.04	1.7
Without the presence of inoculum								
C/Fe = Low	0.99	0.00	1.00		0.666	0.408	0.0108	1.1
C/Fe = Low with Fe (II)	0.73	0.00	0.70		1.072	0.624	0.0108	1.7
C/Fe = High	1.50	0.00	1.50		0.952	0.588	0.018	1.6
C/Fe= High with Fe (II)	1.36	0.00	1.40		1.172	0.804	0.0144	2.0

Table C.6: Mass balance calculation for total C in the Fresh reactor. The calculation has been done based on 30mg in 55ml of solution.

Before					After			
Treatment	**C in solid (mg/30 mg)**	**Solution (mg/55ml)**	**Total C**		**C in solid (mg/30mg)**	**DOC (mg/55ml)**	**Mineralized CO_2-C (mg/30mg)**	**Total C**
Fh	1.29	3.3	4.6		1.79	1.56	2.7	6.1
Fh	1.29	3.3	4.6		1.74	1.44	2.6	5.8
Fh with Fe (II)	0.33	3.3	3.6		0.75	1.56	3.7	6.1
Fh with Fe (II)	0.33	3.3	3.6		0.73	1.44	4.5	6.7
C/Fe= Low	2.54	3.3	5.8		2.84	2.04	3.7	8.6
C/Fe =Low	2.54	3.3	5.8		2.80	1.92	3.4	8.1
C/Fe= Low with Fe (II)	3.16	3.3	6.4		2.85	2.16	3.4	8.4
C/Fe = Low with Fe (II)	3.16	3.3	6.4		2.98	2.28	3.6	8.9
C/Fe =High	4.07	3.3	7.3		3.66	2.04	4.3	10
C/Fe = High	4.07	3.3	7.3		3.83	2.04	5.5	11
C/Fe = High with Fe (II)	4.09	3.3	7.4		3.56	2.16	3.7	9.5
C/Fe = High with Fe (II)	4.09	3.3	7.4		3.51	2.16	4.1	9.8
Media	_	3.3	3.3		_	1.56	3.3	4.9
Media	_	3.3	3.3		_	1.32	4.0	5.4
Without the presence of inoculum								
C/Fe = Low	2.54	4.0	6.6		2.62	1.56	1.19	5.4
C/Fe = Low with Fe (II)	3.16	4.0	7.2		2.61	1.92	1.08	5.6
C/Fe = High	4.07	4.0	8.1		3.47	1.8	2.59	7.9
C/Fe= High with Fe (II)	4.09	4.0	8.1		3.15	2.04	2.30	7.5
Fh	1.29	4.0	5.3		1.58	0.96	2.66	5.2
Fh with Fe(II)	0.33	4.0	4.4		0.49	1.08	3.17	4.7

Table C.7: Mass balance calculation for total C in the Aged reactor. The calculation has been done based on 30mg in 55ml of solution.

Before					After			
Treatment	**C in solid (mg/ 30 mg)**	**Solution (mg/ 55ml)**	**Total C**		**C in solid (mg/ 30mg)**	**DOC (mg/ 55ml)**	**Mineralized CO_2-C (mg/30mg)**	**Total C**
Fh	2.12	4.7	6.8		bdl	2.04	0.63	2.7
Fh	2.12	4.7	6.8		bdl	2.04	0.78	2.8
Fh with Fe (II)	0.84	4.7	5.5		bdl	2.04	0.76	2.8
Fh with Fe (II)	0.84	4.7	5.5		bdl	2.04	0.57	2.6
C/Fe= Low	1.77	4.7	6.4		1.81	2.04	0.78	4.6
C/Fe= Low	1.77	4.7	6.4		1.89	2.04	0.78	4.7
C/Fe= Low with Fe (II)	2.14	4.7	6.8		1.63	2.04	0.74	4.4
C/Fe = Low with Fe (II)	2.14	4.7	6.8		1.61	2.04	0.87	4.5
C/Fe =High	2.09	4.7	6.7		2.48	1.92	0.81	5.2
C/Fe = High	2.09	4.7	6.7		2.36	1.92	0.73	5.0
C/Fe = High with Fe (II)	2.28	4.7	6.9		2.16	2.28	0.55	5.0
C/Fe = High with Fe (II)	2.28	4.7	6.9		1.93	2.16	0.72	4.8
Media	_	4.7	4.7		_	1.2	0.53	1.7
Media	_	4.7	4.7		_	1.32	0.76	2.1
Without the presence of inoculum								
C/Fe = Low	1.77	6.0	7.8		1.97	2.28	0.22	4.5
C/Fe = Low with Fe (II)	2.14	6.0	8.2		1.68	2.40	0.31	4.4
C/Fe = High	2.09	6.0	8.1		2.33	1.92	0.52	4.8
C/Fe= High with Fe (II)	2.28	6.0	8.3		2.29	2.40	0.31	5.0
Fh	2.12	6.0	8.2		bdl	2.28	0.22	2.5
Fh with Fe(II)	0.84	6.0	6.9		bdl	2.28	0.16	2.4

Table C.8: Description of each reactor along with their designated names that have been used in this manuscript.

Treatment name	Description of reactors or vials
Fh	containing Fh, selective media with microbial inoculum
Fh with Fe (II)	containing Fe(II) reacted Fh, selective media with microbial inoculum
C/Fe= Low	containing C/Fe low molar ratio coprecipitates, selective media with microbial inoculum
C/Fe= High	containing C/Fe High molar ratio coprecipitates, selective media with microbial inoculum
C/Fe=Low with Fe (II)	Containing Fe(II) reacted C/Fe low molar ratio coprecipitates, selective media with microbial inoculum
C/Fe=High with Fe (II)	Containing Fe(II) reacted C/Fe High molar ratio coprecipitates, selective media with microbial inoculum
Media	Selective media along with microbial inoculum
Without microbial inoculum	All the reactors under this heading have no microbial inoculum in the reactor vials
C/Fe = Low	containing C/Fe low molar ratio coprecipitates and selective media
C/Fe = High	containing C/Fe High molar ratio coprecipitates and selective media
C/Fe= Low with Fe (II)	Containing Fe(II) reacted C/Fe low molar ratio coprecipitates and selective media
C/Fe= High with Fe (II)	Containing Fe(II) reacted C/Fe High molar ratio coprecipitates and selective media
Fh	containing Fh and selective media
Fh with Fe(II)	containing Fe(II) reacted Fh and selective media
Media	Selective media without microbial inoculum
Media (no glucose)	Selective media but no glucose was added and also without microbial inoculum

Table C.9: Change in pH during the incubation period in Fresh reactor.

Treatments	pH values at each sampling date											
Fh	6.6	7.2	7.2	7.3	7.4	7.3	7.3	7.3	7.3	7.1	7.2	7.2
Fh	6.5	7.2	7.2	7.3	7.4	7.4	7.3	7.3	7.3	7.2	7.3	7.1
Fh with Fe (II)	6.2	6.5	6.6	6.7	6.8	6.7	6.7	6.7	6.9	6.8	6.7	6.8
Fh with Fe (II)	6.2	6.5	6.6	6.6	6.8	6.7	6.8	6.8	6.8	6.8	6.7	6.9
C/Fe= Low	6.3	7.0	7.2	7.2	7.3	7.3	7.3	7.5	7.5	7.3	7.1	7.1
C/Fe= Low	6.4	7.1	7.1	7.2	7.3	7.3	7.4	7.4	7.5	7.4	7.3	7.1
C/Fe=High	6.3	6.9	7.0	7.0	7.2	7.3	7.3	7.3	7.3	7.3	7.3	7.1
C/Fe=High	6.3	6.9	7.0	7.0	7.2	7.2	7.2	7.2	7.2	7.3	7.3	6.8
C/Fe= Low with Fe (II)	6.3	6.7	6.8	6.9	7.1	7.0	7.0	7.1	7.2	7.2	7.1	7.1
C/Fe= Low with Fe (II)	6.2	6.7	6.8	6.9	7.1	7.2	7.2	7.1	7.2	7.1	7.0	7.1
C/Fe = Higwith Fe (II)	6.3	6.6	6.7	6.8	7.0	7.2	7.1	7.1	7.1	7.1	7.0	7.1
C/Fe = High with Fe (II)	6.1	6.6	6.7	6.8	6.9	6.9	7.1	7.1	7.1	7.1	7.1	7.1
Media +MO	6.3	6.6	6.6	6.7	6.7	6.7	6.7	6.8	6.7	6.7	6.6	6.7
Media +MO	6.2	6.5	6.6	6.7	6.8	6.7	6.7	6.8	6.8	6.8	6.7	6.8
Without microbial inoculum												
C/Fe = Low	6.9	6.5	6.7	6.8	6.9	6.8	6.8	7.0	7.0	7.0	7.0	7.0
C/Fe= High	6.9	6.3	6.6	6.7	6.8	6.7	6.8	6.9	6.9	6.9	6.8	6.9
C/Fe = Low with Fe(II)	6.8	5.9	6.5	6.6	6.6	6.5	6.5	6.6	6.6	6.7	6.6	6.7
C/Fe = High with Fe(II)	6.8	6.2	6.5	6.6	6.6	6.5	6.6	6.6	6.6	6.7	6.5	6.6
Media	6.8	6.3	6.1	6.5	6.5	6.3	6.3	6.4	6.4	6.2	6.3	6.4
Media	6.8	6.2	6.4	6.5	6.5	6.4	6.4	6.6	6.5	6.4	6.5	6.5
Media without glucose	6.8	6.8	6.8	6.9	6.9	6.8	6.8	6.9	6.8	6.7	6.7	6.7
Media without microbes	6.8	6.8	6.8	6.9	7.0	6.8	6.9	6.9	6.9	6.8	6.8	6.8
Fh	7.1	6.3	7.0	7.1	7.0	7.0	7.0	7.0	7.0	7.0	7.0	6.9
Fh with Fe(II)	6.8	6.4	6.3	6.4	6.4	6.3	6.3	6.4	6.4	6.4	6.5	6.4

Table C.10: Change in pH during the incubation period in Aged reactor.

Treatment	pH values at each sampling date								
Fh	6.2	7.0	6.9	7.0	6.9	6.8	6.9	6.9	6.7
Fh	6.2	7.1	6.9	6.9	7.0	6.9	6.9	6.9	6.7
Fh with Fe (II)	6.1	6.8	6.7	6.7	6.7	6.7	6.6	6.7	6.5
Fh with Fe (II)	6.1	6.7	6.6	6.6	6.7	6.6	6.6	6.7	6.5
C/Fe = Low	6.3	7.0	6.9	6.9	6.9	6.9	6.9	6.9	6.7
C/Fe =Low	6.3	6.9	7.0	6.9	6.9	6.9	6.9	6.8	6.7
C/Fe =High	6.2	7.0	6.9	6.9	6.8	6.8	6.8	6.7	6.6
C/Fe =High	6.3	6.9	6.9	6.9	6.8	6.8	6.7	6.8	6.5
C/Fe = Low with Fe (II)	6.1	6.8	6.8	6.8	6.8	6.6	6.6	6.6	6.4
C/Fe = Low with Fe (II)	6.1	6.8	6.8	6.7	6.8	6.7	6.7	6.6	6.4
C/Fe = High with Fe (II)	6.2	6.9	6.8	6.7	6.7	6.7	6.6	6.6	6.5
C/Fe =High with Fe (II)	6.3	6.8	6.8	6.7	6.8	6.7	6.6	6.5	6.4
Media +MO	6.2	6.7	6.6	6.6	6.7	6.5	6.5	6.4	6.3
Media +MO	6.3	6.7	6.6	6.6	6.7	6.5	6.5	6.4	6.3
Without microbial inoculum									
C/Fe =Low	7.1	6.8	6.7	6.7	6.7	6.6	6.5	6.5	6.4
C/Fe =High	7.1	6.7	6.7	6.7	6.7	6.5	6.5	6.5	6.3
C/Fe =Low with Fe (II)	7.0	6.7	6.6	6.6	6.6	6.5	6.5	6.4	6.3
C/Fe = High with Fe (II)	7.0	6.7	6.6	6.5	6.6	6.5	6.4	6.3	6.3
Media	7.0	6.6	6.4	6.4	6.4	6.4	6.4	6.3	6.1
Media	7.0	6.6	6.5	6.5	6.4	6.3	6.4	6.3	6.1
Media without glucose	7.0	7.0	6.9	6.9	6.8	6.6	6.6	6.5	6.3
Media without glucose	7.0	7.0	6.9	6.8	6.8	6.6	6.7	6.5	6.3
Fh	7.0	6.8	6.7	6.8	6.7	6.6	6.5	6.5	6.3
Fh with Fe(II)	6.9	6.5	6.4	6.4	6.4	6.3	6.2	6.2	6.1

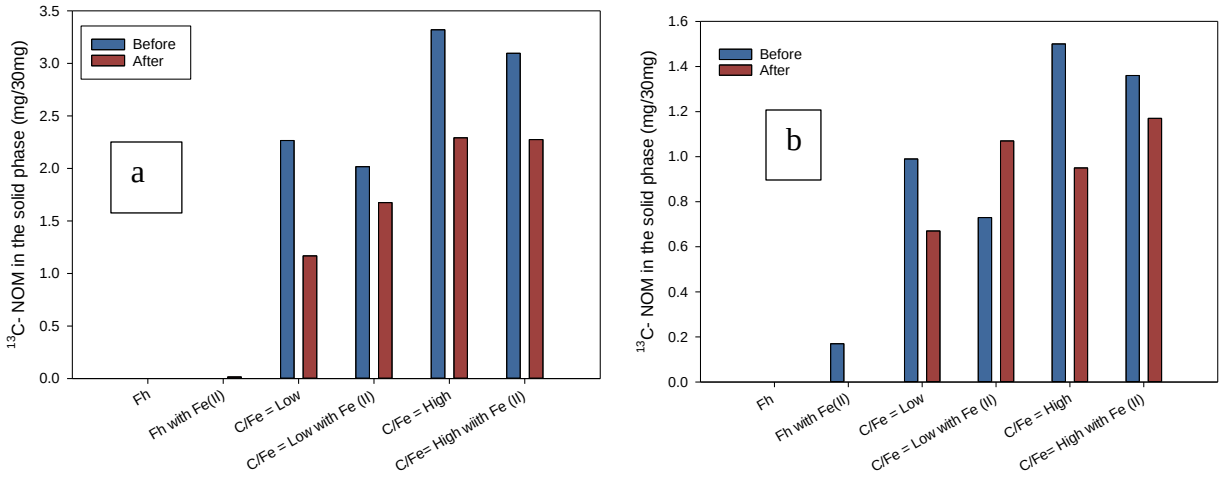

Figure C.1: Added ^{13}C-NOM (mg/30g) in the (a) Fresh and (b) Aged solid sample before and after incubation without microbial inoculum.

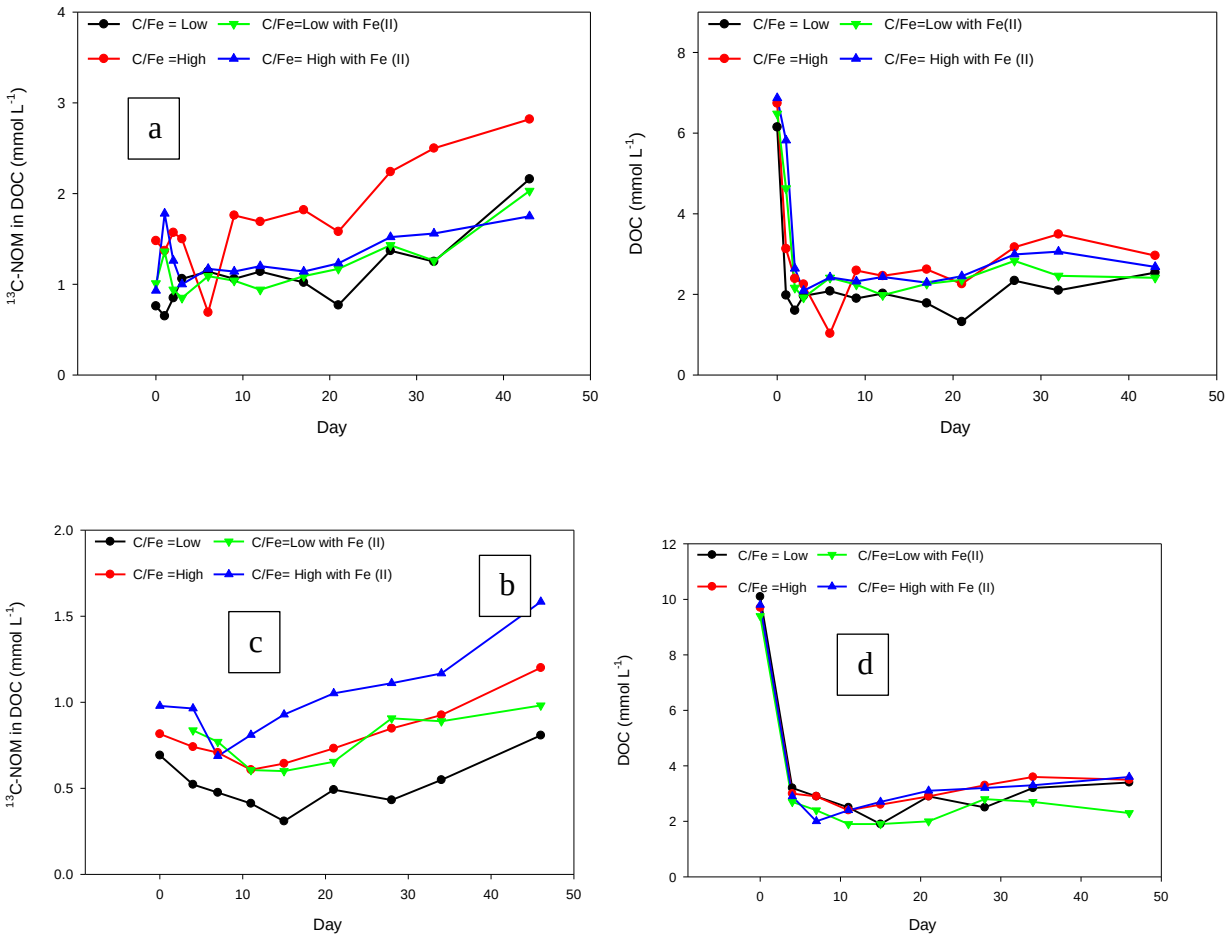

Figure C.2: Added ^{13}C-NOM in DOC and DOC in Fresh (a, b) and Aged (c, d) reactors without microbial inoculum.

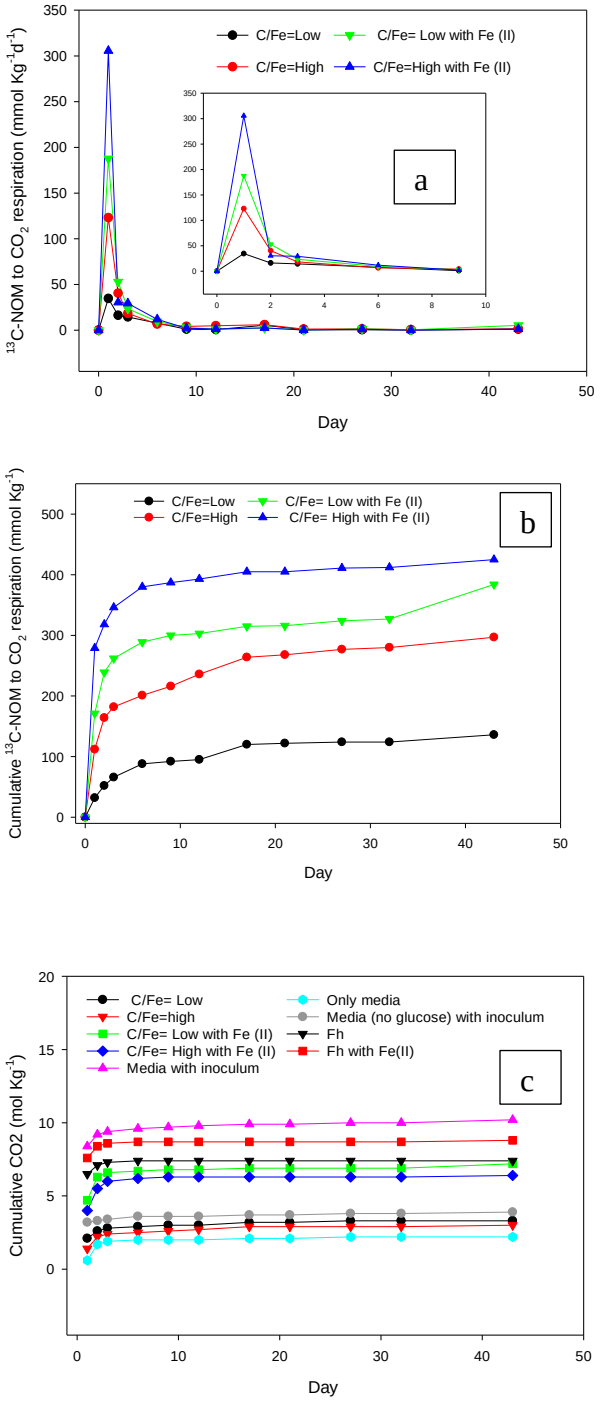

Figure C.3: Added ^{13}C-NOM to CO_2 respiration, cumulative ^{13}C-NOM and Cumulative CO_2 respiration from the Fresh (a,b,c) reactors without microbial incubation.

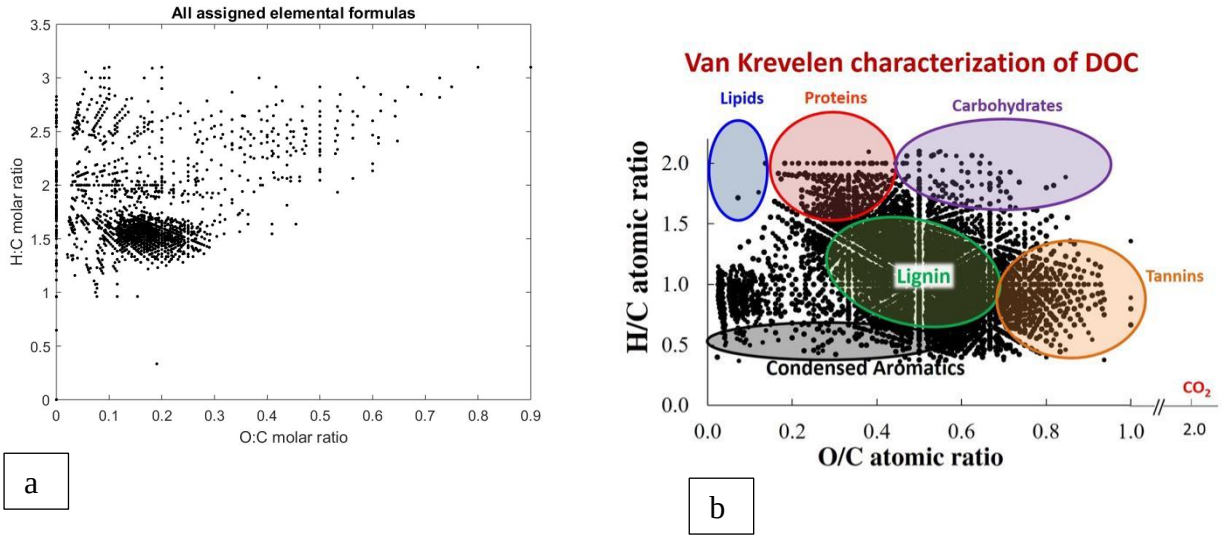

Figure C.4: (a) Van Krevelen space diagram (VKD) of the ^{13}C-DOM used as a C source for preparing the coprecipitate from FTICR analysis. (b) Van Krevelen diagram of DOC from an Arctic stream. Image Source: Dr. Rose Cory (University of Michigan). This image was used to compare our Van Krevelen diagram.

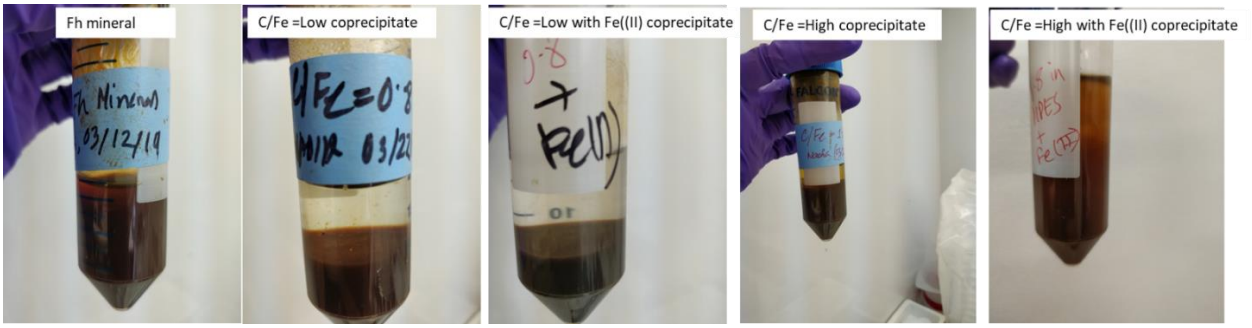

Figure C.5: Images of the 1d reacted coprecipitates along with control.

APPENDIX D

Biodegradation of Ferrihydrite-Humic acid coprecipitate

MATERIALS AND METHODS

Synthesis of Ferrihydrite-Humic acid coprecipitate

Ferrihydrite-Humic acid (Fh-HA) coprecipitates with a C/Fe molar ratio of 1.6 was prepared using Leonardite humic acid standard purchased from the International Humic Substances Society (IHSS). Humic acid was dissolved in 5M KOH to prepare the stock solution. The stock solution later was diluted with 0.1M KOH to achieve the required concentration to prepare the coprecipitates with a C/Fe molar ratio of 1.6. Fe $(NO_3)_3.9H_2O$ was mixed with the required amount of humic acid solution under vigorous stirring following the methods described by Chen et al (Chen et al., 2014). The pH of the suspension was raised from ~2.0 to 7 by slowly adding 0.1 M KOH. After the formation of the coprecipitate, this solution was centrifuged at 12000 rpm for 5 minutes. After washing twice with the 18MΩ DI water the coprecipitate was stored in the glove box (97% N2, 3%H2) before further use.

Microbial inoculum collection

For incubation study under oxic conditions, soil microbial inoculum was obtained from freshly collected soil (0-10 cm depth) from J. Phil Campbell Sr. Research and Education Center, University of Georgia, Athens-GA. The soil was shaken in a 4 mM $CaCl_2$ solution for 24 h and passed through 5 μm filters (Eusterhues et al., 2014b). A small portion of that filtrate was added to Tryptic soy broth (TSB) media and incubated for 12 h at 25°C. The resulting incubated solution was centrifuged at 3000 rpm for 10 min, and the supernatant was discarded. The microbial

inoculums were washed with DI water twice to remove the remaining TSB media and then resuspended in a small amount of selective media containing 0.5 g KH_2PO_4, 1.0 g $NaSO_4$, 2.0 g NH_4Cl, 0.5 mM $CaCl_2$, 0.1 mM $MgSO_4$, and Na lactate (per Liter basis) having concentration of 0, 0.5, 1,2 and 3mM to use for different batches of the experiment. The microorganisms were again incubated in this media for 12 h to give them enough time to adjust to this new media condition before adding to the experimental treatments.

For study under anoxic conditions, *Shewanella oneidensis* MR1 was purchased from American Type Culture Collection (ATCC) and used as the microbial inoculum source. The inoculum was grown on the TSB media and incubated for 12 h at 29°C. Later it was centrifuged at 3000 rpm for 10 min and followed the same procedure that was used for the soil microbial culture solution preparation described above (Ginn et al., 2014).

Experimental setup

The microcosm studies were conducted under both oxic and anoxic conditions in 30ml opaque serum vials containing 30mg of Fh-HA coprecipitate in 20ml of selective media containing (per litre basis) 0.5 g KH_2PO_4, 1.0 g $NaSO_4$, 2.0 g NH_4Cl, 0.5 mM $CaCl_2$, 0.1 mM $MgSO_4$, and Na lactate having a concentration of 0, 0.5, 1, 2 and 3mM. In this study, the effect of the presence of a different concentration of Na lactate on the biodegradation of Fh-HA coprecipitate was also analyzed, therefore, the four different concentration of Na lactate (0.5, 1, 2, 3 mM) was used along with a control containing no Na lactate. The vials under oxic conditions contained soil microorganisms and vials under anoxic conditions contained *Shewanella oneidensis* MR1 along with the coprecipitate and selective media at the rate of $2\times10^{\wedge 8}$ CFU ml^{-1}. To compare the responses of the presence of Na lactate and the microorganisms, there were controls with each batch of experiments containing only Fh-HA coprecipitate and Na lactate containing selective

media; Na lactate containing selective media and microorganisms without the coprecipitates. The incubation study was conducted for 7 days.

The final treatments layout:

Fh-HA+ Inoculum+ Lactate: The reactors contained coprecipitate in sterilized Na lactate containing media with different concentrations (0.5, 1, 2 and 3) along with microbial inoculum.

Fh-HA+ Lactate: Un-inoculated reactors only containing Fh-HA coprecipitate in the media containing different concentrations of Na lactate.

Inoculum + Lactate: The inoculum was suspended in the selective media containing different concentrations of Na lactate (No coprecipitate).

The reactor vials were seal capped with butyl rubber stoppers and continuously shaken on a rotatory shaker. Oxic condition study was conducted in the laminar hood under a laboratory atmosphere, whereas the anoxic condition study was conducted in the glove box (97% N_2, 3%H_2). The reactors were opened during the sampling time with proper measures to prevent contamination. The reactors under oxic condition study were kept open for six hours after each sampling time in the laboratory atmosphere inside the laminar hood to circulate the air inside the reactors with the outside air. This was done to prevent the formation of anoxic conditions in the reactors.

Sample analysis

To measuring the dissolved organic carbon (DOC), acid extractable Fe(II) and emission of CO_2(g) sampling were done at days 0, 3, 5, and 7. 250µl of liquid samples were collected using sterile pipette tips and added 1ml of 0.625 M HCl to measure the Fe (II) concentration following modified ferrozine method (Thompson et al., 2006). The DOC concentration was measured by collecting 750 µl of the solution using 0.22 micron syringe filter and analyzed in the Shimadzu

5050 TOC analyzer. The CO2(g) concentration was measured in LICOR CO_2/H_2O analyzer (Li-840A model).

RESULTS

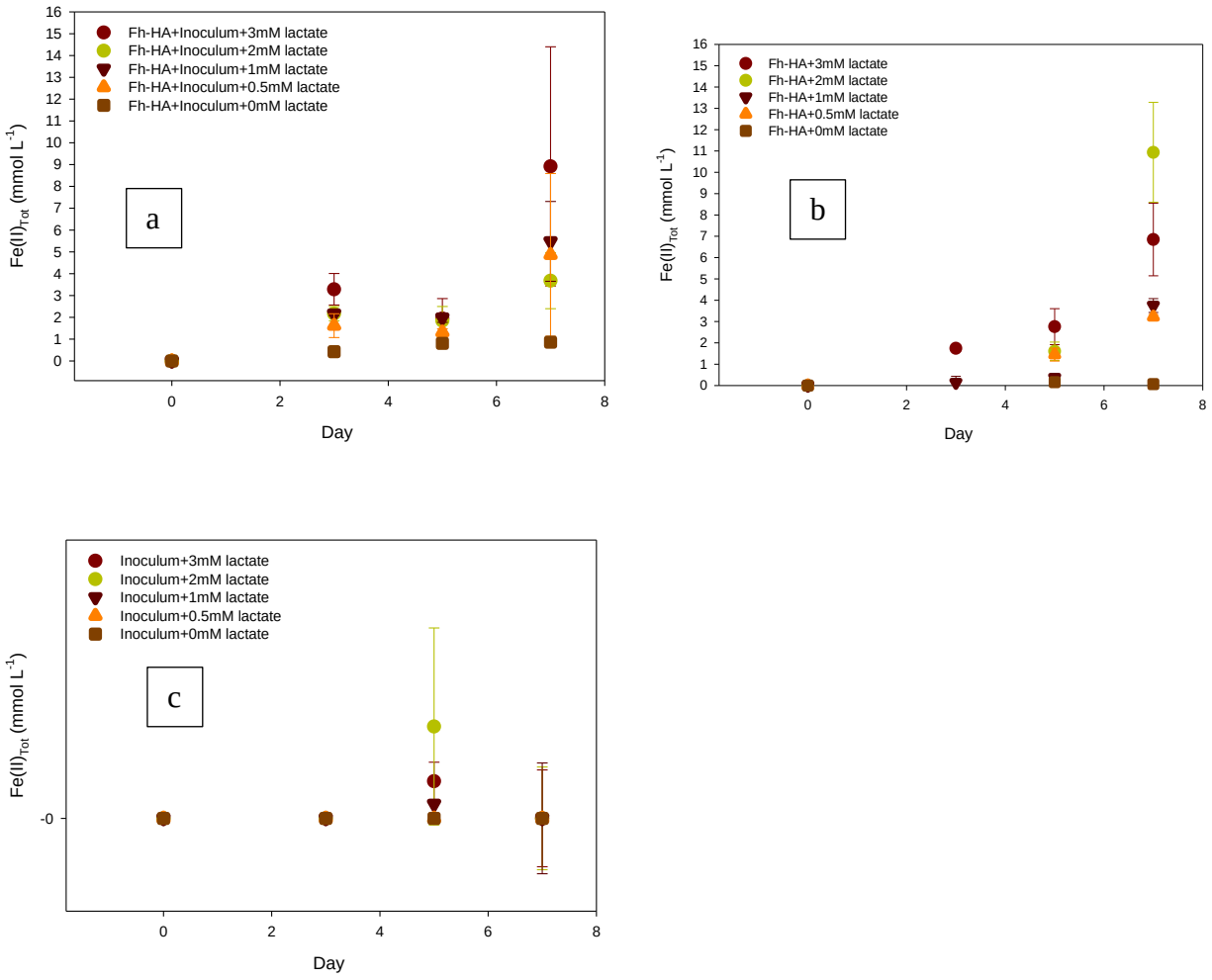

Figure D.1: HCL -extracted Fe (II) over time under anoxic conditions. (a) Fh-HA coprecipitates with microbial inoculum and different concentrations of Na lactate (b) Fh-HA coprecipitate without microbial inoculum (c) Inocumum with different concentrations of lactate.

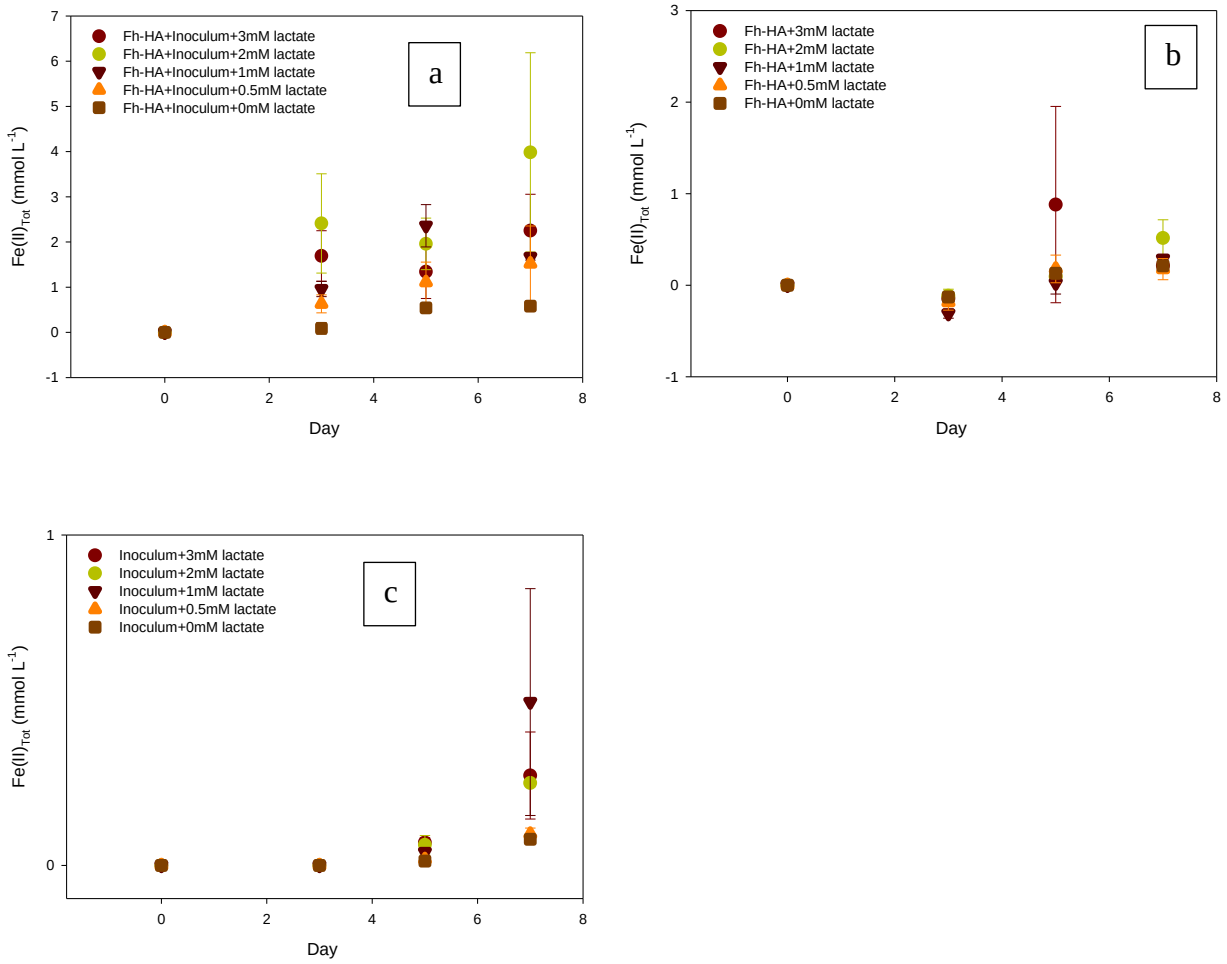

Figure D.2: HCL -extracted Fe (II) over time under oxic condition (a) Fh-HA coprecipitate with microbial inoculum and different concentrations of Na lactate (b) Fh-HA coprecipitate without microbial inoculum(c) Inocumum with different concentrations of lactate.

Under anoxic conditions, over the period of time, the reduction of Fe(III) to Fe(II) increased and it was highest with the presence of 3mM Na lactate (Figure D. 1a). The reduction rate in the reactor containing inoculum and 3mM Na lactate was significantly different from the reactor containing no lactate (Figure D.1a and b). There were differences in the Fe reduction rate in the reactors containing different concentrations of Na lactate but the difference is not significant (Figure D. 1a). Reduction of Fe(III) to Fe(II) also occurred in the reactors without any microbial

inoculum (Figure 1b). The reduction rate was significantly different from the reactor without the lactate (Figure D. 1b). This reduction could be an abiotic reduction process but the experiment was not done in a sterile condition, therefore, this reduction could be the result of microbial contamination in the vials. Fe reduction was not observed in the control (Figure 1c) containing Inoculum and lactate as expected.

Despite being under the oxic condition, a small amount of reduction of Fe was observed in the reactors containing the coprecipitates along with the inoculum and lactate (Figure: 2a). The reduction rate was significantly different from the reactors containing no lactate (zero lactate). No Fe reduction was observed in the reactors containing coprecipitates and lactate (Figure: 2b). The reduction in the oxic condition may have resulted due to the formation of anoxic pockets in the coprecipitates, which triggered the activity of facultative anaerobic microorganisms, resulting in the reduction of Fe(III) to Fe(II).

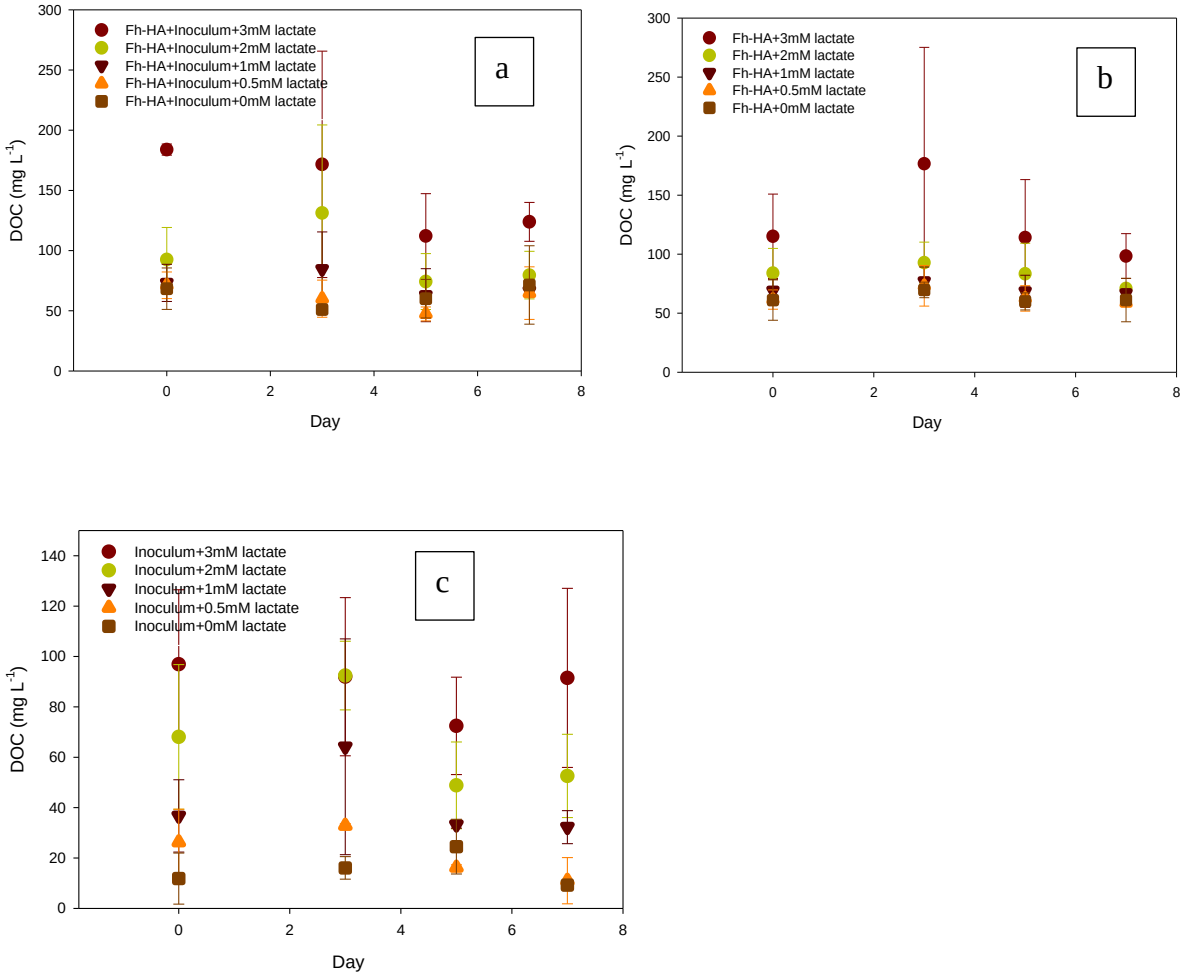

Figure D.3: Dissolve organic carbon (DOC) over time under anoxic condition experiments containing (a) Fh-HA coprecipitate with microbial inoculum and different concentrations of Na lactate (b) Fh-Ha coprecipitate without microbial inoculum(c) Inocumum with different concentrations of lactate.

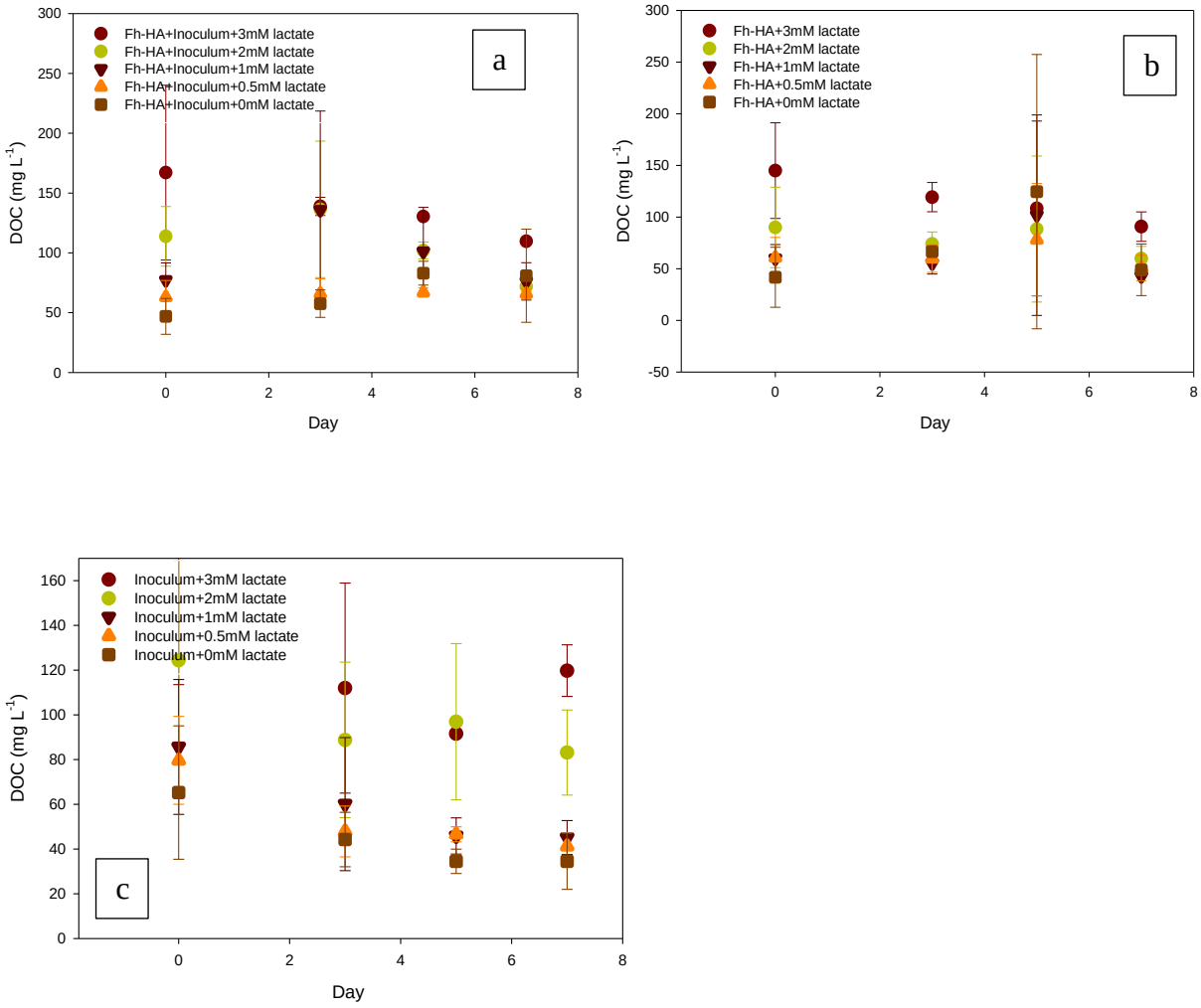

Figure D.4: Dissolve organic carbon (DOC) over time under oxic condition experiments containing (a) Fh-HA coprecipitate with microbial inoculum and different concentrations of Na lactate (b) Fh-Ha coprecipitate without microbial inoculum(c) Inocumum with different concentrations of lactate.

Under anoxic conditions, the concentration of DOC decreased over the period of time in the reactors containing the coprecipitate along with the inoculum and lactate (Figure D. 3a). This rate is significantly different between the reactor containing 3mM lactate and the one with zero lactate (Figure D.3a). The DOC concentration in the reactors containing coprecipitate and lactate

(Figure: 3b) did not change much over the period of time which indicates the decrease in the DOC concentration on the reactors containing coprecipitate along with inoculum and lactate (Figure D. 3a) was occurred due to the sorption of the microbial inoculum on the surface of the coprecipitate minerals. The CO_2 (g) emission data showed no increased in the emission rate over time which also supports this conclusion. Similar trend was observed in the reactors under oxic condition (Figure D. 4).

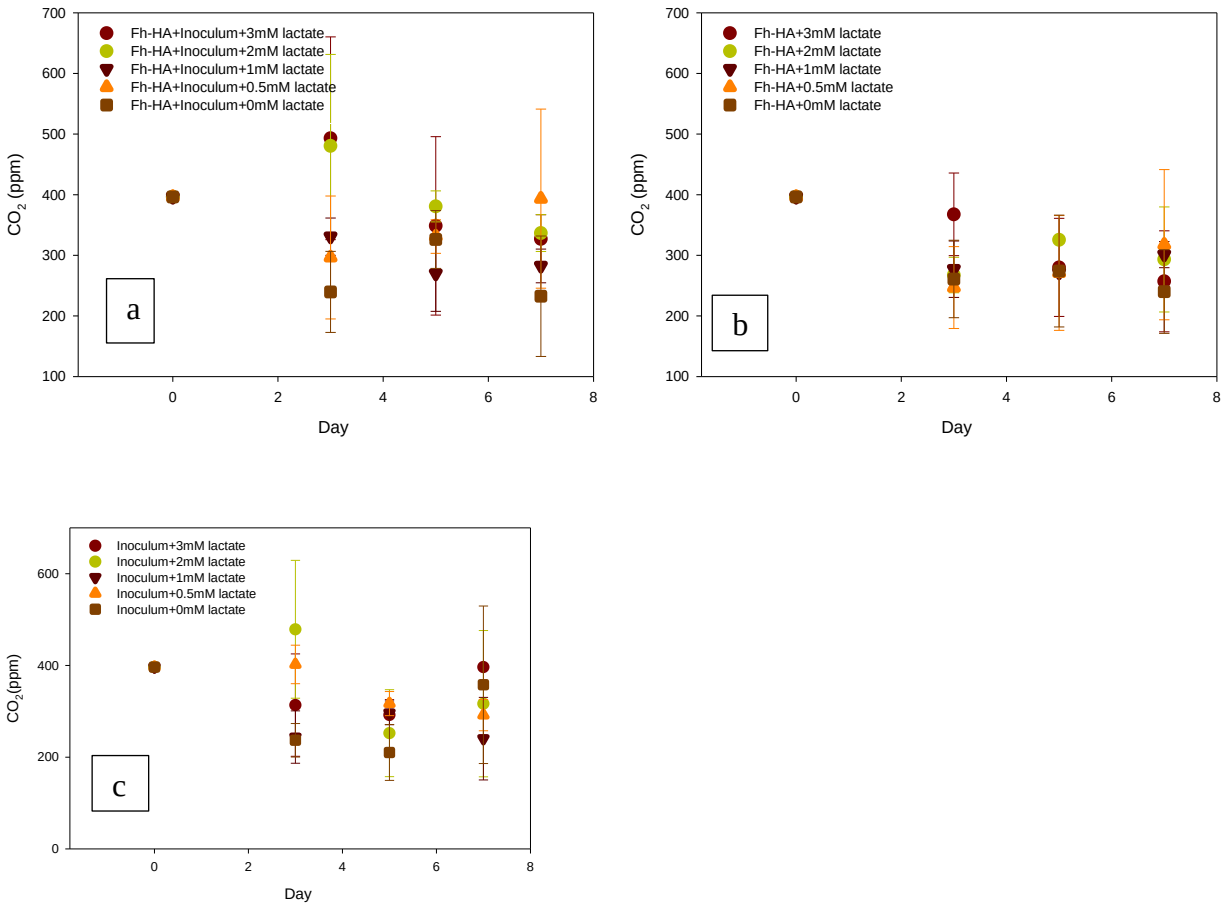

Figure D.5: $CO_{2(g)}$ emission over time under anoxic condition experiments containing (a) Fh-HA coprecipitate with microbial inoculum and different concentrations of Na lactate (b) Fh-Ha coprecipitate without microbial inoculum(c) Inocumum with different concentrations of lactate.

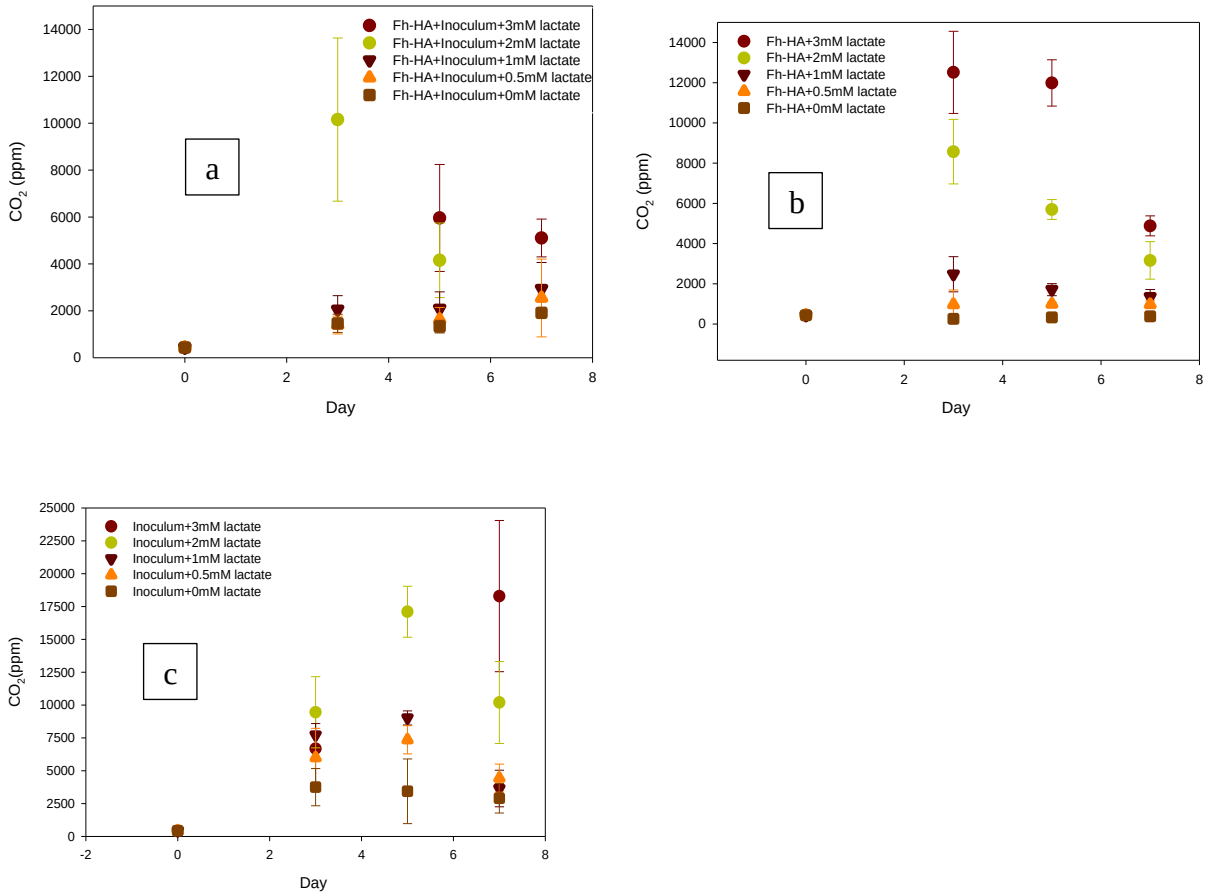

Figure D.6: $CO_{2(g)}$ emission over time under oxic condition experiments containing (a) Fh-HA coprecipitate with microbial inoculum and different concentrations of Na lactate (b) Fh-Ha coprecipitate without microbial inoculum(c) Inocumum with different concentrations of lactate.

Under anoxic conditions, the $CO_{2\,(g)}$ emission did not increase over time which is expected (Figure: 5). Under oxic conditions $CO_{2\,(g)}$ emission increased over time and was maximum in the reactors containing the 3mM Na lactate (Figure D.6).

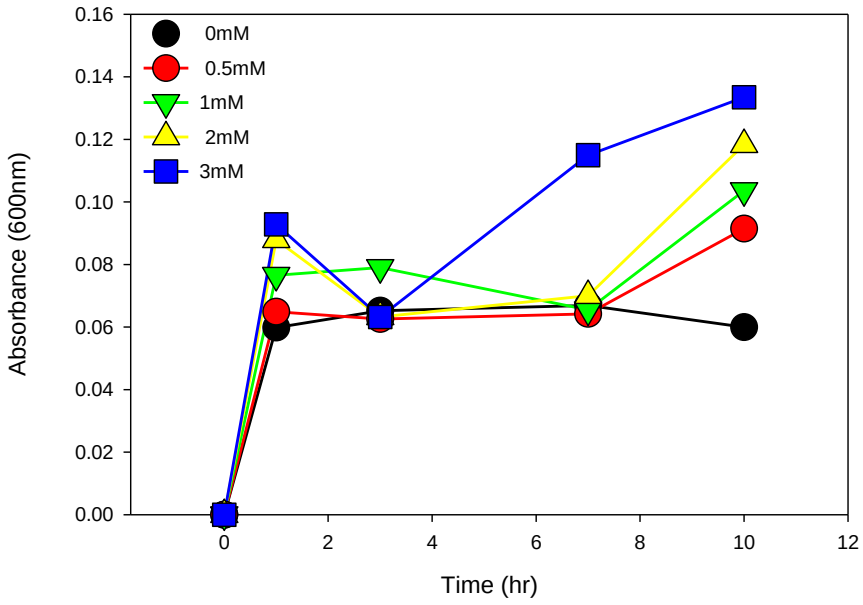

Figure D.7: Growth curve of *Shewanella oneidensis* MR1 over time.

REMARKS

This study was initially conducted to see the effect of different concentrations of Na lactate on the biodegradation of Fh-HA coprecipitate. This experiment was helpful to determine the minimum concentration of Na lactate requires for the survival of the microbial community without causing interference in the microbial interaction with the coprecipitates.

This experiment has some drawbacks such as, not having the Humic acid or the Na lactate being labeled. Which created problems to differentiate the sources of carbon in the solution. Moreover, in controls (Fh-HA and Na lactate, no inoculum) there was no sterilization process adopted apart from autoclaving everything initially, which raised the question of contamination in those vials over the period of time. This issue could have been avoided by using sodium azide in the vials. Na azide has a poisonous impact that prevents the growth of microorganisms. Along with that, this study needed some detailed examination of the coprecipitate samples before and after the incubation period.